DEVELOPING DNA BASED BIOSENSORS FOR

Clostridium difficile DETECTION

DEVELOPING DNA BASED BIOSENSORS FOR

Clostridium difficile DETECTION

By Dingran Chang, B.Sc.

A Thesis

Submitted to the School of Graduate Studies

in Partial Fulfillment of the Requirements

for the Degree

Doctor of Philosophy

McMaster University

DOCTOR OF PHILOSOPHY (2018)   McMaster University

(Biochemistry and Biomedical Sciences)   Hamilton, Ontario

TITLE: New Sensing Strategies and Their Applications in *Clostridium difficile* Detection

AUTHOR: Dingran Chang, B.Sc. (China Pharmaceutical University)

SUPERVISOR: Dr. Yingfu Li

NUMBER OF PAGES: xix, 168

ABSTRACT

Over the last 20 years, the incidence of *Clostridium difficile* infection (CDI) has increased dramatically, making it one of the most common healthcare-associated infections. This has been linked to the emergence of hypervirulent *C. difficile* strains. Currently, cell cytotoxicity assay (CTA) and toxigenic culture are the gold-standard methods for CDI diagnosis. However, they are time-consuming and labour-intensive. Other methods, like enzyme immunoassays (EIAs) and nucleic acid amplification-based tests (NAATs), allow for rapid testing but have poor sensitivity and/or specificity. Additionally, most of these methods target toxins or their associated genes and are unable to discriminate between epidemic and non-epidemic strains. The work described in this dissertation aims to develop easy-to-use and reliable biosensors for *C. difficile*, with a particular focus on epidemic strains of *C. difficile.* The development of the *in vitro* selection technique has allowed for the discovery of a big array of functional DNA, with excellent ability in both target recognition and enzymatic catalysis. My key interest is to employ functional DNA molecules as target recognition elements to develop colorimetric biosensors for *C. difficile* detection.

The first research project aimed to develop a colorimetric detection platform that can be coupled with functional DNA molecules to achieve hypersensitive detection of different targets. This test should be easy-to-use, have broad target applicability and not require expensive equipment. To do so, a colorimetric biosensing platform was created, which takes advantage of the signal amplification ability of rolling circle amplification (RCA) and the simplicity of the classic litmus test. In the presence of the target of interest,

RCA will be triggered, and the biotinylated RCA products can hybridize a number of the urease-labelled single-stranded DNA and immobilize urease onto magnetic beads through streptavidin-biotin interactions. The urease can then be used to hydrolyze urea, resulting in significant pH elevation, that can be detected easily using a litmus test. To prove the concept, we have demonstrated that this platform can be employed to visually detect thrombin and platelet-derived growth factor (PDGF) with high sensitivity, by coupling it with an anti-thrombin aptamer and an anti-PDGF aptamer, respectively. We have also shown that the biosensing platform can be incorporated into simple paper-based devices.

The second project focuses on the development of a colorimetric DNA detection method for epidemic strains of *C. difficile* that utilizes both the polymerase chain reaction (PCR) and the litmus test. The strategy makes use of a modified set of primers for PCR to facilitate ensuing manipulations of resultant DNA amplicons: their tagging with urease and immobilization onto magnetic beads. The amplicon/urease-laden beads are then used to hydrolyze urea, resulting in an increase of pH that can be conveniently reported by a pH-sensitive dye. We have successfully applied this strategy for the detection of two hypervirulent strains of *C. difficile*, which are responsible for the recent increase in the global incidence and severity of *C. difficile* infections. Furthermore, the viability of this test for diagnostic applications is demonstrated using clinically validated stool samples from *C. difficile* infected patients.

The goal of the third project was to isolate RNA-cleaving fluorogenic aptazymes (RFAs) targeting an epidemic strain of *C. difficile*. Four classes of RFA probes were derived using *in vitro* selection approach where a random-sequence DNA library was

reacted with a crude extracellular mixture (CEM) derived from the epidemic *C. difficile* strain BI/027/NAP1, coupled with a subtractive selection strategy to eliminate cross-reactivities to unintended *C. difficile* strains and other bacterial species. The isolated RFDs can be used together to generate specific cleavage patterns for strain-specific identification of *C. difficile*.

Lastly, the final project was to characterize a novel RFA probe (RFA13-1) that was isolated unintentionally using *in vitro* selection. By using CEM prepared from *C. difficile* glycerol stock contaminated by *Klebsiella aerogenes* as the positive target for *in vitro* selection, we isolated a remarkably active RFA probe, RFA13-1, targeting *K. aerogenes*. Further studies demonstrated that RFA13-1 could be activated by CEM prepared from several bacteria from the *Enterobacteriaceae* family. Moreover, the molecular target of RFA13-1 has been identified, which is ribonuclease I. RFA13-1 showed high sensitivity and specificity towards RNase I and could be employed as a tool to study RNase I functions and to detect RNase I or RNase I-containing bacteria.

In summary, I have investigated novel strategies for building a biosensor that is capable of discriminately detecting epidemic strains of *C. difficile*. I hope that my work can take us one step closer towards the development of easy-to-use and reliable biosensors that can be used in the clinical diagnosis of CDI.

ACKNOWLEDGEMENTS

I would like to express my deepest appreciation to my supervisor Dr. Yingfu Li for his excellent mentoring. Thank you for sharing your knowledge and expertise and teaching me invaluable lessons on how to be a great scientist.

I also like to extend my sincere appreciation to my supervisory committee member Dr. Giuseppe Melacini and Dr. Joaquin Ortega for their guidance, insightful comments, and being supportive during this journey.

I have had the great opportunity to work alongside many wonderful people in the Li lab over the years, and I have learned from each and every one of you. Thank you for your encouragement and friendship. In particular, I would like to thank Dr. Kha Tram, Dr. Meng Liu, Dr. Zhifa Shen, Pushpinder Kanda, Qian Feng, Rachel Gysbers, Jim Gu, Wenqing Zhang, Shahrzad Jahanshahi, Kim-Anh Nguyen, Ben Li, Suraj Laxman Gopinathbirla, Mimi Deng, Dr. Natalie Schmitt, Thomas Chang and Alexander Hua for their helpful discussions and general assistance.

In addition, I would like to acknowledge McMaster University for providing me such a great learning environment. I have truly enjoyed my time at this school.

Finally, I would like to thank my family for their unconditional love and always being there for me.

To my parents who have always been there for me

LIST OF CONTENTS

LIST OF FIGURES

LIST OF TABLES

LIST OF ABBREVIATIONS

ATP	adenosine 5'-triphosphate
ABTS	2, 2'-azino-bis (3-ethylbenzothiazoline-6-sulfonic acid)
AuNPs	gold nanoparticles
BP	5′- biotin-labelled DNA primer
BSA	bovine serum albumin
CDI	*Clostridium difficile* infection
CEM	crude extracellular mixture
CT	circular DNA template
CTA	cell cytotoxicity assay
DABCYL	4-([4-(dimethylamino)phenyl]-azo)-benzoic acid succinimidyl ester
DC	DNA capture sequence
DiSC2(5)	3,3′-diethylthiadicarbocyanine
DP	DNA polymerase
DT	DNA target
DMSO	dimethyl sulphoxide
DNA	2'-deoxyribonucleic acid
DNAzyme	deoxyribonucleic acid enzyme
dNTP	2'-deoxyribonucleoside 5'-triphosphate
dsDNA	double-stranded DNA
EDTA	ethylene diamine tetraacetic acid
EIA	enzyme immunoassay
FD	fluorogenic DNA
FNA	functional nucleic acid
FP	forward primer
GDH	glutamate dehydrogenase

GLB	gel loading buffer
GO	graphene oxide
G4-DNAzyme	Peroxidase-mimicking G-quadruplex DNAzyme
HP	hairpin probe
HRP	horseradish peroxidase
Kd	dissociation constant
LAMP	loop-mediated isothermal amplification
MB	magnetic bead
MBS	maleimidobenzoic acid N-hydroxysuccinimide ester
NAAT	nucleic acid amplification-based test
nt	nucleotide
PAGE	polyacrylamide gel electrophoresis
PaLoc	pathogenicity locus
PCR	polymerase chain reaction
PDGF	platelet-derived growth factor
PFGE	pulsed-field gel electrophoresis
Phi29	DNAP phi29 DNA polymerase
PNA	peptide nucleic acid
PNK	T4 polynucleotide kinase
RCA	rolling circle amplification
REA	restriction endonuclease analysis
RFA	RNA-cleaving fluorogenic aptazyme
RFS	RNA-cleaving fluorogenic substrate
rGO	reduced graphene oxide
RNA	ribonucleic acid
RNase	ribonuclease
RP	reverse primer

RPM	5′ biotin-labelled RCA product monomer
SB	selection buffer
SDA	strand displacement amplification
SELEX	systematic evolution of ligands by exponential enrichment
SNP	single nucleotide polymorphisms
SPR	surface plasmon resonance
ssDNA	single-stranded DNA
TMB	3,3′,5,5′-tetramethylbenzidine
UrD	urease-conjugated DNA
WT	wild-type

DECLARATION OF ACADEMIC ACHIEVEMENT

I took the primary role in design of the experiments, interpretation of the data and the writing of the manuscripts. I also performed all experimental work appearing in this document, with the exception of the graphene-based assay in Chapter 2, which I performed with the assistance of Dr. Meng Liu.

In Chapter 1, section 1.2 and 1.4 are a modified version of a published review, which I primarily wrote with help from Dr. Yingfu Li, Sandy Zakaria, Mimi Deng, Nick Allen, and Kha Tram (first citation below).

The study in Chapter 3 has been published (second citation below). It has been modified to fit the format of this thesis. I was responsible for all data collection and analysis. Kha Tram, Qian Feng provided helpful suggestions on urease-mediated litmus tests. Ben Li helped me with the preparation of genomic DNA from stool samples. Zhifa Shen provided helpful suggestions on primer designs. Dr. Salena and Dr. Lee provided stool samples from CDI patients. I wrote the first draft of the manuscript. Dr. Li provided editorial input to generate the final draft of the paper.

Chang, D.; Zakaria, S.; Deng, M.; Allen, N.; Tram, K.; Li, Y. Integrating deoxyribozymes into colorimetric sensing platforms. *Sensors* **2016**, *16*, 2061.

Chang, D.; Tram, K.; Li, B.; Feng, Q.; Shen, Z.; Lee, H.C., Salena, B.J., Li, Y. Detection of DNA amplicons of polymerase chain reaction using litmus test. *Scientific Reports* **2017**, 7, 3110.

Chapter 1

A General Introduction

1.1 *Clostridium difficile* infection

1.1.1 Overview of Clostridium difficile infection

Clostridium difficile (*C. difficile*) is a Gram-positive, anaerobic, spore-forming bacillus that is able to colonize and proliferate in the human gut, especially following changes in the indigenous colonic microbiota after the use of antibiotics[1]. *C. difficile* was first isolated in 1935 from neonates and identified as part of their intestinal microflora[2]. It was originally named *Bacillus difficile* because of its morphology and the encountered difficulties in its cultivation[2]. From 1978, *C. difficile* started to be recognized as the causative agent of enterocolitis and pseudomembranous colitis following the introduction of clindamycin, a broadband antibiotic against Gram-negative anaerobes[3,4].

C. difficile infection (CDI) is toxin-mediated intestinal disease. The clinical outcomes of CDI can range from asymptomatic colonization to mild diarrhea and more severe disease syndromes, including abdominal pain, fever, and leukocytosis[5]. CDI is transmitted by spores that are resistant to heat, acid, and antibiotics. The spores are plentiful in health care facilities and can also be found in the environment and food supply, allowing for both nosocomial and community transmission[6]. Once ingested, spores interact with small molecular germinants, such as bile acids[7,8], triggering a series of events committing

the spores to germinate into toxin-producing bacteria. *C. difficile* then colonizes the large intestine and releases two protein exotoxins, toxin A and toxin B, which are encoded within the pathogenicity locus (PaLoc)[9,10]. Biochemical and molecular studies have shown that the main clinical symptoms of CDI can be largely be explained by the actions of toxin A and toxin B[11]. Both toxins share the same enzymatic activity. Upon entering intestinal epithelial cells, they catalyze the transfer of glucose onto the Rho and Ras family of GTPases[12]. This causes a re-organization of the actin cytoskeleton and destruction of the intestinal barrier function[13]. Besides the genes encoding these toxins (*tcdA* and *tcdB*), the PaLoc also contains genes encoding a sigma factor (*tcdR*), a putative anti-sigma factor (*tcdC*) and *tcdE* which encodes a putative holin protein that may facilitate the release of the toxins into the extracellular environment[14–16]. Notably, *C. difficile* is a genetically diverse species, including both pathogenic and non-pathogenic strains. Strains lacking the PaLoc are not associated with the disease[17]. In addition, colonization of pathogenic *C. difficile* does not always result in symptomatic infection. Both host susceptibility and strain characteristics affect the probability of effective CDI[18,19]. For example, 22-45% of infants are colonized with *C. difficile* during the first year of life, but are asymptomatic, possibly owing to the lack of toxin-binding receptors in the infant's gut[20,21]. Also, upon hospital admission, 7-10% of asymptomatic patients are colonized with toxigenic *C. difficile*[22–24]. However, these asymptomatic carriers of *C. difficile* do play a significant role in onward transmission[25].

1.1.2 C. difficile epidemiology

In the last two decades, both the rate and severity of *C. difficile*-associated disease have increased significantly around the world, especially in North America, Europe, and some regions of Asia[26,27]. *C. difficile* has been recognized as the leading cause of infectious diarrhea that develops in patients after hospitalization and antibiotic treatment. Today, on average, seven CDI cases happen for every 10,000 overnight patients stays in European hospitals[28]. In the US, approximately 4-10% of patients are colonized with pathogenic *C. difficile* on admission to a health-care facility[24]. It is estimated that there are 500,000 CDI cases annually in hospitals and long-term care facilities in the US, resulting in 30,000 deaths[29]. Recent studies have shown that the rate of community-associated CDI (CDI occurring outside the hospital setting) has also increased which is reported more likely to affect younger, healthier patients[30,31]. An extensive US surveillance study published in 2015 demonstrated that more than half of their CDI cases were community-onset and there are around 48 community cases for every 100,000 population[32].

The dramatic increase in the incidence and severity of CDI over the last two decades appear to be linked to the emergence of several epidemic strains of *C. difficile*[33,34]. One such strain is characterized as restriction endonuclease analysis (REA) group BI, North American pulsed-field gel electrophoresis type NAP1, and ribotype type 027 and was subsequently known as BI/NAP1/027[35]. In addition to toxins A and B, this strain produces a binary toxin, which is composed of two proteins, CdtA and CdtB. CdtB binds to host cells and translocates CdtA, the catalytic component, into the cytosol where it ADP-ribosylates actin molecules[36]. Infection by BI/NAP1/027 has been associated with acute clinical

3

response and reports have indicated a high relapse rate and a three-fold increase in mortality within 30 days of infection[37,38]. The emergence and spread of *C. difficile* BI/NAP1/027 correlates with acquired resistance to the antibiotics including fluoroquinolone, gatifloxacin, and moxifloxacin, a trait that was not present in historical strains[35]. Metronidazole has long been the first-line agent for the treatment of CDI. However, a decreased effectiveness of metronidazole in the treatment of BI/NAP1/027 CDI has been documented[39]. In recent years, restoration of protective colonic microbiota by fecal microbiota transplantation has been shown to be more effective in treating BI/NAP1/027 CDI relapse than using antibiotics[11,40]. In the past few years, although the incidence of BI/NAP1/027 has decreased in some areas of western Europe[28], BI/NAP1/027-associated CDI persists in North America (accounting for >25% of CDI) and is increasing in other areas, especially Eastern Europe[32,41,42]. In Australia, similar binary-toxin-producing strains, such as ribotype 244, have emerged[43]. In Asia, non-binary toxin strains such as ribotypes 017, 018 and 014 remain dominant[44]. Further understanding of global CDI epidemiology, especially in developing countries, is hindered by a lack of surveillance.

1.1.3 C. difficile diagnosis

The ability to rapidly and accurately diagnose an incoming patient with pathogenic CDI is crucial for disease management and infection control. Currently, there are two reference standard tests: cell cytotoxicity assay (CTA) and toxigenic culture[45]. CTA is used to monitor the cytopathic effects on tissue culture by toxins from a stool sample. Toxigenic culture assays rely on the anaerobic culture of bacteria from feces and demonstrate the

presence of *C. difficile* isolated with the ability to produce toxins. Thus, toxigenic culture demonstrates the presence of a pathogenic strain of *C. difficile* in a patient but does not necessarily imply active infection, whereas CTA is more closely related to disease but might fail to identify carriers with the potential to transmit toxigenic strains to others. Although CTA generates fewer positive tests than toxigenic culture by ignoring toxigenic strains not currently producing toxin in the patient, its positivity has been shown to correlate more closely with clinical outcome and mortality[46]. However, although these tests confer great accuracy, they have a long turn-around time of 3 days and are labour-intensive[46]. Also, stool culture for *C. difficile* requires anaerobic culture and is not widely available.

The development of enzyme immunoassays (EIAs) has allowed for fast (2-6 hours) and inexpensive detection of toxin A or B in stool samples and these assays have become the primary diagnostic modality in most clinical settings. However, these assays provide reduced diagnostic sensitivity (around 60%)[46]. Glutamate dehydrogenase (GDH) EIA test is another popular screen test for CDI. It detects a cell wall antigen (the GDH enzyme) and provides high sensitivity (75-90%) and a high negative predictive value (95%-100%), but low specificity (<50%) and low positive predictive value[47]. This is because the antibodies used in the GDH test can cross-react with the same enzyme produced by other *Clostridium* species. Thus, the use of toxin EIAs or GDH EIA tests as stand-alone tests is not recommended[48].

Nucleic acid amplification-based tests (NAATs), such as polymerase chain reaction (PCR) and loop-mediated isothermal amplification (LAMP), target the toxin genes (*tcdA* or *tcdB*) and have high sensitivity[49,50]. However, it cannot distinguish asymptomatic

carriers of *C. difficile* from clinically active infections[51]. A prospective observational study by Polage and coworkers demonstrated that detection of toxin genes over-diagnosed clinically relevant CDI[52]; toxin was detected in only half of the NAAT-positive patients[52].

Due to the failure of single tests to accurately diagnose CDI, two-step algorithms for CDI diagnosis have been recommended by the Infectious Diseases Society of America and revised European guidelines on CDI diagnosis[53,54]. The algorithms comprise a rapid and sensitive screening test for *C. difficile*, that is a GDH test or NAAT, followed by a toxin EIA or CTA. Studies showed that using a high sensitivity test (GDH test or NAAT) to screen for *C. difficile* can yield a rapid result with a very high negative predictive value. If the screening test is positive, a second *C. difficile* toxin test (EIA or CTA) provides specificity for CDI. If a two-step approach gives different results, then a third test can be used to increase sensitivity. One example of two-step algorithms for CDI diagnosis is presented in Figure 1-1. The algorithm design requires consideration of cost and speed. Despite the guidelines from the past few years, only 29% of European laboratories are using such a combination of tests, with the majority still using a single test, leading to low diagnostic accuracy of CDI[28].
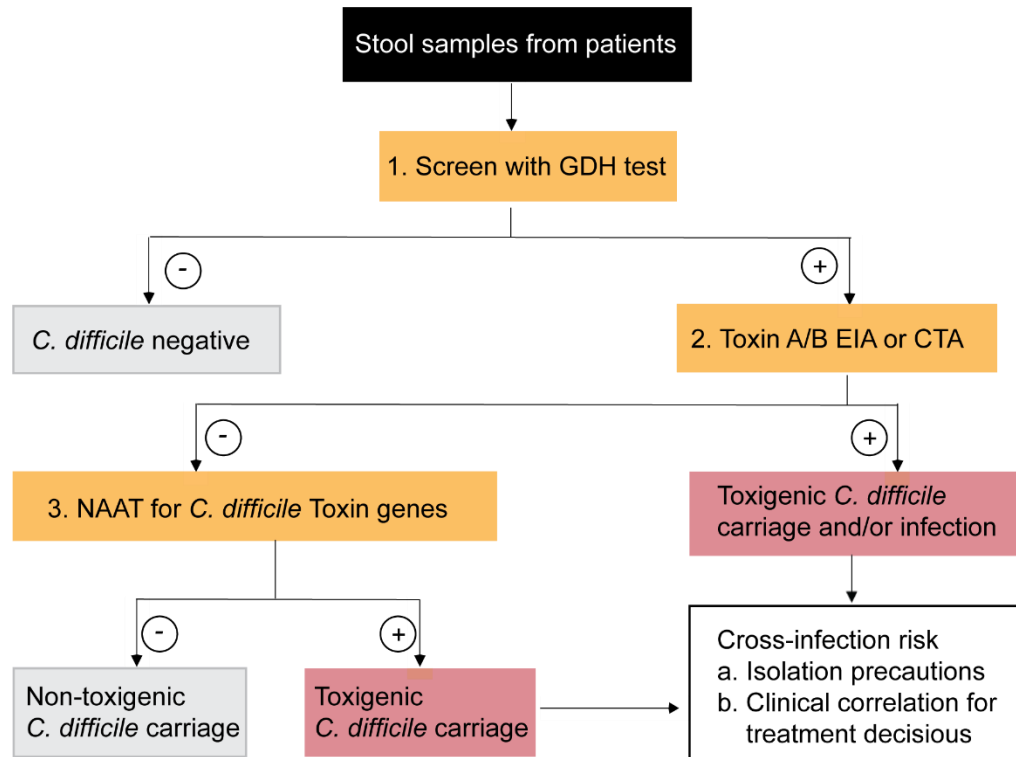
Figure 1-1. Example of two-step algorithms for CDI diagnosis. Diagnostic pathways using GDH as the first-line test. GDH + toxin EIA (1); GDH + CTA (2); and GDH + toxin EIA +PCR (3).

Another challenge for timely and correct diagnosis of CDI is adequate sampling. Currently, only patients with significant diarrhea are requested for *C. difficile* testing[55]. Non-infectious diarrhea is frequent in patients, and clinical discrimination between CDI and non-infectious symptoms is unreliable, which make it difficult to decide whom to test. There are many CDI cases that have been missed due to a failure to test them. A Spanish study tested all unformed stools, regardless of whether the clinician had requested *C. difficile* testing, and found that two-thirds of positive CDI would have been missed[56]. Another study which was performed across 20 countries suggested that one-quarter of

patients with pathogenic CDI were missed due to inadequate sampling and testing strategies[28].

Additionally, to fully understand and manage CDI, it is crucial to examine the relationship between the *C. difficile* strain types and spectrum of *C. difficile* carriage and disease. Then it will be possible to identify patients who require no intervention (those carrying non-pathogenic strains or low-risk strains), those who post an infection risk to others (those carrying hypervirulent strains) and patients who require proper treatment (those infected with hypervirulent strain and having clinical evidence of infection). However, the aforementioned diagnostic methods generally target toxins or their associated toxin genes and are unable to discriminate between *C. difficile* strains.

As a result, there is still a significant desire for an accurate and rapid test that can be easily performed to any patients in clinical settings for strain-specific detection of *C. difficile*. It would help clinicians to make informed decisions on whom to treat, which treatment strategy to use and how to efficiently utilize infection control resources. It will also help improve our understanding of disease epidemiology. The projects described in this thesis are conceived to meet this demand.

1.2 A Brief Outlook of Biosensors

Biosensors are analytical devices that utilize a biological component for the detection of a specific analyte[57]. This idea was first conceptualized in 1962 by Leland Clark with the development of an enzyme-based biosensor that could monitor blood glucose

levels[57]. This biosensor, the first and perhaps the most widely-known example, uses glucose oxidase to generate an electrochemical signal, which is quantified through the use of an oxygen electrode. This system was further developed into the modern-day glucose meter, a device which has become a staple element in the treatment and management of diabetes mellitus, and to this day is the largest stakeholder in the biosensor market[58,59]. Since Clark's invention, interest in biosensors has grown for uses ranging from sensitive laboratory analysis to point-of-care devices.

As the development of biosensors accelerated, two broad categories of biosensors emerged: simple and complex. Simple biosensors, such as the aforementioned glucose monitor, tend to sacrifice sensitivity and throughput with the goal of greatly reducing cost, complexity and size, while remaining functional when faced with the chemical and biological variability of real-world samples. Conversely, complex biosensors such as immunosensors are designed for laboratory use, where factors such as sensitivity, applicability to specialized usage scenarios, and ability to process large amounts of samples are far more important than ease-of-use and cost.

Although the field of biosensors has seen a vast expansion over the last 50 years, the core concept of a biosensor, as shown in Figure 1-2, remains the same. Every biosensor is composed of a recognition element and a transduction element. The recognition elements can be any chemical or biological entity such as small organic molecules, peptides, proteins, nucleic acids or even whole cells. This element ideally should have a low detection limit, high specificity, short response time and good stability[60–62]. Transduction elements are responsible for converting molecular recognition events into detectable signals. In recent

years, the transduction elements in biosensors have seen considerable innovation, particularly in expanding the range of generated response signals. Originally limited to electric signals, modern-day biosensors feature an assortment of output signal types, such as fluorescent, optical, and thermal signals[63–66].
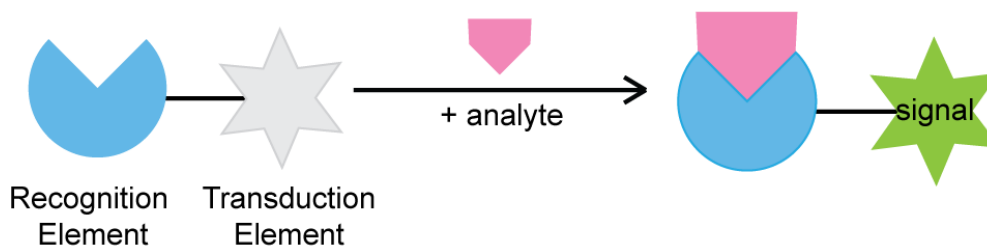
Figure 1-2. Schematic representation of biosensors

To date, the majority of biosensors on the market use protein enzymes or antibodies as their recognition element, and development of new biosensors continues to strongly focus on this model[67]. While proteins have proven to be capable in this task, their use as a recognition element comes with several limitations. Protein enzymes are naturally evolved catalysts that are limited to a target ligand. As a result, they offer little flexibility for developing biosensors to detect analytes that do not have a known natural enzyme that binds to them. While antibodies are more flexible in this regard (i.e., they can be developed for an arbitrary target), antibody isolation is costly and difficult to scale-up for mass production[67].

In response to these limitations of proteins, the last decade has seen increasing research into the use of functional nucleic acids as biosensors, and in biotechnology in general as an alternative to proteins in a variety of uses.

1.3 Functional DNA

1.3.1 Introduction of functional DNA

Historically, nucleic acids are widely known as the carriers of genetic information in every living organism. However, over the past three decades, both naturally occurring and synthetic nucleic acids have been discovered that can perform a wide array of functions[68–73]. These nucleic acid molecules, often referred to as functional nucleic acids, have been extensively studied and used in a broad range of applications such as biosensing, therapeutics, molecular imaging and drug discovery[68–73]. For biosensor development, functional DNA is a more popular candidate because it is significantly (> 100,000-fold) more stable than RNA[74]. In this chapter, we will focus on functional DNA. There are three major classes of functional DNA, DNA enzymes, DNA aptamers, and DNA aptazymes (see Figure 1-3).
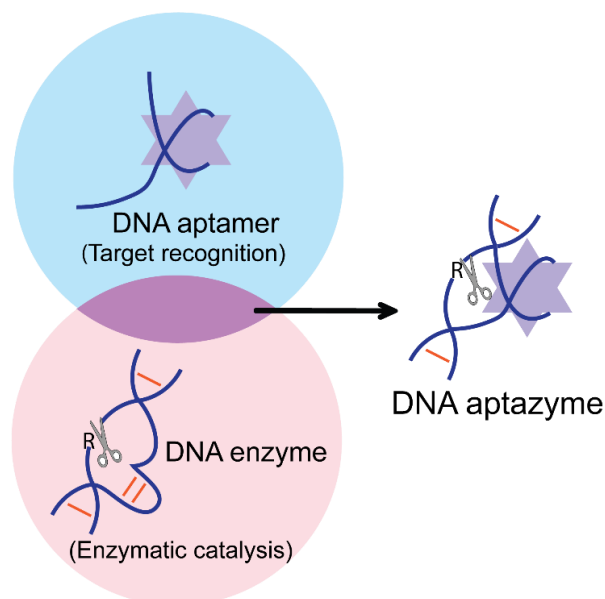
Figure 1-3. Schematic representation of functional nucleic acids

DNA enzymes, namely DNAzymes, are DNA molecules capable of catalyzing chemical reactions. The first-ever DNAzyme, known as GR5, was reported by Joyce and Breaker in 1994[75]. It is an RNA-cleaving DNAzyme that cleave a single RNA linkage in a DNA sequence in the presence of Pb^{2+}. Since then, a wide array of DNAzymes has been isolated to carry a variety of chemical functions, such as RNA cleavage[71], RNA ligation[76], RNA branching[77], DNA capping[78], DNA phosphorylation[77], DNA cleavage[77], and thymine dimer repair[77]. The details of these DNAzymes have been discussed in many reviews[69–73]. The rate enhancement of DNAzyme can be as high as 10^{14} over uncatalyzed reactions comparable to that of protein enzymes[79]. Most DNAzymes require metal irons for their activities, and some even presented metal specificity[80]. Therefore, DNAzymes can be used for metal sensing[80].

DNA aptamers are DNA molecules capable of binding to a target molecule, much like an antibody to its antigen. In the last three decades, hundreds of aptamers have been developed *in vitro* which could bind a wide range of targets including metal ions, small organic molecules, peptides, proteins, cells, and various inorganic materials[70,81]. Aptamers can have strong target binding property with a dissociation constant K_d of less than 1 nM, while the K_d for most antibodies is between 1 and 10 nM[82]. Aptamers also possess high target specificity. For example, the DNA aptamer against the B-chain of the platelet-derived growth factor (PDGF) has a high affinity ($K_d \approx 0.1$ nM) with PDGF-BB or PDGF-AB but has a low affinity with PDGF-AA ($K_d > 10$nM)[82]. With these attributes, aptamers demonstrate the inherent ability to function as recognition elements for biosensor development.

DNA aptazymes are DNA molecules that are able to carry out both target recognition and enzymatic catalysis function. Since they combine the advantages of DNAzymes and aptamers, DNA aptazymes have emerged to be promising molecules for biosensing[70,83].

1.3.2 Isolating functional DNA through in vitro selection

All functional DNAs are artificially created and have not been found in nature. They are generated by a method called Systematic Evolution of Ligands by Exponential Enrichment (SELEX), or *in vitro* selection, which was developed in 1990[84,85]. The method begins by using a library that contains up to 10^{15} unique single-stranded DNA molecules that can fold into a wide array of structures, some of which can bind a given target or catalyze a desired chemical reaction (see Figure 1-4). The DNA pool is subject to a function-based selection step (positive selection) that could separate active sequences from inactive ones. These active sequences are amplified with the use of PCR and are then used for the next round of selection. The cycle is repeated with increasing selective pressure until the sequences that can perform the expected function with the highest efficiency are isolated. The increased selection pressure can be achieved by strategies such as reducing the incubation time with the target and reducing the concentration of the target. During the process of selection, the counter-selection step can also be involved to eliminate sequences that perform undesired functions[86]. The use of the combined positive-selection/counter-selection strategy ensures the derived DNAs have high specificity for the intended target.
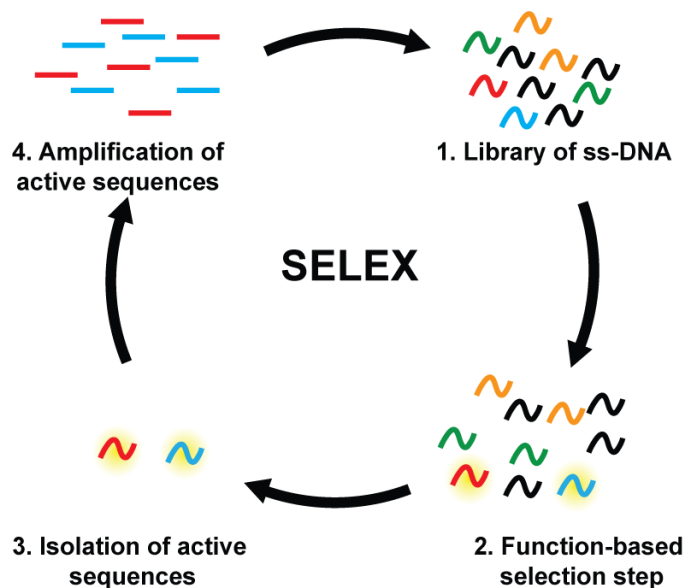
Figure 1-4. A general *in vitro* selection approach for isolating functional nucleic acids

1.3.3 Advantages of functional DNA

Compared with proteins, functional DNA not only has competitive performance, it possesses multiple advantages over proteins for use in biosensors. Functional DNAs are able to detect essentially any target of choice including those for which antibodies are difficult to obtain, such as toxic metal ions and molecules with poor immunogenicity. DNA selection can be carried out at designed conditions to achieve desired performance without involving living cells or animals, and counter selections can be incorporated to remove cross activity, which is difficult to achieve in antibodies. Additionally, functional DNAs are chemically synthesized, rather than expressed in biological systems. This makes

functional DNA production much more commercially scalable, increases consistency between batches, and eliminates biological contamination from expression hosts. Moreover, functional DNA can be easily chemically modified in order to increase stability, as well as to introduce functional groups to allow for conjugation chemistry, enabling the linking of functional DNA to small molecules (dyes, carbohydrates, amino acids), proteins, and various nanomaterials[68,69,73]. Furthermore, functional DNAs are generally smaller than antibodies and can be immobilized with higher density during biosensor development. Lastly, functional DNAs are resistant to thermal denaturation and are able to re-fold into their native structures after heating, a property most proteins lack.

1.3.4 Functional DNA against bacterial pathogens.

Owing to the aforementioned advantages, functional DNAs have been extensively applied for biosensing applications. In this part, I will highlight the functional DNAs isolated against bacterial pathogens.

The most direct targets from bacteria for functional DNA are the cell surface proteins, where the whole cell can be used as a target for *in vitro* selection. A cell's surface is complex and has many different molecules, especially proteins. Using whole cells for selection can produce aptamers specifically bind to a certain bacterium based on these extracellular characteristics and no prior knowledge of bacteria-surface markers is required. By using whole bacterial cells as target for selection, a number of aptamers have been isolated, some of which have been summarized in Table 1-1. For example, a panel of aptamers was isolated by a whole bacterium-based selection with *Staphylococcus aureus*

as a positive target and *S. epidermidis* and *Streptococcus* as counter targets[87]. After five rounds of selection, five aptamers with dissociation constants ranging from 61 to 210 nM were isolated and demonstrated high specificity and affinity to *S. aureus* individually. The study also showed that a set of aptamers could be used in combination to increase the specificity against the target cells. Some drawbacks of using whole cells for selection are that there is little control over the outcome of the selection and it is difficult to identify the molecular target of the selected aptamers.

Table 1-1. Literature examples of using whole bacterial cell as target for SELEX

Bacterial target	K_d	Reference
Escherichia coli	15 ± 4 nM	[88]
Salmonella typhimurium	6.33 ± 0.58 nM	[89]
Salmonella enteritidis	7 nM	[90]
Vibrio parahaemolyticus	16.88 ± 1.92 nM	[91]
Vibrio alginolyticus	27.5 ± 9.2 nM	[92]
Listeria monocytogenes	48.74 ± 3.11 nM	[93]
Shigella dysenteriae	23.47 ± 2.48 nM	[94]
Streptococcus pyonenes	9 nM, 10 nM	[95]
Staphylococcus aureus	61-210 nM	[87]
Proteus mirabilis	7.7 nM, 4.1 nM	[63]
Campylobacter jejuni	292.8 ± 53.1 nM	[96]

Purified molecules from bacteria, such as toxins, have also been used in aptamer selection. Compared with the whole cell-selection, the outcome of selection using purified molecules is more easily controlled, but it requires more steps to identify, express, and purify the protein targets. Moreover, proteins under natural conditions are more complicated than purified proteins used in selection. The proteins could be present in a modified state or can be masked in a physiological context. Under these circumstances, it would be challenging for selected aptamers to recognize the natural structure of some proteins. Despite these challenges, this method has allowed for high-affinity aptamers to be isolated against many targets (see Table 1-2), including protein targets from *C. difficile*. Several aptamers against toxin A, B and binary toxin from *C. difficile* have been isolated by Ochsner and coworkers[97]. They performed selections using truncated recombinant toxins as targets. The selected aptamers have dissociation constants in picomolar to nanomolar range. Their affinities for native toxins were slightly lower but remained in the low nanomolar range for the majority of the candidate sequences. Recently, aptamers against GDH from *C. difficile* have been reported by our group[98]. These aptamers were isolated after 10 rounds of selection and presented low nanomolar affinity against GDH.

Table 1-2. Literature examples of using purified molecules from bacteria as target for SELEX

Target	K_d	Reference
Enterotoxin B	Not reported	[99]
Enterotoxin C1	65.14 ± 11.64 nM	[100]
C. difficile binary toxin	0.02-2.7 nM	[101]
C. difficile toxin A, B and binary toxin	Sub to low nM range	[97]
C. difficile toxin B	47.3 ± 13.7 nM	[102]
C. difficile GDH	3.1- 5.6 nM	[98]
Mycobacterium tuberculosis CFP-10	375 nM/160 nM	[103]
Protective antigen	112 nM	[104]
Botulinum neurotoxin type A heavy chain	Not reported	[105]
Botulinum neurotoxin type A light chain	Not reported	[106]
Cylindrospermopsin	88.78 nM	[107]

The crude extracellular mixture (CEM) of a bacterium has also been proved that can be used in functional DNA selection. By using this strategy, our group has successfully isolated several RNA-cleaving fluorogenic aptazymes (RFAs) targeting bacterial pathogens[86,108,109]. This method allows for sensor development without first identifying a specific target. To isolate probes with high specificity, counter-selection steps are required in each round of selection, where the CEM from unintended bacteria is used as target to remove nonspecific DNA species. This strategy provides a more natural way to select the

"best" biomarker from the complex cellular mixture. By employing selection conditions which are very similar to the testing conditions, the isolated probes are more likely to provide a positive signal in future detection assays. To date, we have successfully applied this approach for two bacteria, *E. coli* and *C. difficile*[108,109]. In the case of *E. coli*, CEM from *E. coli* was used as target for positive selection, while the CEM from *Bacillus subtilis* was used for the counter selection[109]. After 20 rounds of selection, an RFA probe, named RFA-EC1, was isolated that only responded well to *E. coli*, but not to *B. subtilis* and many other bacteria. It also exhibits high sensitivity as it can detect as few as 100 cells. In the case of *C. difficile*, we took it one step further and successfully isolated an RFA probe, RFA-CD1, that can distinguish an epidemic strain of *C. difficile* (BI/027/Hamilton) from other strains of *C. difficile*[108]. It shows both species-specificity and strain-selectivity. The molecular target of RFA-CD1 has also been successfully identified, which is TcdC, a negative regulator of toxin production expressed in *C. difficile*.
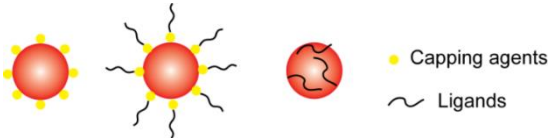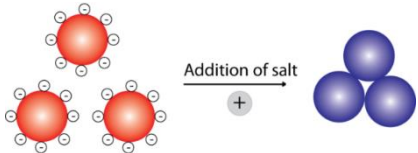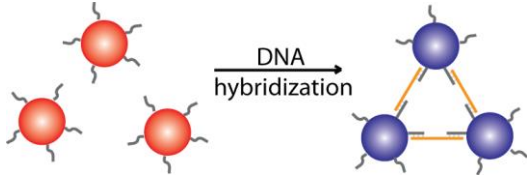
1.4 Constructing functional DNA into colorimetric biosensors

After obtaining functional DNAs with desired functions, the next step is to incorporate them into biosensor designs. Functional DNAs have been employed as recognition elements coupled with a variety of transduction elements to create new biosensors[70]. I am particularly interested in colorimetric biosensors, due to their promising potential for applications in point-of-care devices. The major development of different colorimetric signal transducers applied in functional DNA-based biosensing, including gold nanoparticles, enzymes, and organic dyes, will be discussed in this section.

1.4.1 Gold nanoparticles as signal transducer

Over the last two decades, gold nanoparticles (AuNPs) have been used as the nanoassembly units for creating colorimetric biosensors. AuNPs' intrinsic properties, namely surface plasmon resonance (SPR) and colloidal stability are contributing factors for a colorimetric generation[110,111]. SPR is the mechanism by which AuNPs can produce visible light in response to an electromagnetic field. When AuNPs are exposed to light, the resonant wavelength is absorbed by the AuNPs to induce the oscillation of their surface electrons[110,111]. These oscillating electrons will produce electromagnetic radiation that can be observed by the naked eye. Compared to organic chromophores, AuNPs have much higher extinction coefficient. For example, the extinction coefficients for 13 and 50 nm AuNPs were 2.7×10^8 and 1.5×10^{10}, respectively[112]. These values are 3-5 orders of magnitude higher than those of organic dyes. Therefore, fewer AuNPs (nanomolar) are required for visual detection compared to organic dyes (micromolar). The colloidal stability of AuNPs is determined by two forces counterbalancing one another: Van der Waals and electrostatic force[113]. When one of these forces is weak or absent, the colloid system will destabilize, and the AuNPs will aggregate, resulting in a colour shift from red to blue (the shift of the surface plasmon band to a longer wavelength). This is known as interparticle-plasmon coupling and has been extensively used in colorimetric biosensor development[114]. Currently, techniques such as using colloidal stabilizers and cross-linking agents have shown to be successful in manipulating the dispersal and aggregation of AuNPs for colorimetric generation. These techniques, along with others, are listed in Table 1-3.

Table 1-3. Techniques for AuNPs Dispersal and Aggregation

Techniques	Reference
Colloidal Stabilizers The addition of surface-tethered capping agents (e.g. thiols, amines, phosphines) and ligands (e.g. small charged species, macromolecules, polymers), on the surface of AuNPs, can enhance the stability of colloid AuNPs	115–118
High Salt Concentration High salt concentrations reduce colloid stability via increase of electrostatic interaction. This will result in the aggregation of AuNPs and a colour shift from red to blue will be observed.	119,120
Inter-particle Cross-linking When the surface of AuNPs is modified with ssDNA, AuNPs can be bridged through DNA hybridization. This can lead to the aggregation of AuNPs and a colour shift from red to blue can be observed.	121,122

Due to DNA's programmable nature, the functionalization of AuNPs with DNA molecules provides an attractive option for selective colorimetric sensing. AuNPs are generally coated by ligands during synthesis to stabilize the colloid aqueous solutions[123,124].

These ligands on the surface of AuNPs can be efficiently replaced by thiol-containing molecules because of the thiophilic nature of Au. Based on this principle, thiol-modified DNAs (thiol-DNAs) can be successfully functionalized onto the surface of AuNPs for further biosensing applications[125,126]. In addition to thiol-DNA, unmodified single-stranded DNA (ssDNA) was found to bind AuNPs with sufficient affinity, while double-stranded DNA (dsDNA) could not[127]. By introducing functional DNA into AuNP systems, a series of colorimetric biosensors have been developed for a broad range of targets[128].

For example, when AuNPs are functionalized with thiol-modified DNA, the distance between AuNPs can be controlled by a linking DNA that is complementary to the DNA immobilized on AuNPs. As shown by Lu group, a DNA linker can hybridize with short DNA sequences on each AuNP to create a cross-linked network of AuNPs and induces aggregation[129]. In the presence of Cu^{2+}, the Cu^{2+}-dependent DNA ligation DNAzyme catalyzes the nucleophilic attack of the phosphorus center of substrate S1 by the hydroxyl group on substrate S2, forming a phosphodiester bond with the imidazole acting as a leaving group, as depicted in Figure 1-5A. The ligation product was designed as a DNA linker to assemble AuNPs and lead to a colour shift from red to blue. An alternate design presented by Lu group uses RNA-cleaving DNAzymes to disassemble cross-linked AuNPs[130,131]. In the absence of Pb^{2+}, the DNAzyme remains bound to the AuNPs, and no colour shift is observed. However, when Pb^{2+} is added to the solution, the DNAzyme will respond by cleaving the DNA cross-linker, separating the AuNPs complex[132]. This will result in the dispersal of AuNPs, and a colour shift from blue to red will be observed, as

outlined in Figure 1-5B. Similar designs have been used in detecting UO^{2+} [132], adenosine[133] and infectious pathogens[134].

In addition to manipulating dispersal and aggregation AuNPs for colour change, the red AuNPs can be directly used as signal indicator together with other techniques such as grapheme oxide[135], hydrogel[136–138] and lateral-flow devices[139] for biosensing.
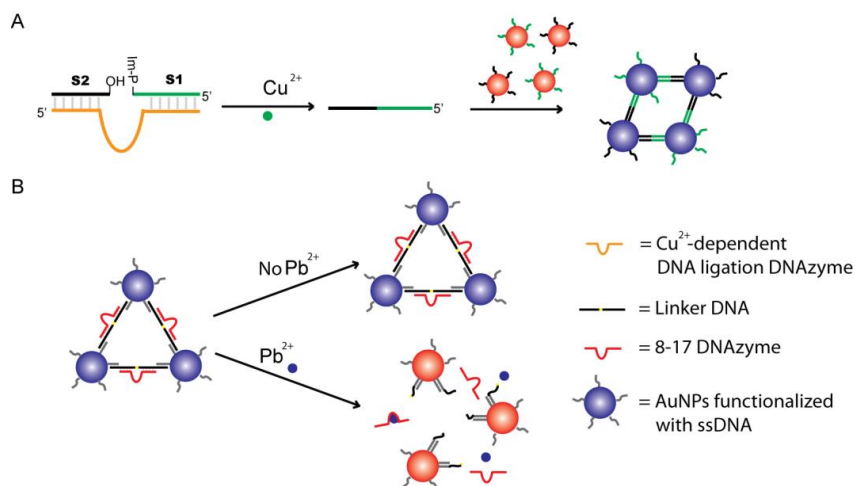
Figure 1-5. DNAzyme-directed AuNP assemblies as biosensors for a) Cu^{2+} and b) Pb^{2+}.

1.4.2 Protein Enzymes as Signal Transducer

Protein enzymes have been coupled with functional DNAs for colorimetric biosensor development. For example, peroxidases are a family of enzymes that catalyze the oxidation of a wide variety of substrates using H_2O_2 or other peroxides[140]. The enzyme horseradish peroxidase (HRP) has the ability to produce a coloured, fluorescent, or luminescent product when incubated with their respective substrates. As a result, it has been

extensively used as a signal transducer in various techniques such as western blotting and ELISA. H_2O_2-mediated oxidation of 3,3′,5,5′-tetramethylbenzidine (TMB) by HRP is a well-researched area of colour-based sensing[141]. When used in conjunction with target-specific functional DNA and solid supports, HRP-based systems can report trace amounts of target and has been applied in detecting targets like thrombin[142], aflatoxin B1[143], and Lipocalin-2[101].
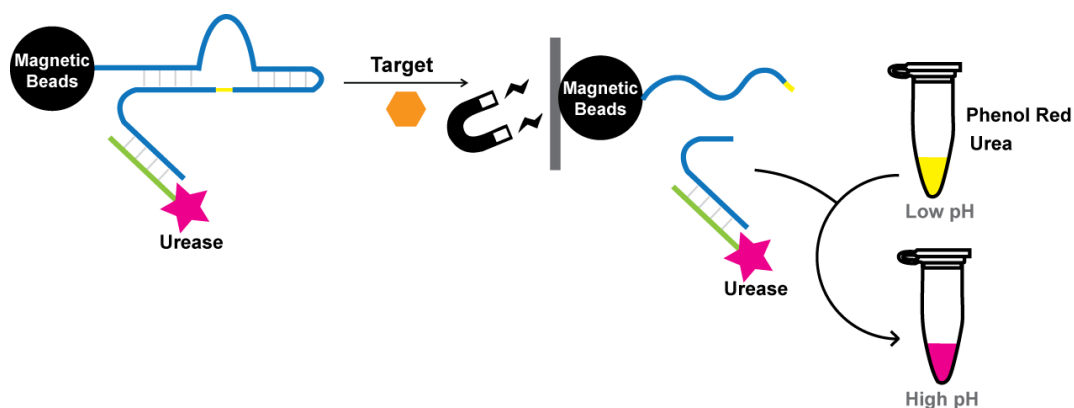
Figure 1-6. Conceptual schematic of DNAzyme-litmus test. The signal is transduced through hydrolysis of urea and reported through a colour change of phenol red.

Urease is a highly efficient protein enzyme that is capable of converting urea into carbon dioxide and ammonia. The generation of ammonia in solution will cause the pH of the solution to increase, and this change in pH can be monitored by an indicator dye. By taking advantage of urease and RNA-cleaving DNAzymes, our group has created a modified litmus test for targets like *E. coli* and uranyl[144,145]. The assay involved a DNAzyme with a 5′ biotin moiety for binding to streptavidin-coated magnetic beads (MB) and a 3′-end for hybridization with urease-conjugated DNA (UrD). To prepare UrD, urease

was attached to a 5′-amino-modified DNA oligonucleotide using maleimidobenzoic acid N-hydroxysuccinimide ester. In the presence of the target, the DNAzyme catalyzes cleavage at a ribonucleic site along the sequence, releasing the 3′ end of DNAzyme and its bounded UrD into solution. After removal of MB-immobilized cleavage product *via* magnetic separation, urea was added to the solution. A colour change can be detected by using phenol red (Figure 1-6).

1.4.3 *Peroxidase-mimicking DNAzyme (G4-DNAzyme) as Signal Transducer*

A DNAzyme with peroxidase-like activity was first reported by Sen and co-workers in the late 1990s[146–148]. Two G-rich DNA aptamers (PS2.M and PS5.M) were found to display selectivity towards N-methyl mesoporphyrin IX and hemin through *in vitro* selection procedure[147,149]. Later, it was found that these aptamers could act as DNAzymes to catalyze porphyrinmetallation[148]. Compared to free hemin, PS2.M had 250-fold enhanced peroxidase activity. The proposed secondary structure of PS2.M with hemin is shown in Figure 1-7. In such a DNAzyme, each guanine is linked with neighbouring guanine *via* two hydrogen bonds by Hoogsteen pairing. These cyclic guanine quartets then stack on each other in a helical fashion, forming a G-quadruplex structure. Hemin, with its Fe^{III}-centered core, stacks externally on the terminal G-quartet through strong π-π interactions. The proximity between the oxygen atoms of guanine and Fe^{III} allows for this interaction, which is essential for peroxidation activity[150].
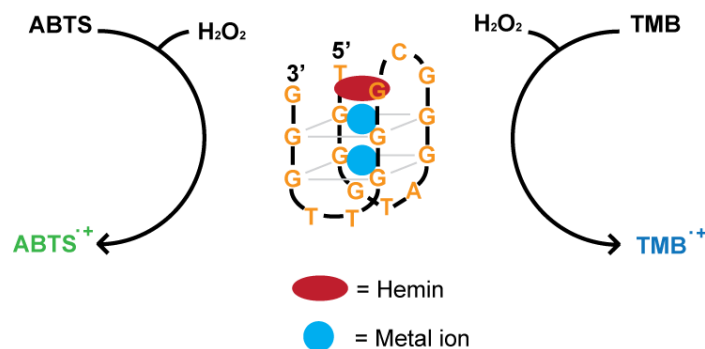
Figure 1-7. The proposed structure of the 18-nucleotide G4-DNAzyme (middle); the DNAzyme can catalyze the oxidation of ABTS (left) or TMB (right) to enable a colour change.

Visual detection can be achieved using 2, 2'-azino-bis (3-ethylbenzothiazoline-6-sulfonic acid) (ABTS) as the substrate, which is converted to a green soluble product in the presence of H_2O_2 upon oxidation[150]. TMB is an alternative chromogenic substrate, producing a blue coloured product upon oxidation. In comparison with HRP, G4-DNAzymes possess numerous advantages including small size, ease of synthesis, facile manipulation and amenability to the rational design of allosteric control. G4-DNAzymes have been extensively exploited to replace HRP for the development of colorimetric biosensors and molecular machines. Several signalling strategies of colorimetric biosensors using G4-DNAzymes as the signal transducer will be discussed here.
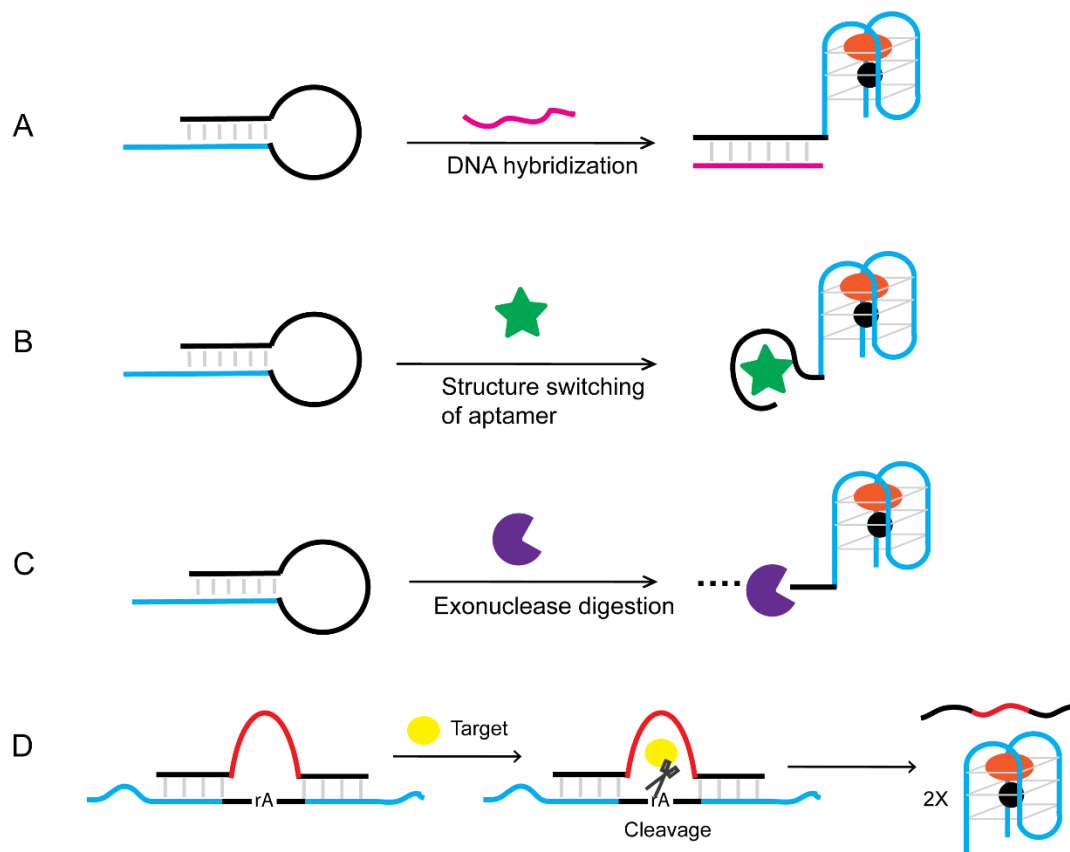
Figure 1-8. G4-DNAzyme-based biosensors signalling though removal of blocker DNA. Hairpin can be opened through a) DNA hybridization; b) structure switching of an aptamer; c) exonuclease mediated digestion; d) DNAzyme-mediated cleavage.

Being nucleic acids permits hybridization of single-stranded G4 DNA molecule to its complementary sequence (blocker DNA) that prevents the formation of the G-quadruplex structure and inhibits its catalytic ability. Various colorimetric biosensors have been developed based on the target-dependent removal of this blocker DNA. For example, blocker DNA could be released through DNA hybridization (Figure 1-8A). Willner and coworkers designed the first G4-DNAzyme containing a hairpin structure, whose duplex structure at the stem prohibited the self-assembly[150]. Following target DNA hybridization,

the loop region opens and leads to the formation of a hemin/G-quadruplex structure that could oxidize ABTS to the coloured ABTS$^{•+}$. This assay allows colorimetric detection of DNA at a concentration of 0.2 μM[151].

The blocker DNA can also be part of an aptamer. In the presence of its target ligand, the formation of the respective ligand–aptamer complex opens up the hairpins and result in the self-assembly of the activated G4-DNAzyme (Figure 1-8B). Several biosensors were reported that were based on this principle and the use of aptamers with different targets, such as AMP[152], ATP[153], methamphetamine[154], and Ochratoxin A[155].

The blocking DNA could also be digested by exonucleases (Figure 1-8C). Yu and coworkers describe a colorimetric strategy for estimating the activity of polynucleotide kinase (PNK) by taking advantage of the efficient cleavage of exonuclease and the G4-DNAzyme signal amplification. The 5′-OH of the hairpin DNA was first phosphorylated in the presence of PNK and then digested by an exonuclease[156]. The blocked G4-DNAzyme sequence was then released and activated due to the removal of its completely complementary sequence. Tang and coworkers reported a strategy that applied G4-DNAzyme-containing hairpin into PCR[157,158]. During the annealing step of PCR amplification, the hairpin DNA probe would open and form a stable duplex with one single-stranded PCR product. *Taq* DNA polymerase has an inherent 5′-3′ exonuclease activity and cleaves a part of the probe that is hybridized to the PCR template and releases the G4-DNAzyme. Detection of as low as 10 copies of HBV DNA was achieved based on this method.

The blocked G4-DNAzyme can also be released by DNAzyme-mediated cleavage. Willner and coworkers described a supermolecular construct which comprised of target-dependent RNA-cleaving DNAzymes, their substrate sequences, and G4-DNAzymes[159], as shown in Figure 1-8D. The RNA-cleaving DNAzyme is hybridized to its RNA-substrate sequence that includes a G4-DNAzyme on each end of the substrate sequence. The partial hybridization between G4-DNAzyme domains and RNA-cleaving DNAzyme prohibits the self-assembly of the G-quadruplex. In the presence of target, the DNAzyme cleaves the RNA, fragmenting the sequence into two parts, which destabilizes the complex and enables the formation of an activated G4-DNAzyme. By making use of this strategy, the Willner group successfully developed colorimetric assays that can sensitively and specifically detect Pb^{2+}, L-histidine, UO_2^{2+} or Mg^{2+}[159,160].

G4-DNAzyme would lose its peroxidase activity if the G-quadruplex sequence was split into two halves, but once it is reconstructed with the assistance of designated template, the catalytic activity can be restored. Kolpaschikov demonstrated this concept by using a single-stranded synthetic DNA as the template for two equally split (1:1) G4-DNAzyme sequences[161] (Figure 1-9A). In coupling with different recognition element, this concept was successfully applied to achieve visual detection of many different targets, such as PCR products[162], and thrombin[163]. Moreover, Willner and coworkers have developed an amplification platform that involves the use of split fragments of G4-DNAzyme that upon recognition of the target DNA, can trigger an autonomous cross-opening process to produce hemin/G4 DNAzyme wires[164] (Figure 1-9B). The resulting nanowires then enable

colorimetric or chemiluminescent readout of the sensing process. This analytical platform

allows the sensing of target DNA with a detection limit of 0.1 pM[164].
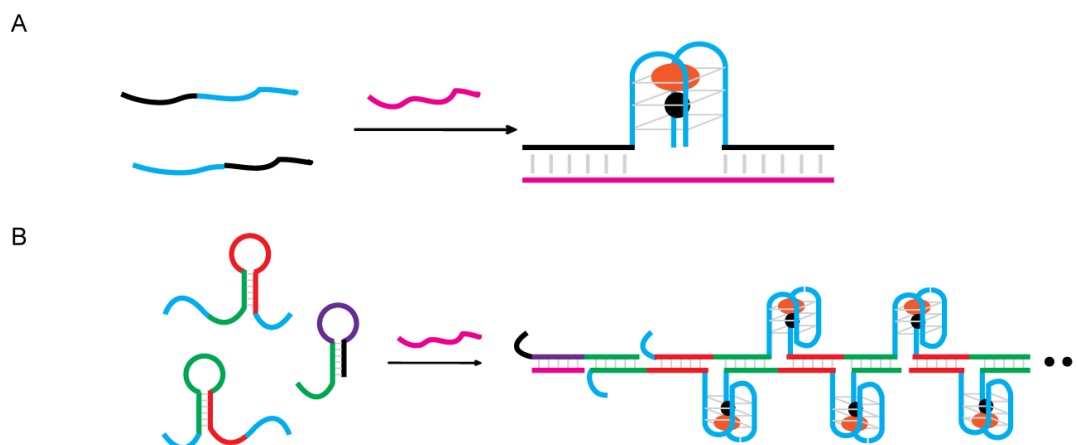
Figure 1-9. Biosensors signalling by reconstructing split fragments of G4-DNAzyme. a) Reconstructing G4-DNAzyme by using target DNA as template. b) Scheme for the amplified detection of DNA through the enzyme-free autonomous assembly of G40 DNAzyme Nanowires.

G4-DNAzymes can also be synthesized by DNA polymerases in various biosensing

platforms. Polymerase-stimulated synthesis, such as rolling circle amplification (RCA)[165]

or strand displacement amplification (SDA) reaction[166], to produce G4-DNAzymes was

adopted by many researchers to develop analytical methods with high sensitivity (see

Figure 1-10). Upon recognition of the input analyte, the amplification reaction is activated,

and numerous G4-DNAzymes are synthesized, which in turn, generate colorimetric signals.

Thus, a single recognition event can be translated into an amplified signal.
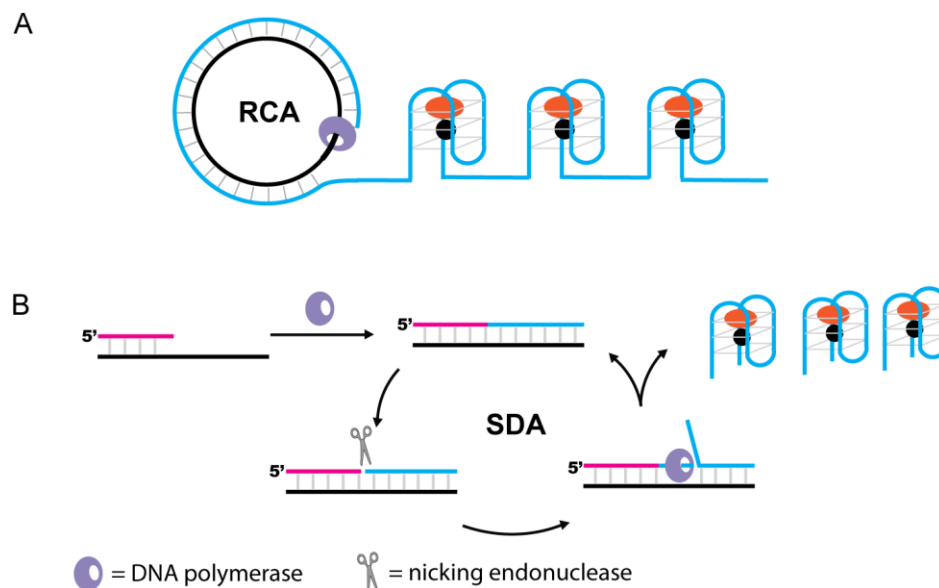
Figure 1-10. G4-DNAzyme-based biosensors signalling by polymerase-stimulated DNAzyme synthesis. a) Synthesis of G4-DNAzymes using RCA. b) Synthesis of G4-DNAzymes using SDA.

DNA detection can also be achieved using target DNA as a linker to bridge surface-immobilized DNA with free-floating G4-DNAzymes (Figure 1-11A). The signal could be further enhanced by using AuNPs immobilized with G4-DNAzymes (Figure 1-11B). AuNPs possess a very high surface-to-volume ratio, which offers an opportunity to attach multiple kinds of biomolecules, such as aptamers, DNAzymes, and antibodies, as multifunctional nanoprobes[165]. When AuNPs were used as carriers for the G4-DNAzyme labels, a single recognition event could be converted to multi-labels of G4-DNAzymes, significantly improving the sensitivity. This kind of signal amplification has been named ''bio-bar-code'' amplification[165]. G4-DNAzyme-functionalized AuNPs were used as biocatalytic conjugates by Park and coworkers for the construction of colorimetric sensors for the amplified detection of Chlamydia gene with a detection limit of 50 fM[167]. Similar

designs have also been reported for the detection of the *invA* gene of *Salmonella*[168], thrombin[169], ATP[170], and myoglobin[171].
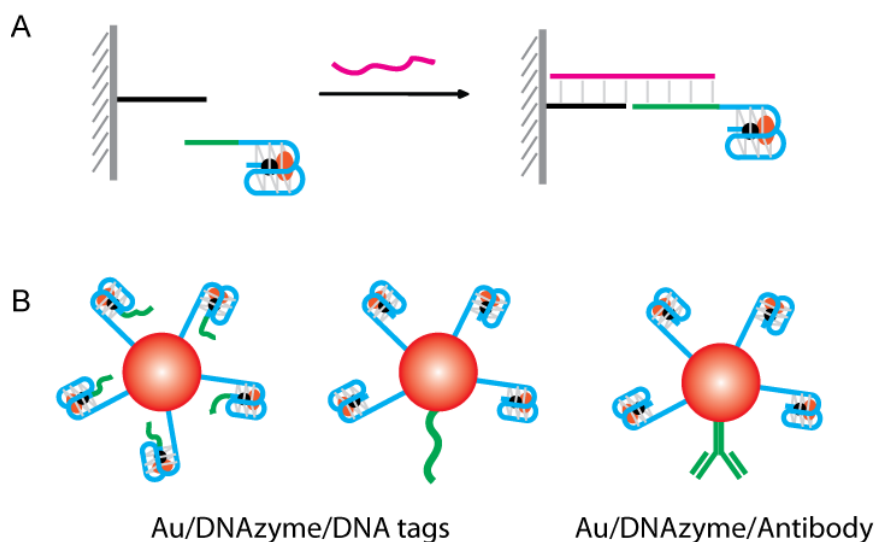
Figure 1-11. G4-DNAzyme-based biosensors signalling by solid support mediated separation. a) Target DNA mediated G4-DNAzyme immobilization. b) ''Bio-bar-code'' amplification.

1.4.4 Organic Dyes as Colorimetric Signal Transducer

Through the years, organic dyes have become useful for not only their pigmentation but also their physical and chemical properties that can be engineered to induce a colour change. For example, Stojanovic and coworkers reported a colorimetric sensor for cocaine, taking advantage of anti-cocaine aptamer and cyanine dye[172]. They suggested that cocaine could displace the cyanine in the aptamer binding pocket and release the dye into solution. The dye then formed dimers in solution whose absorbance spectrum is different from that

of the monomer, leading to a colour change. However, to detect the colour change, high

concentration (20 μM) of aptamer and a waiting time of 12 h were required.
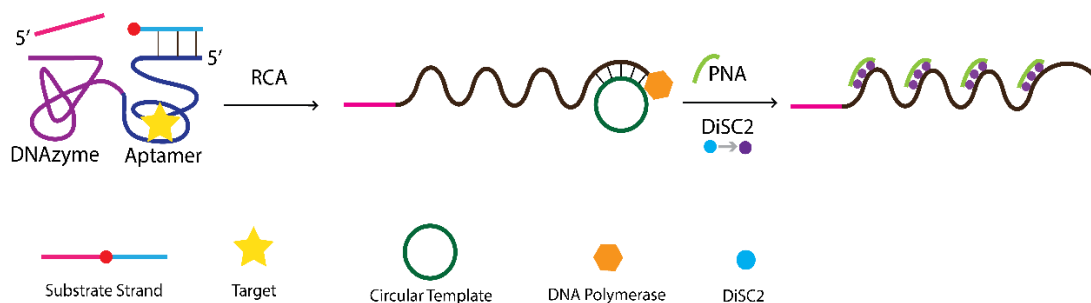
Figure 1-12. Colorimetric detection involving an RNA-cleaving DNAzyme for RCA initiation and signal generation by DiSC2(5).

DNA duplex-binding dyes, such as DiSC2(5) (3,3′-diethylthiadicarbocyanine), have also been employed to generate colour change. For example, our group has developed a method that utilized RNA-cleaving aptazyme, RCA, and DiSC2(5)[173]. As shown in Figure 1-12, the recognition element is an allosteric DNAzyme whose RNA-cleaving activity is regulated by an aptamer. Target binding to the aptamer induces a conformation change, enabling the allosteric DNAzyme to cleave its RNA-containing substrate, generating a DNA primer. DNA polymerase uses the DNA primer to initiate an RCA reaction, resulting in the production of a long DNA chain with tandem repeats that can bind a peptide nucleic acid (PNA). The PNA hybridizes to the RCA product to form highly stable duplex structures that can bind DiSC2(5). When bound, DiSC2(5) undergoes a colour change from blue to purple, indicating the presence of the target. Signal amplification offered by RCA is able to provide a detection limit of 100 μM when ATP target is tested.

Since the emergence of the glucose meter, the field of biosensors has expanded tremendously. The development of the *in vitro* selection technique has allowed for the discovery of a great range of functional DNAs over the last 20 years, with excellent ability in both target recognition and enzymatic catalysis. Functional DNAs have shown great potential to serve as target recognition elements and replace antibodies in biosensor development. The substantial development in functional DNA-based colorimetric biosensors, as spotlighted in this chapter, further validates the idea that functional DNAs can be easily integrated with various colorimetric signal transduction elements, such as AuNPs, HRP, and organic dyes, to achieve practically useful applications.

1.5 Thesis objective and outline

C. difficile has emerged as an important gut pathogen that accounts for thousands of infections and deaths around the world annually. Early and accurate detection of *C. difficile,* especially epidemic strains of *C. difficile* is of great importance for disease management and infection control. Many current detection strategies confront several technical and cost limitations. One technology that has the potential to overcome the gap is functional DNA based biosensor. The objective of this thesis aims to 1) investigate the use of functional DNA in *C. difficile* detection; 2) construct colorimetric biosensors for *C. difficile*. Below I will outline the coverage of the thesis chapter by chapter.

Chapter 2: A colorimetric biosensing platform based on rolling circle amplification and urease-mediated litmus test. In this chapter, we constructed a colorimetric detection platform that can be coupled with functional DNA molecules to detect different targets.

Previously, our group has validated that urease can be coupled with RNA-cleaving DNAzymes for biosensing. Here we will demonstrate that urease can also work with aptamers and RCA to achieve visual detection of different targets with high sensitivity. This novel platform has the potential to be applied to any targets for which an aptamer can be created, including *C. difficile*.

Chapter 3: Detecting epidemic strains of *Clostridium difficile* using PCR and urease-mediated litmus test. PCR has become a widely adopted technique in clinical laboratories. However, the lack of simple yet effective signal transduction mechanisms that permit detection of PCR products without the use of expensive equipment (such as real-time PCR machine) and complicated processes (such as DNA separation by gel electrophoresis) is one of the barriers that prevent PCR from becoming a popular point-of-care field tool. To address this issue, in this chapter, we will expand the use of urease-mediated litmus test to PCR products. This strategy will be applied for the detection of two hypervirulent strains of C. *difficile* that are responsible for the recent increase in the global incidence and severity of *C. difficile* infections. The viability of this test for diagnostic applications will also be demonstrated using clinically validated stool samples from *C. difficile* infected patients.

Chapter 4: Isolation of RNA-cleaving fluorogenic aptazymes for identification of epidemic strains of *C. difficile*. In early efforts, our group has isolated an RNA-cleaving fluorogenic aptazyme (RFA13-1) targeting *C. difficile* BI/027-H that is isolated from a CDI patient in Hamilton. However, further studies indicated that *C. difficile* BI/027-H is not the

epidemic strain BI/027/NAP1 despite the same REA type and ribotype. As a result, in this chapter, we aim to isolate RFAs targeting the epidemic strain of *C. difficile* (BI/027/NAP1).

Chapter 5: RFA 13-1, an unintentionally isolated RNase I-cleaving fluorogenic DNA probe. In one attempt of isolating RFAs for *C. difficile*, the glycerol stock of *C. difficile* used for *in vitro* selection was contaminated by another bacterium, leading to the isolation of an RNase I-cleaving fluorogenic probe, RFA13-1. Despite the unexpected result, RFA13-1 may serve as a useful probe for RNase I or RNase I-containing bacteria as it exhibited high sensitivity and was able to detect as low as 5 pM of RNase I. It also presented great specificity as it only responds to specific types of RNase I expressed in *Enterobacteriaceae* bacteria. This story will be shared in this chapter.

In the final chapter of my thesis, I will summarize the major achievements of this thesis.

1.6 References

1. Wilson, K. H., Sheagren, J. N., Freter, R., Weatherbee, L. & Lyerly, D. Gnotobiotic models for study of the microbial ecology of *Clostridium difficile* and Escherichia coli. *J. Infect. Dis.* **153,** 547–51 (1986).

2. Hall, I. C. & O'Toole, E. Intestinal flora in new-born infants. *Am. J. Dis. Child.* **49,** 390 (1935).

3. Ünal, C. M., Steinert, M. & Steinert, M. Expert Opinion on Therapeutic Targets Novel therapeutic strategies for *Clostridium difficile* infections Novel therapeutic strategies for *Clostridium difficile* infections. **8222,** (2016).

4. Lusk, R. H. *et al.* Clindamycin-induced enterocolitis in hamsters. *J. Infect. Dis.* **137,** 464–475 (1978).

5. Rupnik, M., Wilcox, M. H. & Gerding, D. N. *Clostridium difficile* infection : new developments in epidemiology and pathogenesis. **7,** (2009).

6. Rupnik, M. Is *Clostridium difficile*-associated infection a potentially zoonotic and foodborne disease? *Clin. Microbiol. Infect.* **13,** 457–459 (2007).

7. Sorg, J. A. & Sonenshein, A. L. Bile Salts and Glycine as Cogerminants for *Clostridium difficile* Spores. *J. Bacteriol.* **190,** 2505–2512 (2008).

8. Britton, R. A. & Young, V. B. Interaction between the intestinal microbiota and host in *Clostridium difficile* colonization resistance. *Trends Microbiol.* **20,** 313–319 (2012).

9. Thelestam, M. & Chaves-Olarte, E. Cytotoxic effects of the *Clostridium difficile* toxins. *Curr Top Microbiol Immunol* **250,** 85–96 (2000).

10.   Braun, V., Hundsberger, T., Leukel, P., Sauerborn, M. & Von Eichel-Streiber, C. Definition of the single integration site of the pathogenicity locus in *Clostridium difficile*. *Gene* **181,** 29–38 (1996).

11.   Lee, C. H. *et al.* Frozen vs Fresh Fecal Microbiota Transplantation and Clinical Resolution of Diarrhea in Patients With Recurrent *Clostridium difficile* Infection. *JAMA* **315,** 142 (2016).

12.   Jank, T., Giesemann, T. & Aktories, K. Rho-glucosylating *Clostridium difficile* toxins A and B: New insights into structure and function. *Glycobiology* **17,** (2007).

13.   Pothoulakis, C. Effects of *Clostridium difficile* toxins on epithelial cell barrier. *Ann N Y Acad Sci* **915,** 347–356 (2000).

14.   Mani, N. & Dupuy, B. Regulation of toxin synthesis in *Clostridium difficile* by an alternative RNA polymerase sigma factor. **98,** (2001).

15.   Matamouros, S., England, P. & Dupuy, B. *Clostridium difficile* toxin expression is inhibited by the novel regulator TcdC. *Mol. Microbiol.* **64,** 1274–1288 (2007).

16.   Tan, K. S., Wee, B. Y. & Song, K. P. Evidence for holin function of tcdE gene in the pathogenicity of *Clostridium difficile*. *J. Med. Microbiol.* **50,** 613–9 (2001).

17.   Braun, V., Hundsberger, T., Leukel, P., Sauerborn, M. & von Eichel-Streiber, C. Definition of the single integration site of the pathogenicity locus in *Clostridium difficile*. *Gene* **181,** 29–38 (1996).

18.   Abou Chakra, C. N., Pepin, J., Sirard, S. & Valiquette, L. Risk Factors for Recurrence, Complications and Mortality in *Clostridium difficile* Infection: A Systematic Review. *PLoS One* **9,** e98400 (2014).

19. Walker, A. S. *et al.* Relationship Between Bacterial Strain Type, Host Biomarkers, and Mortality in *Clostridium difficile* Infection. *Clin. Infect. Dis.* **56,** 1589–1600 (2013).

20. Rousseau, C. *et al. Clostridium difficile* Carriage in Healthy Infants in the Community: A Potential Reservoir for Pathogenic Strains. *Clin. Infect. Dis.* **55,** 1209–1215 (2012).

21. Stoesser, N. *et al.* Molecular epidemiology of *Clostridium difficile* strains in children compared with that of strains circulating in adults with *Clostridium difficile-*associated infection. *J. Clin. Microbiol.* **49,** 3994–6 (2011).

22. Zacharioudakis, I. M., Zervou, F. N., Pliakos, E. E., Ziakas, P. D. & Mylonakis, E. Colonization With Toxinogenic *C. difficile* Upon Hospital Admission and Risk of Infection: A Systematic Review and Meta-Analysis. *Am. J. Gastroenterol.* **110,** 381–390 (2015).

23. McFarland, L. V., Mulligan, M. E., Kwok, R. Y. Y. & Stamm, W. E. Nosocomial Acquisition of *Clostridium difficile* Infection. *N. Engl. J. Med.* **320,** 204–210 (1989).

24. Curry, S. R. *et al.* Use of Multilocus Variable Number of Tandem Repeats Analysis Genotyping to Determine the Role of Asymptomatic Carriers in *Clostridium difficile* Transmission. *Clin. Infect. Dis.* **57,** 1094–1102 (2013).

25. Clabots, C. R., Johnson, S., Olson, M. M., Peterson, L. R. & Gerding, D. N. Acquisition of *Clostridium difficile* by hospitalized patients: evidence for colonized new admissions as a source of infection. *J. Infect. Dis.* **166,** 561–7 (1992).

26. Martin, J. S. H., Monaghan, T. M. & Wilcox, M. H. *Clostridium difficile* infection:

Epidemiology, diagnosis and understanding transmission. *Nat. Rev. Gastroenterol. Hepatol.* **13,** 206–216 (2016).

27.　Kouhsari, E. *et al. Clostridium difficile* infection：a review. *Rev. Med. Microbiol.* **29,** 103–109 (2018).

28.　Davies, K. A. *et al.* Underdiagnosis of *Clostridium difficile* across Europe: The European, multicentre, prospective, biannual, point-prevalence study of *Clostridium difficile* infection in hospitalised patients with diarrhoea (EUCLID). *Lancet Infect. Dis.* **14,** 1208–1219 (2014).

29.　Lessa, F. C. *et al.* Burden of *Clostridium difficile* infection in the United States. *N. Engl. J. Med.* **372,** 825–834 (2015).

30.　Chitnis, A. S. *et al.* Epidemiology of Community-Associated *Clostridium difficile* Infection, 2009 Through 2011. *JAMA Intern. Med.* **173,** 1359 (2013).

31.　Khanna, S. *et al.* The Epidemiology of Community-Acquired *Clostridium difficile* Infection: A Population-Based Study. *Am. J. Gastroenterol.* **107,** 89–95 (2012).

32.　Lessa, F. C., Winston, L. G., McDonald, L. C. & Emerging Infections Program *C. difficile* Surveillance Team. Burden of *Clostridium difficile* Infection in the United States. *N. Engl. J. Med.* **372,** 2368–2370 (2015).

33.　Freeman, J. *et al.* The changing epidemiology of *Clostridium difficile* infections. *Clin. Microbiol. Rev.* **23,** 529–49 (2010).

34.　He, M. *et al.* Emergence and global spread of epidemic healthcare-associated *Clostridium difficile*. *Nat. Genet.* **45,** 109–13 (2013).

35.　McDonald, L. C. *et al.* An epidemic, toxin gene-variant strain of *Clostridium difficile*.

N. Engl. J. Med. **353,** 2433–41 (2005).

36.   Vedantam, G. *et al. Clostridium difficile* infection: toxins and non-toxin virulence factors, and their contributions to disease establishment and host response. *Gut Microbes* **3,** 121–34 (2012).

37.   Pépin, J., Valiquette, L. & Cossette, B. Mortality attributable to nosocomial *Clostridium difficile*-associated disease during an epidemic caused by a hypervirulent strain in Quebec. *CMAJ* **173,** 1037–1041 (2005).

38.   Nap, B. I. Association of Relapse of *Clostridium difficile* Disease with. **50,** 4078–4082 (2012).

39.   Pépin, J., Valiquette, L., Gagnon, S., Routhier, S. & Brazeau, I. Outcomes of *Clostridium difficile*-Associated Disease Treated With Metronidazole or Vancomycin Before and After the Emergence of NAP1/027. *Am. J. Gastroenterol.* **102,** 2781–2788 (2007).

40.   Rohlke, F. & Stollman, N. Fecal microbiota transplantation in relapsing *Clostridium difficile* infection. *Therap. Adv. Gastroenterol.* **5,** 403–20 (2012).

41.   Ahmetagic, S. *et al. Clostridium Difficile* Infection in Hospitalized Patients at University Clinical Center Tuzla, Bosnia and Herzegovina: a 4 Year Experience. *Mater. Socio Medica* **25,** 153 (2013).

42.   Tenover, F. C. *et al.* Comparison of Strain Typing Results for *Clostridium difficile* Isolates from North America. *J. Clin. Microbiol.* **49,** 1831–1837 (2011).

43.   Lim, S. K. *et al.* Emergence of a Ribotype 244 Strain of *Clostridium difficile* Associated With Severe Disease and Related to the Epidemic Ribotype 027 Strain.

Clin. Infect. Dis. **58,** 1723–1730 (2014).

44.   Collins, D. A., Hawkey, P. M. & Riley, T. V. Epidemiology of *Clostridium difficile* infection in Asia. *Antimicrob. Resist. Infect. Control* **2,** 21 (2013).

45.   Peng, Z. *et al.* Advances in the diagnosis and treatment of *Clostridium difficile* infections. *Emerg. Microbes Infect.* **7,** 15 (2018).

46.   Planche, T. D. *et al.* Differences in outcome according to *Clostridium difficile* testing method: a prospective multicentre diagnostic validation study of *C. difficile* infection. *Lancet. Infect. Dis.* **13,** 936–45 (2013).

47.   Khan, F. Y. & Elzouki, A. N. *Clostridium difficile* infection: A review of the literature. *Asian Pac. J. Trop. Med.* **7,** S6–S13 (2014).

48.   Surawicz, C. M. *et al.* Guidelines for diagnosis, treatment, and prevention of *Clostridium difficile* infections. *Am. J. Gastroenterol.* **108,** 478–98; quiz 499 (2013).

49.   Jensen, M. B. F. *et al.* Diagnosis of *Clostridium difficile*: real-time PCR detection of toxin genes in faecal samples is more sensitive compared to toxigenic culture. *Eur. J. Clin. Microbiol. Infect. Dis.* **34,** 727–736 (2015).

50.   Norén, T., Alriksson, I., Andersson, J., Åkerlund, T. & Unemo, M. Rapid and sensitive loop-mediated isothermal amplification test for *Clostridium difficile* detection challenges cytotoxin B cell test and culture as gold standard. *J. Clin. Microbiol.* **49,** 710–711 (2011).

51.   Longtin, Y. *et al.* Impact of the type of diagnostic assay on *Clostridium difficile* infection and complication rates in a mandatory reporting program. *Clin. Infect. Dis.* **56,** 67–73 (2013).

52.   Polage, C. R. *et al.* Overdiagnosis of *Clostridium difficile* Infection in the Molecular

       Test Era. *JAMA Intern. Med.* **175,** 1792 (2015).

53.   Crobach, M. J. T., Dekkers, O. M., Wilcox, M. H. & Kuijper, E. J. European Society

       of Clinical Microbiology and Infectious Diseases (ESCMID): Data review and

       recommendations for diagnosing *Clostridium difficile*-infection (CDI). *Clin.*

       Microbiol. Infect. **15,** 1053–1066 (2009).

54.   Cohen, S. H. *et al.* Clinical Practice Guidelines for *Clostridium difficile* Infection in

       Adults: 2010 Update by the Society for Healthcare Epidemiology of America

       (SHEA) and the Infectious Diseases Society of America (IDSA). *Infect. Control*

       Hosp. Epidemiol. **31,** 431–455 (2010).

55.   Wilcox, M. H., Hawkey, P. M., Patel, B., Planche, T. & Stone, S. Updated guidance

       on the management and treatment of *Clostridium difficile* infection. *Public Heal.*

       Engl. 1–29 (2013).

56.   Alcalá, L. *et al.* Laboratory diagnosis of *Clostridium difficile* infection in Spain: a

       population-based survey. *J. Hosp. Infect.* **79,** 13–17 (2011).

57.   Turner, A. P. F., Karube, I. & Wilson, G. S. *Biosensors : fundamentals and*

       applications. (Oxford University Press, 1987).

58.   Turner, A. P. F. Biosensors: sense and sensibility. *Chem. Soc. Rev.* **42,** 3184 (2013).

59.   Wang, J. Glucose Biosensors: 40 Years of Advances and Challenges. *Sensors Updat.*

       10, 107–119 (2002).

60.   Campàs, M., Carpentier, R. & Rouillon, R. Plant tissue-and photosynthesis-based

       biosensors. *Biotechnol. Adv.* **26,** 370–378 (2008).

61.   Bousse, L. Whole cell biosensors. *Sensors Actuators B Chem.* **34,** 270–275 (1996).

62.   Wang, J. Electrochemical nucleic acid biosensors. *Anal. Chim. Acta* **469,** 63–71 (2002).

63.   Savory, N. *et al.* In silico maturation of binding-specificity of DNA aptamers against *Proteus mirabilis. Biotechnol. Bioeng.* **110,** 2573–2580 (2013).

64.   Wang, J., Jiang, Y., Zhou, C. & Fang, X. Aptamer-based ATP assay using a luminescent light switching complex. *Anal. Chem.* **77,** 3542–6 (2005).

65.   Stojanovic, M. N., de Prada, P. & Landry, D. W. Aptamer-Based Folding Fluorescent Sensor for Cocaine. *J. Am. Chem. Soc.* **123,** 4928–4931 (2001).

66.   Stojanovic, M. N. & Landry, D. W. Aptamer-Based Colorimetric Probe for Cocaine. *J. Am. Chem. Soc.* **124,** 9678–9679 (2002).

67.   Luong, J. H. T., Male, K. B. & Glennon, J. D. Biosensor technology: Technology push versus market pull. *Biotechnol. Adv.* **26,** 492–500 (2008).

68.   Chang, D. *et al.* Integrating deoxyribozymes into colorimetric sensing platforms. *Sensors (Switzerland)* **16,** (2016).

69.   Gysbers, R., Tram, K. Manochehry, S. Chang, D.& Li, Y. *Selection and Application of Catalytically Active Oligonucleotides*. **2,** (2016).

70.   Liu, J., Cao, Z. & Lu, Y. *Functional Nucleic Acid Sensors Functional Nucleic Acid Sensors*. **109,** (2009).

71.   Liu, M., Chang, D. & Li, Y. Discovery and Biosensing Applications of Diverse RNA-Cleaving DNAzymes. *Acc. Chem. Res.* **50,** 2273–2283 (2017).

72.   Silverman, S. K. Artificial Functional Nucleic Acids: Aptamers, Ribozymes, and

Deoxyribozymes Identified by *In Vitro* Selection. *Funct. Nucleic Acids Anal. Appl.* 47–108 (2009).

73. Silverman, S. K. Catalytic DNA: Scope, Applications, and Biochemistry of Deoxyribozymes. *Trends Biochem. Sci.* **41,** 595–609 (2016).

74. Li, Y. & Breaker, R. R. Kinetics of RNA Degradation by Specific Base Catalysis of Transesterification Involving the 2'-Hydroxyl Group. *J. Am. Chem. Soc.* **121,** 5364–5372 (1999).

75. Breaker, R. R. & Joyce, G. F. A DNA enzyme that cleaves RNA. *Chem. Biol.* **1,** 223–9 (1994).

76. Flynn-Charlebois, A. *et al.* Deoxyribozymes with 2'−5' RNA Ligase Activity. *J. Am. Chem. Soc.* **125,** 2444–2454 (2003).

77. Wang, Y. & Silverman, S. K. Deoxyribozymes that synthesize branched and lariat RNA. *J. Am. Chem. Soc.* **125,** 6880–1 (2003).

78. Li, Y., Liu, Y. & Breaker, R. R. Capping DNA with DNA. *Biochemistry* **39,** 3106–3114 (2000).

79. Chandrasekar, J. & Silverman, S. K. Catalytic DNA with phosphatase activity. *Proc. Natl. Acad. Sci.* **110,** 5315–5320 (2013).

80. Zhou, W., Saran, R. & Liu, J. Metal Sensing by DNA. *Chem. Rev.* **117,** 8272–8325 (2017).

81. Mok, W. & Li, Y. Recent progress in nucleic acid aptamer-based biosensors and bioassays. *Sensors* **8,** 7050–7084 (2008).

82. Brody, E. N. *et al.* The use of aptamers in large arrays for molecular diagnostics.

Mol. Diagn. **4,** 381–8 (1999).

83. Famulok, M. Allosteric aptamers and aptazymes as probes for screening approaches. *Curr. Opin. Mol. Ther.* **7,** 137–43 (2005).

84. Ellington, a D. & Szostak, J. W. *In vitro* selection of RNA molecules that bind specific ligands. *Nature* **346,** 818–22 (1990).

85. Tuerk, C. & Gold, L. Systematic Evolution of Ligands By Exponential Enrichment - Rna Ligands To Bacteriophage-T4 DNA-Polymerase. *Science* **249,** 505–510 (1990).

86. Zhang, W., Feng, Q., Chang, D., Tram, K. & Li, Y. *In vitro* selection of RNA-cleaving DNAzymes for bacterial detection. *Methods* **106,** 66–75 (2016).

87. Cao, X. *et al.* Combining use of a panel of ssDNA aptamers in the detection of Staphylococcus aureus. *Nucleic Acids Res.* **37,** 4621–8 (2009).

88. Peng, Z., Ling, M., Ning, Y. & Deng, L. Rapid Fluorescent Detection of Escherichia coli K88 Based on DNA Aptamer Library as Direct and Specific Reporter Combined With Immuno-Magnetic Separation. *J. Fluoresc.* **24,** 1159–1168 (2014).

89. Duan, N. *et al.* Selection and Characterization of Aptamers against Salmonella typhimurium Using Whole-Bacterium Systemic Evolution of Ligands by Exponential Enrichment (SELEX). *J. Agric. Food Chem.* **61,** 3229–3234 (2013).

90. Kolovskaya, O. S. *et al.* Development of Bacteriostatic DNA Aptamers for Salmonella. *J. Med. Chem.* **56,** 1564–1572 (2013).

91. Duan, N., Wu, S., Chen, X., Huang, Y. & Wang, Z. Selection and Identification of a DNA Aptamer Targeted to Vibrio parahemolyticus. *J. Agric. Food Chem.* **60,**

4034–4038 (2012).

92.   Tang, X., Zheng, J., Yan, Q., Li, Z. & Li, Y. Selection of aptamers against inactive

Vibrio alginolyticus and application in a qualitative detection assay. *Biotechnol. Lett.*

35, 909–914 (2013).

93.   Duan, N. *et al.* Selection, identification and application of a DNA aptamer against

Listeria monocytogenes. *Food Control* **33,** 239–243 (2013).

94.   Duan, N. *et al. In vitro* selection of a DNA aptamer targeted against Shigella

dysenteriae. *J. Microbiol. Methods* **94,** 170–174 (2013).

95.   Hamula, C. L. A., Le, X. C. & Li, X.-F. DNA Aptamers Binding to Multiple

Prevalent M-Types of *Streptococcus pyogenes*. *Anal. Chem.* **83,** 3640–3647 (2011).

96.   Dwivedi, H. P., Smiley, R. D. & Jaykus, L.-A. Selection and characterization of

DNA aptamers with binding selectivity to Campylobacter jejuni using whole-cell

SELEX. *Appl. Microbiol. Biotechnol.* **87,** 2323–2334 (2010).

97.   Ochsner, U. A., Katilius, E. & Janjic, N. Detection of *Clostridium difficile* toxins A,

B and binary toxin with slow off-rate modified aptamers. *Diagn. Microbiol. Infect.*

Dis. **76,** 278–285 (2013).

98.   Liu, M., Yin, Q., Brennan, J. D. & Li, Y. Selection and characterization of DNA

aptamers for detection of glutamate dehydrogenase from *Clostridium difficile*.

Biochimie **145,** 151–157 (2018).

99.   Bruno, J. G. & Kiel, J. L. Use of Magnetic Beads in Selection and Detection of

Biotoxin Aptamers by Electrochemiluminescence and Enzymatic Methods.

Biotechniques **32,** 178–183 (2002).

100. Huang, Y. *et al.* Selection and characterization of DNA aptamers against Staphylococcus aureus enterotoxin C1. *Food Chem.* **166,** 623–9 (2015).

101. Ochsner, U. A., Green, L. S., Gold, L. & Janjic, N. Systematic selection of modified aptamer pairs for diagnostic sandwich assays. *Biotechniques* **56,** (2014).

102. Hong, K. L., Maher, E., Williams, R. M. & Sooter, L. J. *In Vitro* Selection of a Single-Stranded DNA Molecular Recognition Element against *Clostridium difficile* Toxin B and Sensitive Detection in Human Fecal Matter. *J. Nucleic Acids* **2015,** 1–12 (2015).

103. Tang, X.-L. *et al.* CFP10 and ESAT6 aptamers as effective Mycobacterial antigen diagnostic reagents. *J. Infect.* **69,** 569–580 (2014).

104. Cella, L. N. *et al.* Nano Aptasensor for Protective Antigen Toxin of Anthrax. *Anal. Chem.* **82,** 2042–2047 (2010).

105. Tok, J. B.-H. & Fischer, N. O. Single microbead SELEX for efficient ssDNA aptamer generation against botulinum neurotoxin. *Chem. Commun.* **0,** 1883 (2008).

106. Qian, J., Lou, X., Zhang, Y., Xiao, Y. & Soh, H. T. Generation of Highly Specific Aptamers via Micromagnetic Selection. *Anal. Chem.* **81,** 5490–5495 (2009).

107. Elshafey, R., Siaj, M. & Zourob, M. *In Vitro* Selection, Characterization, and Biosensing Application of High-Affinity Cylindrospermopsin-Targeting Aptamers. *Anal. Chem.* **86,** 9196–9203 (2014).

108. Shen, Z. *et al.* A Catalytic DNA Activated by a Specific Strain of Bacterial Pathogen. *Angew. Chem. Int. Ed. Engl.* **55,** 2431–4 (2016).

109. Ali, M. M., Aguirre, S. D., Lazim, H. & Li, Y. Fluorogenic DNAzyme Probes as

Bacterial Indicators. *Angew. Chemie Int. Ed.* **50,** 3751–3754 (2011).

110. Daniel, M.-C. & Astruc, D. Gold nanoparticles: assembly, supramolecular chemistry, quantum-size-related properties, and applications toward biology, catalysis, and nanotechnology. *Chem. Rev.* **104,** 293–346 (2004).

111. Rechberger, W. *et al.* Optical properties of two interacting gold nanoparticles. *Opt. Commun.* **220,** 137–141 (2003).

112. Storhoff, J. J. *et al.* What Controls the Optical Properties of DNA-Linked Gold Nanoparticle Assemblies? *J. Am. Chem. Soc.* **122,** 4640–4650 (2000).

113. Verwey, E. Theory of the stability of lyophobic colloids: the interaction of sol particles having an electric double layer. (1962).

114. Xiang, Y., Wu, P., Tan, L. H. & Lu, Y. DNAzyme-functionalized gold nanoparticles for biosensing. *Adv. Biochem. Eng. Biotechnol.* **140,** 93–120 (2014).

115. Turkevich, J., Stevenson, P. C. & Hillier, J. A study of the nucleation and growth processes in the synthesis of colloidal gold. *Discuss. Faraday Soc.* **11,** 55 (1951).

116. Manson, J., Kumar, D., Meenan, B. J. & Dixon, D. Polyethylene glycol functionalized gold nanoparticles: the influence of capping density on stability in various media. *Gold Bull.* **44,** 99–105 (2011).

117. Glomm, W. R. Functionalized Gold Nanoparticles for Applications in Bionanotechnology. *J. Dispers. Sci. Technol.* **26,** 389–414 (2005).

118. Häkkinen, H. The gold–sulfur interface at the nanoscale. *Nat. Chem.* **4,** 443–455 (2012).

119. Hunter, R. Foundations of colloid science. (2001).

120. Napper, D. Polymeric stabilization of colloidal dispersions. (1983).

121. Kim, H. K. *et al.* Metal-dependent global folding and activity of the 8-17 DNAzyme studied by fluorescence resonance energy transfer. *J. Am. Chem. Soc.* **129,** 6896–6902 (2007).

122. Elghanian, R., Storhoff, J. J., Mucic, R. C., Letsinger, R. L. & Mirkin, C. A. Selective colorimetric detection of polynucleotides based on the distance-dependent optical properties of gold nanoparticles. *Science* **277,** 1078–81 (1997).

123. Park, J., Joo, J., Kwon, S. G., Jang, Y. & Hyeon, T. Synthesis of Monodisperse Spherical Nanocrystals. *Angew. Chemie Int. Ed.* **46,** 4630–4660 (2007).

124. Jadzinsky, P. D., Calero, G., Ackerson, C. J., Bushnell, D. A. & Kornberg, R. D. Structure of a thiol monolayer-protected gold nanoparticle at 1.1 A resolution. *Science* **318,** 430–3 (2007).

125. Hakkinen, H. The gold-sulfur interface at the nanoscale. Nat Chem 4 (6): 443–455. (2012).

126. Li & Rothberg, L. J. Label-Free Colorimetric Detection of Specific Sequences in Genomic DNA Amplified by the Polymerase Chain Reaction. *J. Am. Chem. Soc.* **126,** 10958–10961 (2004).

127. Wang, Z., Lee, J. H. & Lu, Y. Label-Free Colorimetric Detection of Lead Ions with a Nanomolar Detection Limit and Tunable Dynamic Range by using Gold Nanoparticles and DNAzyme. *Adv. Mater.* **20,** 3263–3267 (2008).

128. Wei, H., Li, B., Li, J., Dong, S. & Wang, E. DNAzyme-based colorimetric sensing of lead (Pb $^{2+}$) using unmodified gold nanoparticle probes. *Nanotechnology* **19,**

095501 (2008).

129. Liu, J. & Lu, Y. Colorimetric Cu2+ detection with a ligation DNAzyme and nanoparticles. *Chem. Commun.* 4872 (2007).

130. Liu, J. & Lu, Y. A Colorimetric Lead Biosensor Using DNAzyme-Directed Assembly of Gold Nanoparticles. *J. Am. Chem. Soc.* **125,** 6642–6643 (2003).

131. Liu, J., Lu, Y., About, M. & Article, T. Accelerated Color Change of Gold Nanoparticles Assembled by DNAzymes for Simple and Fast Colorimetric Pb Detection. *ACS Publ.* 12298–12305 (2004).

132. Lee, J. H., Wang, Z. D., Liu, J. W. & Lu, Y. Highly Sensitive and Selective Colorimetric Sensors for Uranyl (UO22+): Development and Comparison of Labeled and Label-Free DNAzyme-Gold Nanoparticle Systems. *J. Am. Chem. Soc.* **130,** 14217–14226 (2008).

133. Liu, J. & Lu, Y. Adenosine-Dependent Assembly of Aptazyme-Functionalized Gold Nanoparticles and Its Application as a Colorimetric Biosensor. *Anal. Chem.* **76,** 1627–1632 (2004).

134. Zagorovsky, K. & Chan, W. C. W. A Plasmonic DNAzyme Strategy for Point-of-Care Genetic Detection of Infectious Pathogens. *Angew. Chemie Int. Ed.* **52,** 3168–3171 (2013).

135. Li, C., Wei, L., Liu, X., Lei, L. & Li, G. Ultrasensitive detection of lead ion based on target induced assembly of DNAzyme modified gold nanoparticle and graphene oxide. *Anal.Chim.Acta* **831,** 60–64 (2014).

136. Yin, B. C., Ye, B. C., Wang, H., Zhu, Z. & Tan, W. Colorimetric logic gates based

on aptamer-crosslinked hydrogels. *Chem. Commun.* **48,** 1248–1250 (2012).

137. Lin, H. *et al.* DNAzyme crosslinked hydrogel: a new platform for visual detection of metal ions. *Chem. Commun.* **47,** 9312 (2011).

138. Huang, Y. *et al.* Target-Responsive DNAzyme Cross-Linked Hydrogel for Visual Quantitative Detection of Lead. *Anal. Chem.* **86,** 11434–11439 (2014).

139. Wang, Z. *et al.* A test strip for lead(II) based on gold nanoparticles multi-functionalized by DNAzyme and barcode DNA. *J. Anal. Chem.* **70,** 339–345 (2015).

140. Hamid, M. & Khalil-ur-Rehman. Potential applications of peroxidases. *Food Chem.* **115,** 1177–1186 (2009).

141. Zhang, H. *et al.* Magnetic beads-based DNAzyme recognition and AuNPs-based enzymatic catalysis amplification for visual detection of trace uranyl ion in aqueous environment. *Biosens. Bioelectron.* **78,** 73–79 (2016).

142. Mir, M., Vreeke, M. & Katakis, I. Different strategies to develop an electrochemical thrombin aptasensor. *Electrochem. commun.* **8,** 505–511 (2006).

143. Sun, L. & Zhao, Q. Competitive horseradish peroxidase-linked aptamer assay for sensitive detection of Aflatoxin B1. *Talanta* **179,** 344–349 (2018).

144. Tram, K., Kanda, P., Salena, B. J., Huan, S. & Li, Y. Translating bacterial detection by DNAzymes into a litmus test. *Angew. Chemie - Int. Ed.* **53,** 12799–12802 (2014).

145. Manochehry, S., McConnell, E. M., Tram, K. Q., Macri, J. & Li, Y. Colorimetric Detection of Uranyl Using a Litmus Test. *Front. Chem.* **6,** 332 (2018).

146. Li, T., Dong, S. & Wang, E. G-Quadruplex Aptamers with Peroxidase-Like DNAzyme Functions: Which Is the Best and How Does it Work? *Chem. - An Asian*

J. **4,** 918–922 (2009).

147. Travascio, P., Bennet, A. J., Wang, D. Y. & Sen, D. A ribozyme and a catalytic DNA with peroxidase activity: active sites versus cofactor-binding sites. *Chem. Biol.* **6,** 779–787 (1999).

148. Travascio, P., Li, Y. & Sen, D. DNA-enhanced peroxidase activity of a DNA aptamer-hemin complex. *Chem. Biol.* **5,** 505–517 (1998).

149. Liu, J. & Lu, Y. Stimuli-responsive disassembly of nanoparticle aggregates for light-up colorimetric sensing. *J. Am. Chem. Soc.* **127,** 12677–12683 (2005).

150. Keniry, M. A. Quadruplex structures in nucleic acids. *Biopolymers* **56,** 123–146 (2000).

151. Xiao, Y. *et al.* Catalytic Beacons for the Detection of DNA and Telomerase Activity. *J. Am. Chem. Soc.* **126,** 7430–7431 (2004).

152. Teller, C., Shimron, S. & Willner, I. Aptamer−DNAzyme Hairpins for Amplified Biosensing. *Anal. Chem.* **81,** 9114–9119 (2009).

153. Liu, F., Zhang, J., Chen, R., Chen, L. & Deng, L. Highly Effective Colorimetric and Visual Detection of ATP by a DNAzyme-Aptamer Sensor. *Chem. Biodivers.* **8,** 311–316 (2011).

154. Mao, K. *et al.* G-quadruplex–hemin DNAzyme molecular beacon probe for the detection of methamphetamine. *RSC Adv.* **6,** 62754–62759 (2016).

155. Yang, C., Lates, V., Prieto-Simón, B., Marty, J. L. & Yang, X. Aptamer-DNAzyme hairpins for biosensing of Ochratoxin A. *Biosens. Bioelectron.* **32,** 208–212 (2012).

156. Jiang, C., Yan, C., Jiang, J. & Yu, R. Colorimetric assay for T4 polynucleotide

kinase activity based on the horseradish peroxidase-mimicking DNAzyme combined with λ exonuclease cleavage. *Anal. Chim. Acta* **766,** 88–93 (2013).

157. Yang, L., Du, F., Chen, G., Yasmeen, A. & Tang, Z. Analytica Chimica Acta A novel colorimetric PCR-based biosensor for detection and quantification of hepatitis B virus. *Anal. Chim. Acta* **840,** 75–81 (2014).

158. Du, F. & Tang, Z. Colorimetric Detection of PCR Product with DNAzymes Induced by 5′-Nuclease Activity of DNA Polymerases. *ChemBioChem* **12,** 43–46 (2011).

159. Elbaz, J., Shlyahovsky, B. & Willner, I. A DNAzyme cascade for the amplified detection of Pb2+ ions or L-histidine. *Chem. Commun.* 1569–1571 (2008).

160. Moshe, M., Elbaz, J. & Willner, I. Sensing of UO_2^{2+} and Design of Logic Gates by the Application of Supramolecular Constructs of Ion-Dependent DNAzymes. *Nano Lett.* **9,** 1196–1200 (2009).

161. Kolpashchikov, D. M. Split DNA Enzyme for Visual Single Nucleotide Polymorphism Typing. *J. Am. Chem. Soc.* **130,** 2934–2935 (2008).

162. Darius, A. K. L., Ling, N. J. & Mahesh, U. Visual detection of DNA from salmonella and mycobacterium using split DNAzymes. *Mol. Biosyst.* **6,** 792–794 (2010).

163. Zhang, L., Zhu, J., Li, T. & Wang, E. Bifunctional Colorimetric Oligonucleotide Probe Based on a G-Quadruplex DNAzyme Molecular Beacon. *Anal. Chem.* **83,** 8871–8876 (2011).

164. Shimron, S., Wang, F., Orbach, R. & Willner, I. Amplified Detection of DNA through the Enzyme-Free Autonomous Assembly of Hemin/G-Quadruplex DNAzyme Nanowires. *Anal. Chem.* **84,** 1042–1048 (2012).

165. Ali, M. M. *et al.* Rolling circle amplification: a versatile tool for chemical biology, materials science and medicine. *Chem. Soc. Rev.* **43,** 3324 (2014).

166. Zhao, Y., Zhou, L. & Tang, Z. Cleavage-based signal amplification of RNA. *Nat. Commun.* **4,** 1493 (2013).

167. Fu, R., Li, T. & Park, H. G. An ultrasensitive DNAzyme-based colorimetric strategy for nucleic acid detection. *Chem. Commun.* 5838–5840 (2009).

168. Luo, R. *et al.* A colorimetric assay method for invA gene of Salmonella using DNAzyme probe self-assembled gold nanoparticles as single tag. *Sensors Actuators B Chem.* **198,** 87–93 (2014).

169. Rao, X. *et al.* Au nanoparticle-DNAzyme dual catalyst system for sensitively colorimetric detection of thrombin. *Chem. Res. Chinese Univ.* **29,** 868–873 (2013).

170. Li, S. *et al.* An ultrasensitive colorimetric aptasensor for ATP based on peptide/Au nanocomposites and hemin-G-quadruplex DNAzyme. *RSC Adv.* **4,** 23185–23190 (2014).

171. Wang, Q., Yang, X., Yang, X., Liu, F. & Wang, K. Visual detection of myoglobin via G-quadruplex DNAzyme functionalized gold nanoparticles-based colorimetric biosensor. *Sensors Actuators B Chem.* **212,** 440–445 (2015).

172. Stojanovic, M. N. & Landry, D. W. Aptamer-based colorimetric probe for cocaine. *J. Am. Chem. Soc.* **124,** 9678–9679 (2002).

173. Ali, M. M. & Li, Y. Colorimetric sensing by using allosteric-DNAzyme-coupled rolling circle amplification and a peptide nucleic acid-organic dye probe. *Angew. Chem. Int. Ed. Engl.* **48,** 3512–5 (2009).

Chapter 2

A Colorimetric Biosensing Platform based on Rolling Circle Amplification and Urease-mediated Litmus Test

2.1 Abstract

We report on a sensitive colorimetric sensing platform that takes advantage of both the strong amplification power of rolling circle amplification (RCA) and the high efficiency of simple urease-mediated litmus test. The presence of the target triggers the RCA reaction, and urease-labelled DNA can be hybridized to the generated RCA products and then immobilized onto magnetic beads. The urease laden beads are then used to hydrolyze urea, leading to the increase of pH that can be detected by a simple litmus test. To demonstrate the versatility, we applied this approach to detect thrombin and platelet-derived growth factor (PDGF) utilizing structure-switching signalling aptamers for target recognition. Furthermore, we demonstrated that the colorimetric sensing platform could be integrated into a simple paper-based device for sensitive DNA detection.

2.2 Introduction

Highly sensitive and easy-to-use biosensors are highly desirable in point-of-care diagnostic applications[1,2]. Standard biosensors, composed of a recognition element and a transduction element, are generally not sensitive enough when the biomarker for a disease exists only at extremely low concentration. Therefore, considerable efforts have been directed towards incorporating a signal amplification element into the biosensor design to enhance the detection sensitivity.

Rolling circle amplification (RCA) is an isothermal DNA replication process that produces extremely long linear single-stranded DNA with thousands of periodic sequences from a circular DNA[3]. The power of this technique is conferred by the strong abilities of Phi29 DNA polymerase: this enzyme can generate more than 70,000 nucleotide additions before its dissociation from the circular template and possesses strong strand displacement ability that can unwind double-stranded DNA without requiring the assistance of DNA helicase[4,5]. Benefiting from its unique DNA synthesis reaction, RCA has been popularly used as a signal amplification element for the development of biosensors[3,6–11]. In order to monitor the RCA process or detect the products, a variety of signal readout techniques have been developed. In particular, colorimetric methods have attracted great attention due to their many distinct advantages, including simplicity and low-cost. For example, gold nanoparticles (AuNPs) can be assembled into RCA products through complementary nucleotides thus allowing colorimetric visualization of the RCA products[12]. In addition to

AuNPs, some intercalating dyes, such as 3,3-diethylthiadicarbocyanine iodide (DiSC2(5)), can be used to generate a colour change when binding to the duplex between RCA products and peptide nucleic acids (PNA)[13]. RCA can also synthesize a significant amount of G-quadruplex horseradish peroxidase-mimicking DNAzymes in situ[14]. Upon binding of hemin, these DNAzymes catalyze chemical reactions that produce coloured products. Despite the progress, a simple and sensitive colorimetric assay for RCA is still in demand due to some major drawbacks of current methods, such as limited chemical stability, time-consuming processes, high background and aqueous solubility of the substrates.

Urease is a highly efficient enzyme that catalyzes the hydrolysis of urea into carbon dioxide and ammonia[15]. The reaction can cause the elevation of the solution pH which can be easily detected using a litmus test. By employing urease as a transducer and an anti-bacteria DNAzyme as a recognition element, we recently developed an approach which adopts the classic litmus test for bacterial detection[16]. Herein, we report a biosensing platform which takes advantage of the strong amplification power of RCA and the robust activity of urease. In using this double-amplification strategy, we are attempting to achieve ultrasensitive detection of the target molecules by the naked eye.

2.3 Results

2.3.1 Principle of the RCA-urease based biosensing platform

The principle of our strategy is illustrated in Figure 2-1. A 5′- biotin-labelled DNA primer (BP) was hybridized to a circular DNA template (CT), triggering the RCA reaction

in the presence of Phi29 DNA polymerase (DP) and dNTPs. Urease-labeled ssDNA (UrD) (with an inverted T at the 3′ end) was also added to the mixture simultaneously. Thus, the RCA products contained hundreds of tandem-repeat sequences that could serve as a template for binding of UrD. Upon magnetic separation through streptavidin-biotin interaction, the free UrD was then washed away and the immobilized urease can be used to hydrolyze urea in the presence of a litmus dye for colour generation. Phenol red was used as a litmus dye as it produced a rather sharp, yellow-to-pink transition.
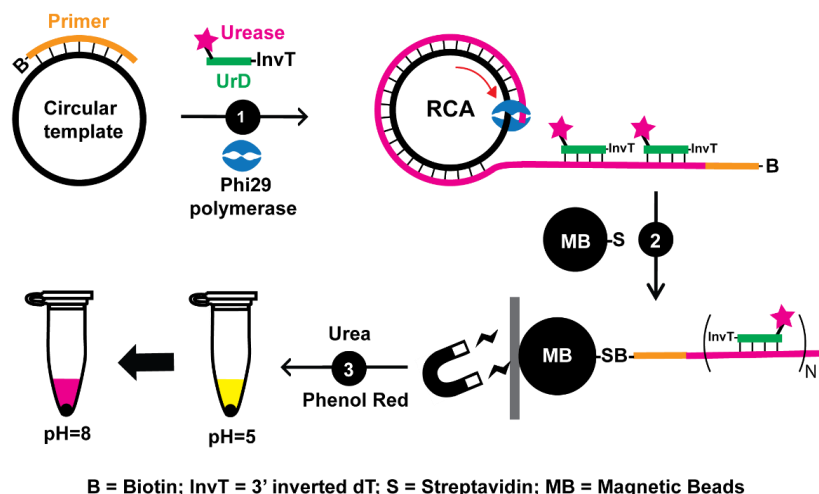
Figure 2-1. Principle of the RCA-urease based sensing platform. (1) RCA reaction. (2) Immobilization of RCA products and urease labelled DNA onto magnetic beads. (3) Litmus test.

We prepared UrD according to previously reported methods[16,17]. To validate our design, we carried out the urease-mediated litmus test for RCA products. As shown in Figure 2-2a, dPAGE analysis indicated that a significant amount of RCA products was produced when BP was incubated with CT with (lane 1) or without UrD (lane 2). After

magnetic separation and washing steps, an intense colour change was observed for the sample containing RCA products and UrD (Figure 2-2b). In contrast, the colour of the reaction mixture without RCA products or urease remained unchanged. These results demonstrate that the urease-mediated litmus test can be used for naked-eye detection of RCA products.
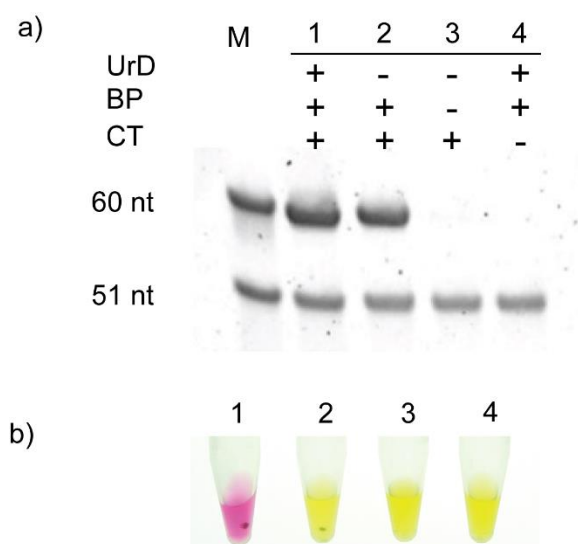
Figure 2-2. Validation of RCA-urease based assay. a) Analysis of digested RCA products by 10% dPAGE. Top band: digested RCA monomer (60 nt). Bottom band: DNA loading control (51 nt). b) Litmus test for the RCA reactions. The photograph was taken at 15 min.

2.3.2 Optimization of the RCA-urease based biosensing platform

To improve the efficiency of the biosensing platform, we first investigated the best timing for introducing UrD into the system. It is interesting to note that a high amount of RCA products can induce the aggregation of magnetic beads after magnetic separation (Figure 2-3a). This observation has been reported previously[18,19]. We found the litmus test

can be largely affected if UrD was introduced following aggregation (Figure 2-3b). This

contributes to a decreased hybridization rate of UrD and aggregated RCA products, which

was confirmed using fluorogenic DNA as a tool to trace the DNA hybridization reaction

(Figure 2-3c). Therefore, we decided to introduce UrD during the RCA reaction in our tests.
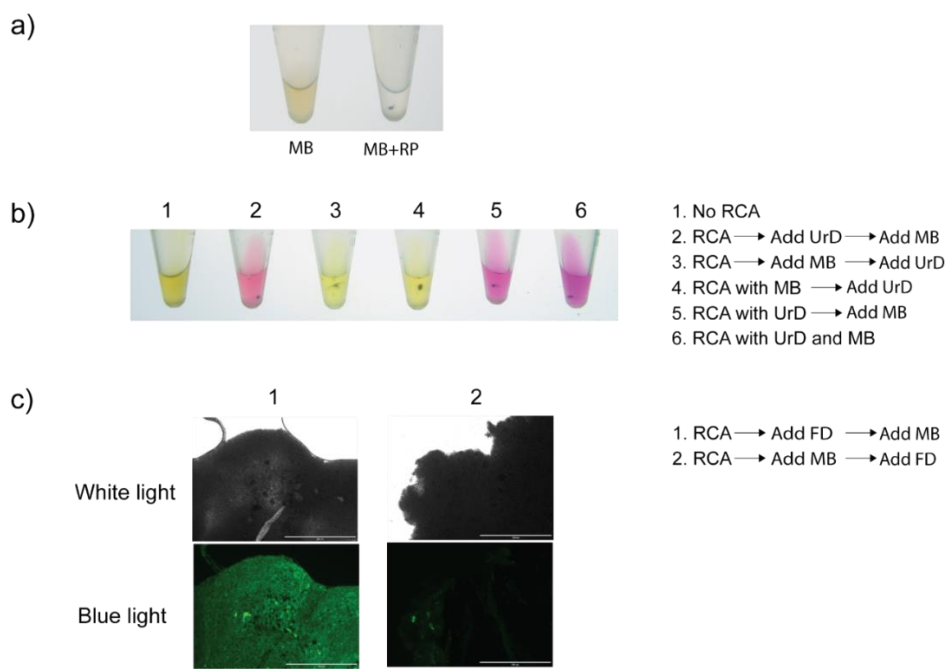
Figure 2-3. Effect of aggregation of magnetic beads on RCA-urease based assay. a) Observation of aggregation of magnetic beads in the presence of high concentration RCA products. b) RCA-litmus test affected by the aggregation of magnetic beads c). Using fluorogenic DNA(FD) as a tool to investigate the effect of magnetic bead aggregation on DNA hybridization. Scale bar is 200 μm.

Although UrD does not contain a biotin modifier, the UrD was found to non-

specifically bind to magnetic beads at high concentrations and increase the background

signal. To prevent the non-specific binding, several blocking reagents were incubated with

magnetic beads for 1 hour before the addition of UrD. After thorough washing of the beads with washing buffer, we performed the litmus test and found 5% skim milk served the best in decreasing the background signal (Figure 2-4a). However, skim milk is known to contain low amounts of biotin which may bind to streptavidin molecules on the MB and prevent immobilization of the RCA products. To investigate whether this is the case, we incubated 5′ biotin-labelled RCA product monomer (RPM, sequence information is listed in Table 2-1) and UrD with skim milk-blocked MB. The results showed that RPM was successfully immobilized on the blocked MB and was able to induce a sharp colour change (Figure 2-4b). As a result, skim milk was employed as a blocking reagent for litmus tests. In addition, we noticed that the background signal could be further decreased by introducing the blocking reagent into not only the blocking step but also the UrD-RPM-MB incubation step (see Figure 2-4b).

Compared to previously developed DNAzyme-mediated litmus tests[16], our design has several distinct advantages. In conventional DNAzyme-mediated litmus tests, the urease molecules are released into the supernatant in the presence of the target, and the litmus test is then applied. In this case, the initial volume and pH of the initial sample can affect later litmus test, leading to a compromised detection sensitivity. In our design, the urease molecules are immobilized onto the MB, allowing for washing steps to remove the initial sample. Thus, the pH and volume of the litmus test are not impacted by the initial sample and the performance (reaction time and detection sensitivity) of the test can be optimized. As shown in Figure 2-4c, we performed the litmus test in the presence of substrate solution containing acetic acid buffer of different pH and found the detection

sensitivity could be improved by elevating the starting pH of the substrate solution from 5 to 6. The reaction volume was also optimized and set to 50 μL to increase the colour-changing rate and reduce the incubation time (see Figure 2-4d).
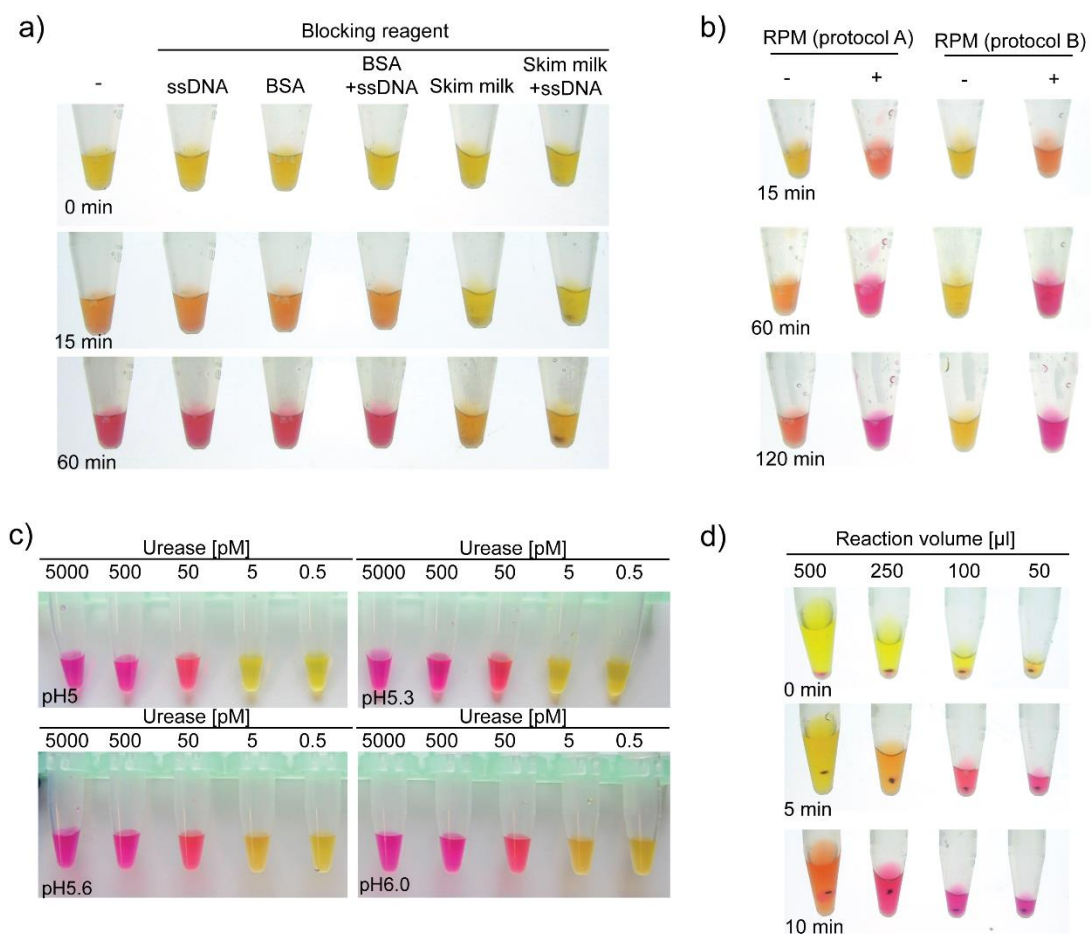
Figure 2-4. Optimization of the RCA-urease based biosensing platform. a) Evaluation of different blocking reagents in decreasing background signal. ssDNA: 20nt single-stranded DNA, 1 μM. BSA: 10% Bovine serum albumins dissolved in binding buffer. Skim milk: 5% skim milk dissolved in binding buffer. b) Litmus test for skim milked blocked MB with/without RPM. Protocol A: 5% skim milk was only used in the blocking step. Protocol B: 5% skim milk was used in both the blocking step and UrD-RPM-MB incubation step. c) Evaluation of the sensitivity of the litmus test using various concentration of urease and

substrate solution with different initial pH. Incubation time: 60 minutes. d) Litmus test with
RCA products in different reaction volumes.

2.3.3 Evaluation of the sensitivity of the RCA-urease based biosensing platform
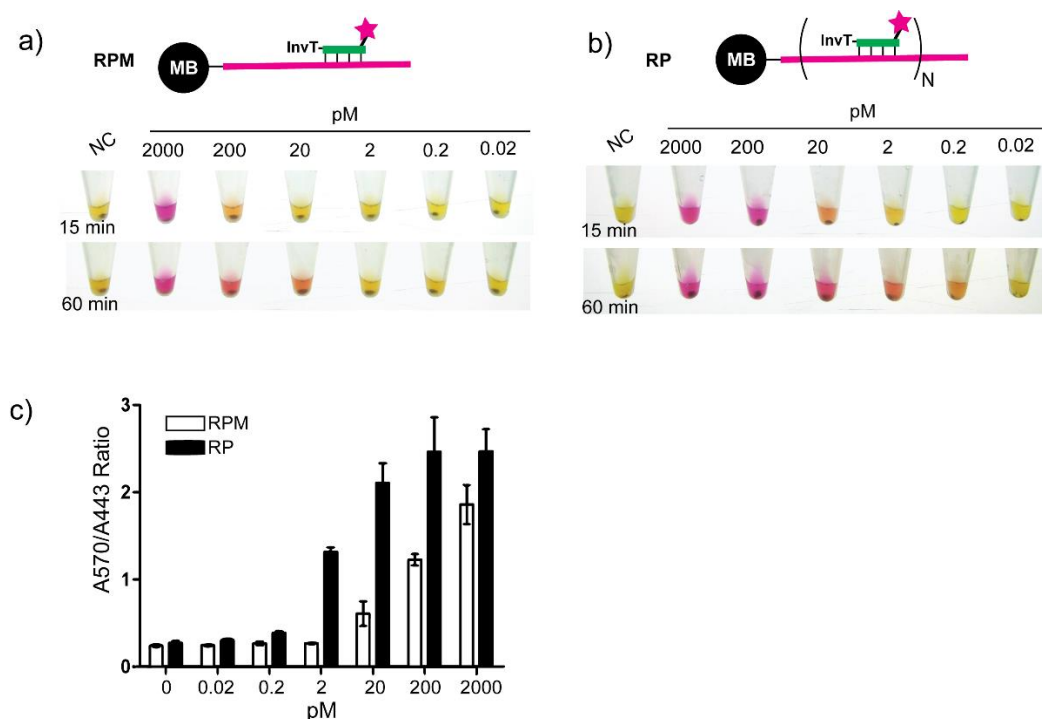
Figure 2-5. Evaluation of the sensitivity of the litmus test with or without RCA. a). Litmus
test for various concentrations of RPM. b) Litmus test for RCA products obtained with
various concentrations of BP as a primer. RCA time is 2 hours. The photograph was taken
after a signal-producing time of 15 minutes and 60 minutes. c). Quantification of the litmus
tests. The litmus reactions were 60 minutes. The absorbance of the reactions at 570 nm and
443 nm (A570 and A443) was measured. A570/A443 was plotted against concentrations
of BP or RPM. Error bars denote standard deviation (n=3).

We then evaluated the sensitivity of the urease-mediated litmus test in detecting

RPM and RCA products. The litmus test was first performed using varying concentrations

of RPM without RCA amplification. As shown in Figure 2-5a, after 60 minutes of colour

development, a subtle colour transition was observed down to 20 pM of RPM. We then

performed litmus tests with decreasing concentration of BP and 2 hours of RCA

amplification (Figure 2-5b). A colour transition was observed at 20 pM of RCA products

after incubation for 15 minutes (top panel). However, a subtle but detectable colour

transition, in comparison to the reference samples (without target), was observed down to

0.2 pM after a colour development of 60 minutes. The sensitivity from this method was

found to be higher than the dPAGE analysis (Figure 2-6). We have also performed

spectroscopic analysis to quantify the detection sensitivity by plotting OD570/OD443 vs

concentration of RCA products and RPM (Figure 2-5c) based on the fact that the colour of

phenol red exhibits a gradual transition from yellow ($\lambda_{max} = 443$ nm) to red ($\lambda_{max} = 570$ nm)

when the pH of a test solution changes from acidic to basic. These tests indicated that the

litmus test with RCA has a sensitivity limit that is ~2 orders of magnitude lower than that

of litmus test without RCA amplification under the same condition, which confirms the

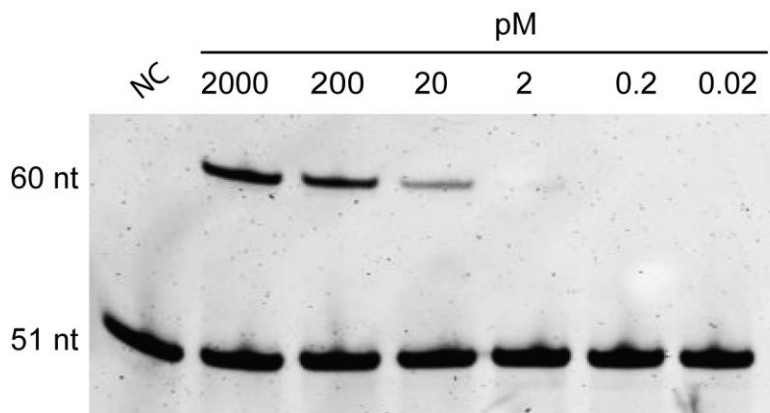strong signal amplification ability of RCA.

Figure 2-6. dPAGE analysis of digested RCA products. The top band: digested RCA monomer (60 nt); the bottom band: DNA loading control (51 nt).

2.3.4 Application 1: Thrombin detection using RCA-urease based biosensing platform

To confirm the general applicability of the RCA-urease based biosensing platform in biomarker detection, we first incorporated the platform into thrombin detection using our previously developed strategy and an anti-thrombin aptamer[20]. The anti-thrombin aptamer used in this study has high affinity (K_d in the range of 25-200 nM) and great specificity and has been widely studied and used for the development of aptamer-based diagnostics[21]. As illustrated in Figure 2-7a, our detection platform features three components: reduced graphene oxide (rGO) as a transducing mediator, an anti-thrombin DNA aptamer as a receptor and UrD as a signal reporter. Initially, the anti-thrombin DNA aptamers are expected to bind onto the rGO surface non-specifically, making them unavailable for the RCA reaction. However, the presence of thrombin will induce the conformational change of the adsorbed DNA aptamers, thus facilitating their release from the rGO surface. The released aptamers can then serve as primers to initiate the RCA reactions and enable a colour response. Using this method, 50 pM of thrombin could be detected with naked eyes or spectroscopic analysis (Figure 2-7b). This detection sensitivity is high enough in monitoring thrombin levels in human blood samples which is within nanomolar range [22]. Control experiments with other proteins, platelet-derived growth factor (PDGF) and bovine serum albumin (BSA), demonstrated that the litmus test was dependent on the matching target for the aptamer, thus indicating the high specificity of this assay (Figure 2-7c).
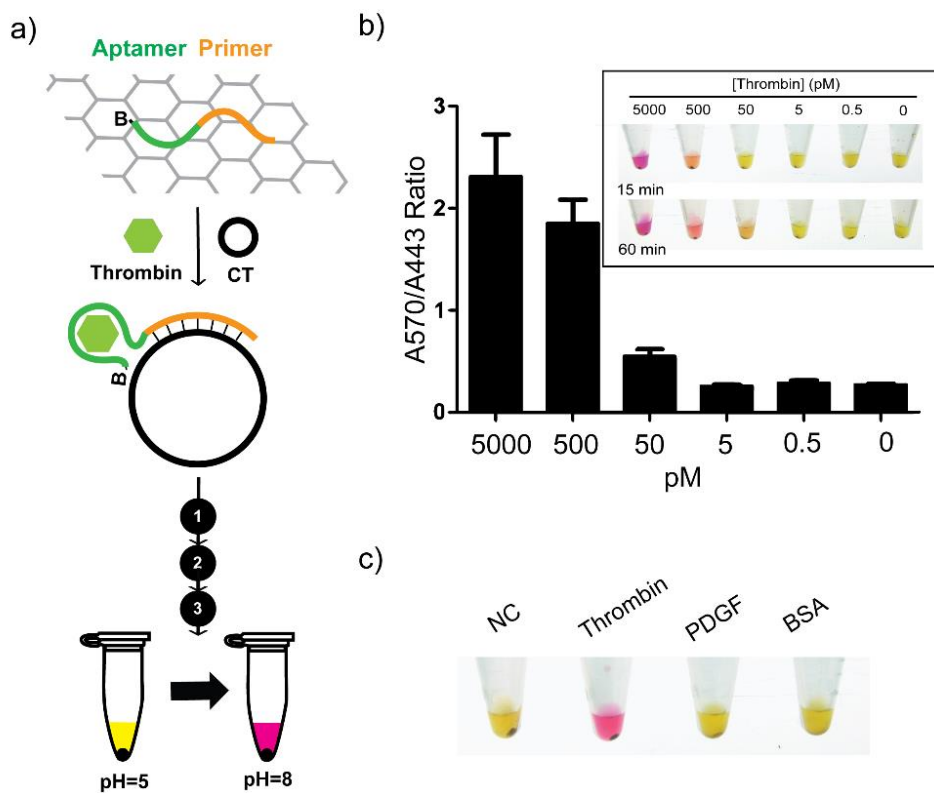
Figure 2-7. RCA-litmus test coupled with anti-thrombin aptamer and graphene for thrombin detection. a) Working principle. Sequence in green: anti-thrombin aptamer; Sequence in orange: RCA primer. (1) RCA reaction. (2) Immobilization of RCA products and urease labelled DNA onto magnetic beads. (3) Litmus test. b) Litmus test for RCA in the presence of different concentrations of thrombin. A570 and A443 were measured after a signal-producing time of 60 minutes. A570/A443 was plotted against concentrations of thrombin. Error bars denote standard deviation (n=3). (C) Litmus test with various protein targets. The photograph was taken after a signal-producing time of 30 minutes.

2.3.5 Application 2: PDGF detection using RCA-urease based biosensing platform

We also applied the RCA-urease based sensing platform for the detection of PDGF, which is a growth factor that plays a significant role in blood vessel formation[23]. It is expressed at low levels in normal cells but is found to be overexpressed in human malignant tumors[24]. As a potential biomarker of cancer diagnosis, a simple and sensitive sensor has been desired. Herein, we developed a novel strategy for the detection of PDGF, which takes advantage of the structure-switching ability of DNA aptamers, the nucleolytic and polymeric function of Phi29 DP, and the litmus test (Figure 2-8a). A functional hairpin probe (HP) was designed and contains an anti-PDGF aptamer sequence (in green) at the 5′ end, a primer sequence (in orange) for RCA in the loop region and a blocking sequence (in grey) at the 3′ end which is complementary to the sequence at the 5′ end. Phi29 DP is known to have the ability to digest single-stranded DNA from the 3′ end[10,25]. The hairpin duplex structure can prevent Phi29 DP from performing the nucleolytic function. However, the presence of PDGF triggers the structure-switching reaction, exposing the 3′ element of HP for nucleolytic trimming. In turn, this converts HP into a mature primer to enable RCA which can then follow with the litmus test.
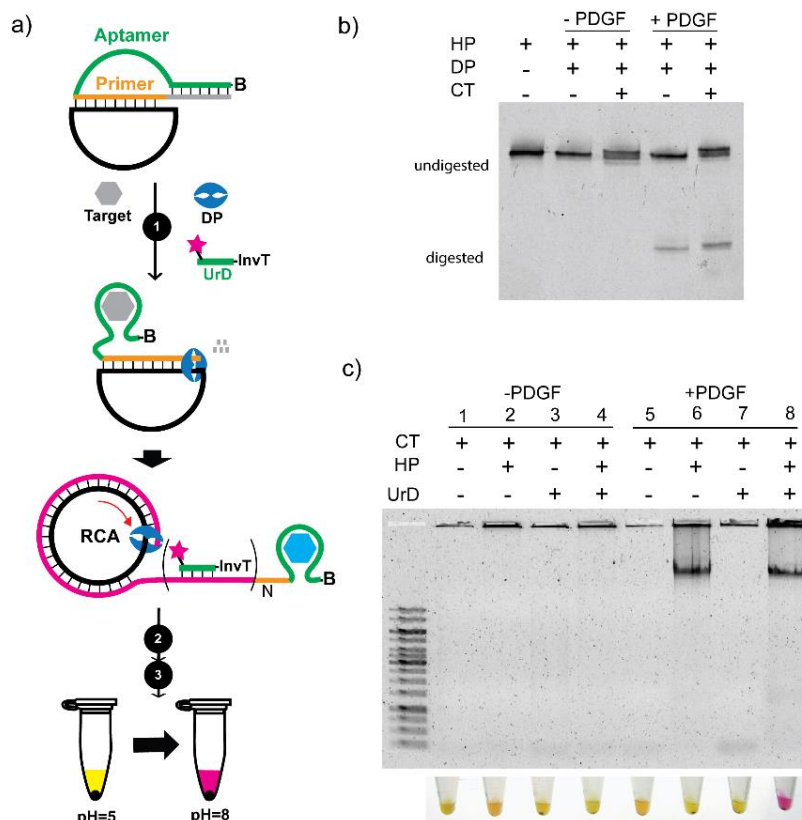
Figure 2-8. Litmus test coupled with anti-PDGF aptamer for PDGF detection. a) Schematic illustration of the litmus test in PDGF detection. (1) RCA reaction. (2) Immobilization of RCA products and urease labelled DNA onto MB. (3) Litmus test. b) Digestion of 20 nM HP with 0.1 U μL^{-1} of Phi29 DP for 30 min in the absence and presence of 20 nM CT or 50 nM PDGF. C) Agarose gel analysis and litmus test of RCA products in RCA reaction containing various combinations of 20 nM HP, 20 nM CT and 20 nM UrD in the absence and presence of 50 nM PDGF. The RCA reaction was 120 minutes. The photograph was taken after a signal-producing time of 60 minutes.

We first assessed the digestion of HP in the absence and presence of PDGF. As shown in Figure 2-8b, no degradation was observed in the absence of PDGF with or without CT. However, when PDGF was present, a significant amount of digestion products was generated. These results indicate that HP digestion is PDGF-dependent.
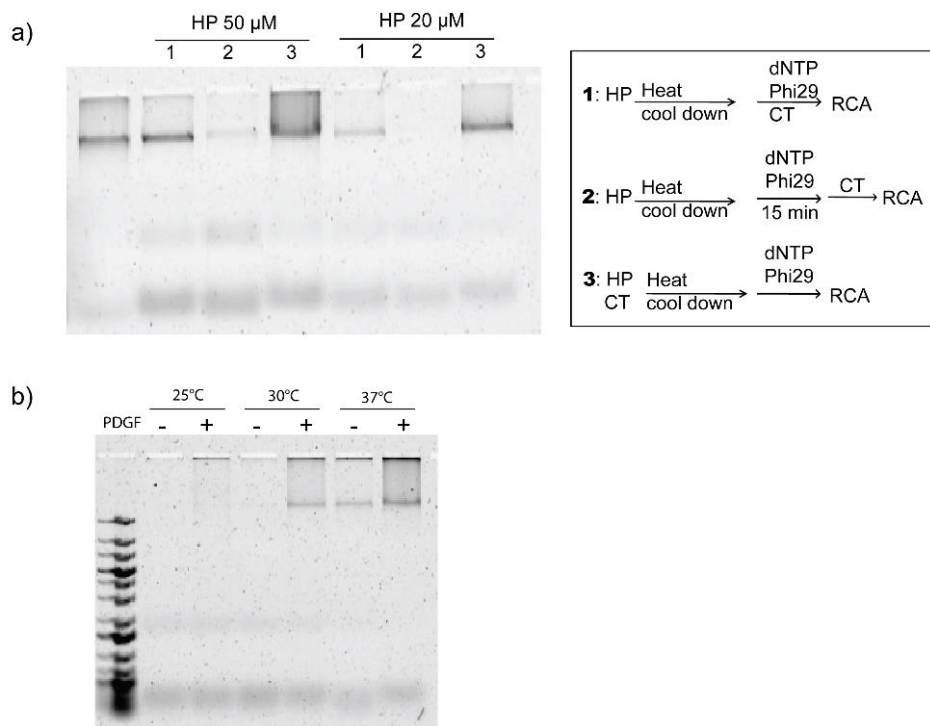
Figure 2-9. Optimization of RCA-urease based biosensing platform for PDGF detection. a) Agarose gel-based analysis for RCA reactions using HP following different protocols. RCA was performed at 30 °C for 2 hours. b) Agarose gel-based analysis for RCA products in PDGF detection performed at different temperatures (25 •C, 30 •C or 37 •C).

We next investigated the PDGF-promoted RCA reaction. To eliminate the background signal which can be generated by improperly folded HP, three different protocols were tested as shown in Figure 2-9a. We found that by treating the HP (20 μM) with Phi29 DP and dNTP for 15 mins before adding the circle could effectively decrease the background signal. This result can be attributed to the nucleolytic and polymeric ability of Phi29 DP. For example, if an HP molecule is misfolded and has a 3′-end overhang, Phi29 DP can digest the overhang and leave a blunt end; if an HP molecule has a 5′-end overhang,

the Phi29 DP can use the overhang as template and elongate its 3′ end until it has a blunt end. As a result, by using this protocol, improperly folded HP molecules will be forced to present blunt ends which cannot initiate RCA, leading to a decreased background signal. We also optimized the reaction temperature for the PDGF-promoted structure switching reaction (see Figure 2-9b). We chose 30 °C as reaction temperature for our following experiments as under this temperature, a relatively high positive signal and a low background signal was observed.

We then examined the applicability of PDGF-promoted RCA reactions using the litmus test. As shown in Figure 2-8c, agarose gel-based analysis indicated that a significant amount of RCA products were produced when HP and CT were incubated with PDGF, both with (lane 8) and without UrD (lane 6). In addition, RCA products were not observed when CT or PDGF was omitted. The litmus test was then performed and showed that the generated RCA products could produce an intense colour signal.
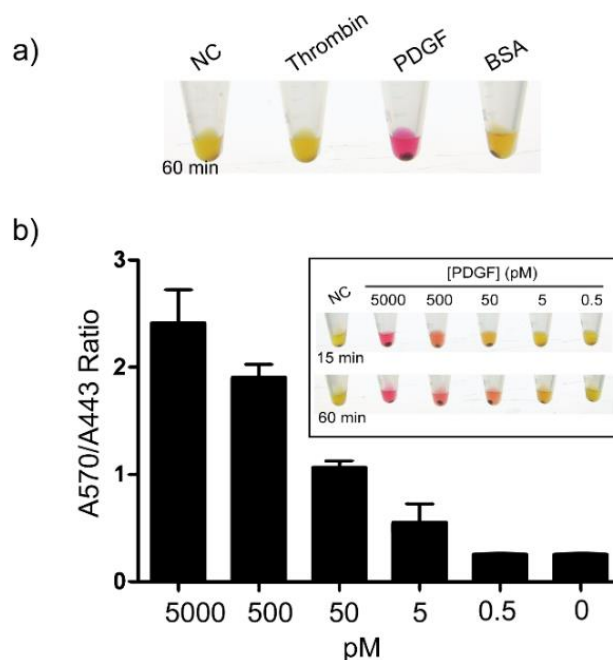
Figure 2-10. Examination of RCA-urease based biosensing platform for PDGF detection. a) Litmus test with various protein targets. b) Quantitative analysis of RCA-litmus test in the presence of different concentration of PDGF. Inset: a photograph for visual detection of PDGF at various concentrations.

Specificity and sensitivity of this method in PDGF detection were then evaluated. Thrombin and BSA were chosen for the specificity test. As shown in Figure 2-10a, neither thrombin nor BSA was able to trigger the colour transition, suggesting that this method has excellent specificity. Various concentrations of PDGF were used to examine the sensitivity of our method. A PDGF concentration as low as 5 pM was able to be detected after one hour of colour generation (see Figure 2-10b). To be noted, the concentration range of PDGF in healthy people is 46-110 pM for urine and the number is even higher in cancer patients[26]. Therefore, this method is sensitive enough in monitoring PDGF in human samples. We then assessed the effectiveness of our method for human applications by analyzing PDGF

in a matrix of human urine. A 1:5 dilution of urine was used in the tests. Figure 2-11 shows

that 50 pM of PDGF spiked in urine can be detected using our method indicating that the

method could be used for protein detection in biological media.
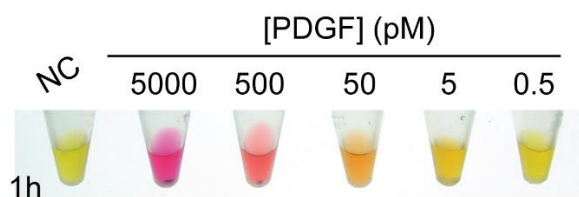
Figure 2-11. Using anti-PDGF aptamer-mediated RCA-litmus test to detect PDGF in urine.
RCA reactions were performed in 20% of urine for 2 hours.

2.3.6 RCA-urease based biosensing platform on paper-based devices

Paper-based devices provide a platform for portable, low-cost, low-volume, and

simple sensors, which are particularly well suited for point-of-care diagnostic

applications[27]. A previous study in our lab has proved that paper-based devices are capable

of carrying out target-induced RCA to produce massive amounts of DNA amplicons[7].

Herein, we will demonstrate that the RCA-urease biosensing platform can be incorporated

into simple paper-based devices and used for DNA detection.

Nitrocellulose paper, which is known to have a high affinity for protein binding,

was used for this study. We first immobilized 5′-biotinylated DNA primer (DP2)-

streptavidin conjugate onto a nitrocellulose surface (see Figure 2-12a). Blocking reagent

(5% skim milk in 1 ×PBS) was then added to prevent the nonspecific binding of proteins,

such as urease, to the paper surface. We then performed RCA in a volume of 10 µL by

placing a mixture of CT, Phi29 DP, dNTPs, reaction buffer, and UrD onto the paper

platform, followed by incubation at room temperature for 60 minutes. The free UrD was

then removed through a washing step and the litmus test was performed. We found that a

high concentration of UrD could bind to the paper surface and increase the background

signal even after the blocking step. To circumvent this issue, the concentration of UrD used

in this assay was optimized and 10 nM was chosen for further testing (see Figure 2-12b).

The result in Figure 2-12c indicates that RCA-urease mediated litmus test can be

successfully performed on the paper-based device and induce a colour change in the

presence of RCA products.
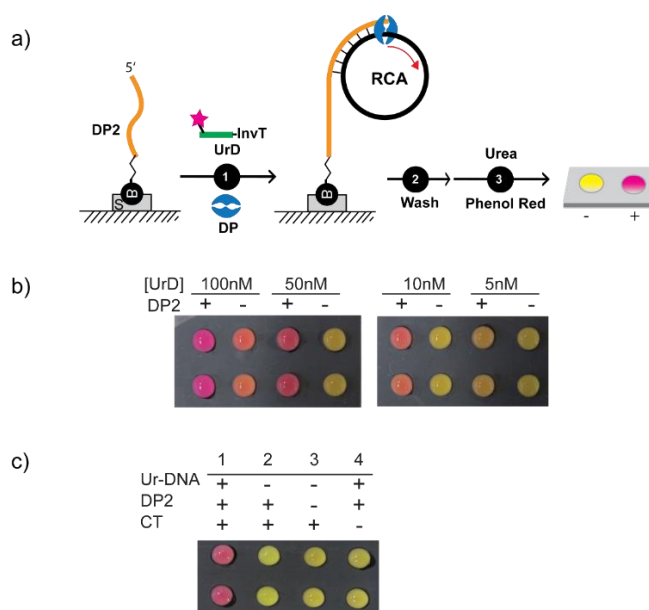
Figure 2-12. Detecting RCA primer (DP2) using paper-based RCA-litmus test. a). Assay principle. (1) RCA reaction. (2) Immobilization of RCA products and urease labelled DNA onto magnetic beads. (3) Litmus test. b). Photographs of visual detection of DP2 on paper using different concentration UrD. The photographs were taken after 20 min of colour development. c). Paper-based RCA litmus test in the presence of a various combination of UrD, DP2, and CT. The photographs were taken after 20 min of colour development.

To achieve DNA detection, the 3′-biotinylated DNA capture sequence (DC) was designed to be immobilized onto the paper surface to capture the DNA target (DT). As shown in Figure 2-13a, DT contains two sequence domains: a 5′ domain that binds to DC and a 3′ domain that can serve as the RCA primer. In the presence of DT, RCA products can be generated and immobilized onto the paper. In testing this design, a sharp colour change was observed in the presence of immobilized RCA products (see Figure 2-13b, lane 8). In contrast, no colour change was found in any of the negative controls (the first six lanes, RCA should not occur when DT or CT is omitted). Interestingly, a subtle colour change was also observed in lane 7 (with DT, without DC). dPAGE analysis (Figure 2-13c) of monomeric RCA products on paper showed that RCA products in lane 7 were not completely removed after the washing step indicating a strong affinity of RCA products to the nitrocellulose surface. We then examined the sensitivity of this method for detecting DT. After 20 minutes of colour development, the paper device was photographed and analyzed using Image J software. As shown in Figure 2-13d, 0.1 nM of DT can be detected with the naked eye. With the help of Image J analysis, the detection limit is capable of decreasing to 0.01 nM.
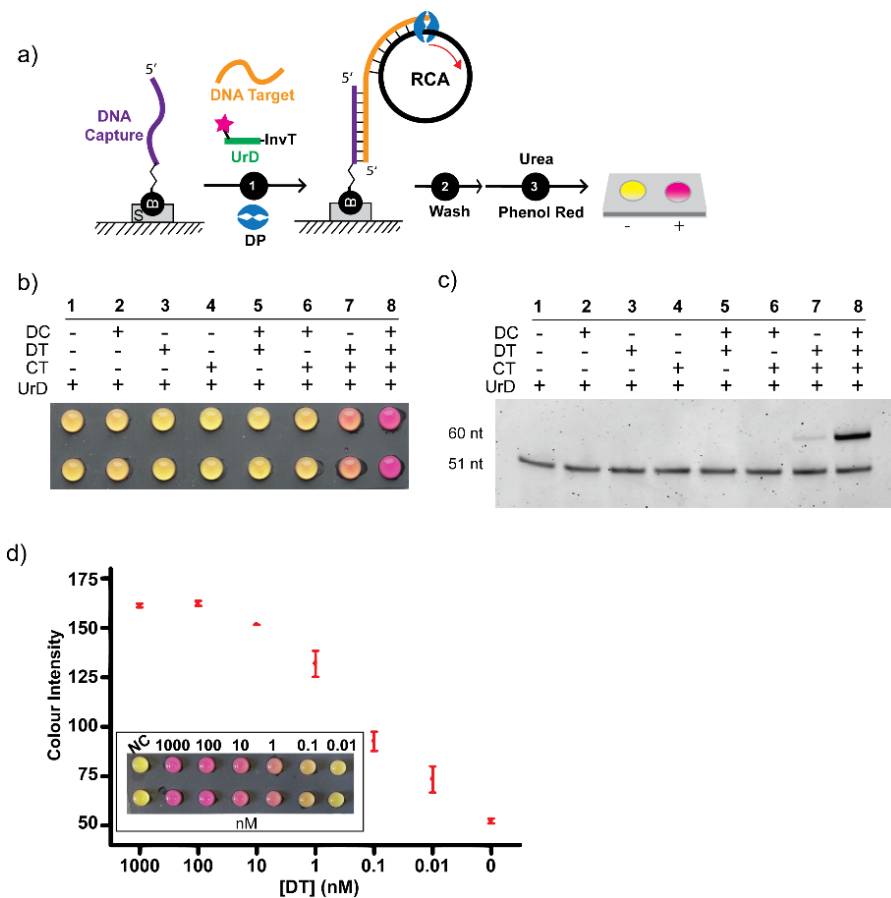
Figure 2-13. Paper-based RCA-litmus test for DNA detection. a). Working principle. (1) RCA reaction. (2) Immobilization of RCA products and urease labelled DNA onto magnetic beads. (3) Litmus test. b). Paper-based litmus test and c) dPAGE analysis for digested RCA products from RCA reaction containing various combinations of 1 μM BI, 1 μM DT, 100 nM CT and 10 nM UrD. The RCA reaction is 60 minutes at room temperature. d). Dose-responsive curves for detection of DT using the paper-based test. Inset: a photograph for visual detection on a paper array at DT at various concentrations. Two rows represent two repeats. The photograph was taken after a signal-producing time of 20 minutes.

2.4 Summary

In conclusion, we have demonstrated a colorimetric double-amplified biosensing platform that uniquely takes advantage of the signal amplification power of RCA and the simplicity of urease-mediated litmus test. To the best of our knowledge, our work represents the first example of employing the classic litmus test for RCA products detection. By integrating structure-switching signalling aptamers for target recognition, this platform can be adopted for colorimetric detection of different targets. This approach can turn an aptamer with a relatively low affinity for its target into an ultra-sensitive colorimetric biosensing system. With a wide variety of aptamers currently available and new aptamers that can be conveniently produced by *in vitro* selection, we envision that the described strategy will find diverse applications in biological, medical, and environmental fields. A range of aptamers targeting toxins or GDH from *C. difficile* have been reported in recent years. We believe this colorimetric biosensing platform can be employed in couple with these aptamers in simple and sensitive detection of *C. difficile*. We have also demonstrated that the colorimetric biosensing platform can be incorporated into simple paper-based devices, making it particularly suitable for point-of-care diagnostic applications.

2.5 Experiments

2.5.1 Materials and reagents

All DNA oligonucleotides (Table2-1) were obtained from Integrated DNA Technologies (Coralville, IA, USA), and purified by 10% denaturing (8 M urea) polyacrylamide gel electrophoresis (dPAGE), and their concentrations were determined spectroscopically. T4 polynucleotide kinase, T4 DNA ligase, Phi29 DNA polymerase, FastDigest *Eco*RI, ATP, and deoxynucleoside 5′-triphosphates (dNTPs) were purchased from Thermo Scientific (Ottawa, ON, Canada). SYBR Gold (10,000× stock in DMSO) was obtained from Life Technologies (Burlington, ON, Canada). Streptavidin-coated magnetic beads of 1.5 μm (BioMag-SA) was purchased from Bangs Laboratories Inc. Urease powder from Canavaliaensiformis (Jack bean), maleimidobenzoic acid N-hydroxy-succinimide ester (MBS), and phenol red were obtained from Sigma-Aldrich. Water was purified with a Milli-Q Synthesis A10 water purification system. All other chemicals were purchased from Bioshop Canada and used without further purification.

Table 2-1. Sequences used in RCA-litmus test. Note: lnvdT on the 3′ end of the sequence is an inverted T sequence added on the 3′ end to prevent extension and degradation.

Name	Sequences (5'-3')
Circular Template (CT)	AAGGAGTGAAGCGTGCGTAATAGTGTCAAGGAATTCAATCAA CGTAAAGCTGAAGAAGCT
LigationTemplate (LT)	CTCCTTAGCTTCTTCA
NH$_2$-DNA	AmMC6T-TTTTTTAGTGAAGCGTGCGTAATAGTGTCAAG-InvdT
Biotin-DNA Primer (BP)	Bio-CTCCTTAGCTTCTTCA
Fluorogenic DNA (FD)	AGTGAAGCGTGCGTAATAGTGTCAAG-FAM
RCA product monomer (RPM)	Bio-TCTTCAGCTTTACGTTGATTGAATTCCTTGACACTATTACG CACGCTTCACTCCTTAGCT
DNA loading control	TTCGGAAGAGATGGCGACGCCGAACTATCTCTCGAGCTGATC CTGATGGAA
Thrombin Probe (TP)	Bio-AGGTTGGTGTGGTTGGAACTCCTTAGCTTCTTCA
Hairpin probe (HP)	Bio-CAGGCTACGGCACGTAGAGCATCACCATGATCCTGCTCC TTAGCTTCTTCATTTTTGCCGTAGCCTG
DNA Target (DT)	ACCTTCTCTGTTCTACGATTTCTCCTTAGCTTCTTCA
DNA Capture (DC)	TCGTAGAACAGAGAAGGT-3BioTEG
Biotin-DNA Primer (BP2)	5BioTEG-CTCCTTAGCTTCTTCA

2.5.2 Preparation of circular DNA templates

Circular DNA templates were prepared from 5′-phosphorylated linear DNA oligonucleotides through template-assisted ligation with T4 DNA ligase. Linear circle template (CT) was phosphorylated as follows: a reaction mixture (50 μL) was made to contain 1 nmol of CT, 20 U PNK (U: unit), 1× PNK buffer A (50 mM Tris-HCl, pH 7.6 at 25°C, 10 mM MgCl$_2$, 5 mM DTT, 0.1 mM spermidine), and 2 mM ATP. The mixture was incubated at 37°C for 40 min, followed by heating at 90 °C for 5 min. The circularization reaction was conducted in a volume of 400 μL, produced by adding 306 μL of H$_2$O and 2 μL of a DNA template (LT, 500 μM) to the phosphorylation reaction mixture above. After heating at 90°C for 3 min and cooling down at room temperature for 10 min, 40 μL of 10×

T4 DNA ligase buffer (400 mM Tris-HCl, 100 mM MgCl$_2$, 100 mM DTT, 5 mM ATP, pH 7.8 at 25°C) and 2 μL of T4 DNA ligase (5 U/μL) were added. This mixture was incubated at RT for 2 hours before heating at 90°C for 5 min to deactivate the ligase. The ligated circular DNA molecules were concentrated by standard ethanol precipitation and purified by 10% dPAGE. The concentration of the circular DNA template was determined spectroscopically.

2.5.3 DNA-urease conjugation

Urease-DNA was prepared according to a previously reported method[16,17]. An MBS solution (6.4 mM) was made by dissolving 2 mg MBS (6.4μmol) in 1 mL of dimethyl sulphoxide (DMSO). Similarly, a urease solution was produced by dissolving 1.5 mg urease (3.3 nmol) powder in 1 mL of 1× PBS buffer (pH 7.2). 1 nmol UrD and 3.2 μL of the MBS solution (20 nmol) were mixed and adjusted to a final reaction volume of 100 μL with 1× PBS buffer, and allowed to react at room temperature. After 2 h, the mixture was passed through a membrane-based molecular sizing centrifugal column with a molecular weight cut-off of 3,000 Daltons (NANOSEP OMEGA, Pall Incorporation) in order to remove excess MBS. The column was washed with 50 μL of 1× PBS buffer 3 times, and the DNA was resuspended in 100 μL of 1× PBS buffer. The urease solution (1 mL, 3.3 nmol) was then added to the MBS activated DNA. The conjugation reaction was allowed to proceed at room temperature for 1 h. The mixture was filtered through 300,000-Dalton cut-off centrifugal column. The DNA-urease conjugate (UrD) was then washed with 50 μL of 1×

PBS buffer 3 times and resuspended in 100 μL of 1× PBS buffer. The concentration of the UrDNA was quantified based on previously developed method[17]. Details are provided in 3.5.7.

2.5.4 RCA reactions

The RCA reactions were performed in 50 μL. 1 μL of 0.1 μM CT (the final concentration is 2 nM) was mixed with 1 μL of BP, 5 μL of 10 mM each of dGTP, dATP, dTTP and dCTP, 5 μL 10×RCA buffer (330 mM Tris-acetate, 660 mM K-acetate, 100 mM Mg-acetate, 1% tween 20, 10 mM DTT, pH 7.9) and 37.5 μL of H_2O. After heating at 90 °C for 3 min, the solution was cooled to RT for 10 min. 0.5 μL of 10 U/μL Phi29 DNA polymerase and 1μL of 2 μM UrD were then added, followed by incubation at 30°C for 120 min.

2.5.5 Litmus test

15 μL of magnetic beads (MB) was incubated with binding buffer (10 mM Tris-HCl, pH 7.5, 3M NaCl, 1 mM $MgCl_2$, 0.01% tween 20, 5% skim milk) for 1 h. Then the supernatant was removed through magnetic separation. 50 μL of the above RCA reaction mixture was incubated with 50 μL of binding buffer along with the MB for 15 min. Then it was placed in a magnet holder to separate the supernatant and MB. MB was then washed with 100 μL of washing buffer (10 mM Tris-HCl, pH 7.5, 3 M NaCl, 1 mM $MgCl_2$, 0.01% tween20) four times and then resuspended in 60 μL of acetic acid buffer (0.1 mM, pH 6).

Then 20 μL of 0.04% phenol red and 100 μL of substrate solution (3 M NaCl, 60 mM MgCl$_2$, 50 mM urea, 1 mM HCl) were added. Note that this substrate solution should have a starting pH of 6.0. After a signal producing time of 1 hour, measurements at 443 nm and 570 nm were performed by using a microplate scanning spectrometer (TECAN M1000).

2.5.6 Restriction digestion and analysis of monomeric RCA products

The digestion reaction was performed in 10 μL. A 5-μL aliquot of the above RCA reaction mixture was heated to 65 °C for 10 min to deactivate the polymerase and cooled at room temperature for 10 min. This was followed by the addition of 2 μL of FastDigest *Eco*RI and 3 μL of H$_2$O. The reaction mixture was then incubated at 37°C for 16 hours. The above digestion mixture was combined with 10 μL of 2× denaturing gel loading buffer (GLB), and 4μL of 200nM DNA loading control in 1× GLB; The final volume of this DNA mixture was 24 μL. A 5-μL aliquot was then run on a 10% dPAGE gel. After electrophoresis, the gel was stained with 1× SYBR Gold (diluted from the 10,000×concentratedstock solution). A fluorescent image of the stained gel was obtained using Typhoon 9200 and analyzed using Image Quant software (Molecular Dynamics).

2.5.7 DNA probe adsorption by rGO

Graphene oxide (GO) was prepared according to a previously reported method[28]. Absorption of graphene was initially done by adding rGO (40 μg/mL) in a total volume of 50 μL with 1× thrombin binding buffer (20 nM PBS, 150 mM NaCl, 20 mM KCl, 5 mM

MgCl$_2$, pH 7.5), 100 nM of Thrombin probe (TP) and the rest of the volume with ddH$_2$O. This reaction incubated at room temperature for 60 min and then centrifuged at 14,000 g for 5 min.

2.5.8 DNA probe release by thrombin

48μL of the TP-rGO mixture was transferred into a 1.5-mL microcentrifuge tube and combined with 2 μL of a thrombin stock solution with a defined concentration of thrombin. The reaction mixture was incubated at 30 °C for 30 min, then centrifuged for 10 min at 14,000 g to remove the rGO. 5 μL of the supernatant was used as a primer for RCA reactions as described above.

2.5.9 RCA reaction with the PDGF sensing system

In a typical experiment, 5 μL of 10× RCA reaction buffer, 1.5 μL of HP (1 μM), and 35 μL of water were mixed. The mixture was heated at 90 °C for 3 min and cooled to room temperature for 20 min. 5 U of Phi29 DP and 5 μL of 10 mM dNTPs were then added to the mixture. After incubation at 30 °C for 15 min, 1 μL of 1 μM CT, 1 μL of 2 μM UrD and 1 μL of PDGF were added. The mixture was then incubated at 30 °C for 2 h.

2.5.10 Preparation of bioactive paper

To facilitate the immobilization of DNA primers on paper, streptavidin was used to bind the biotinylated BP2 or DC. Briefly, 1 nmol of BP2 or DC and 30 µL of 2 mg/mL streptavidin were added to 1 mL of $1 \times$ PBS buffer. After incubating at room temperature for 2 h, 10 µL of the above solution was dropped onto each test zone and allowed to dry at room temperature. After immersion in PBS buffer (containing 5% skim milk, 0.01%(v/v) tween 20) for 20 min and washing twice, the obtained bioactive paper was dried at room temperature and stored at 4 °C in a desiccant container.

2.5.11 RCA-litmus test on paper

In a typical experiment, 1 µL of $10\times$ RCA reaction buffer, 5 U of Phi 29 DP, 1 µL of 10 mM dNTPs, 1 µL of 0.1 µM CT and 1 µL of 2 µM UrD were mixed with 1µL of different concentrations of DT and then added (total volume: 15 µL) to the test zones. The reaction was allowed to proceed at room temperature for 1 h. Then the paper was immersed in $1\times$PBS buffer (containing 0.01%(v/v) tween 20) for 20 min and washed three times. 6 µL of acetic acid buffer (0.1 mM, pH 6), 1.5 µl of 0.04% phenol red and 7.5 µL of substrate solution (3 M NaCl, 60 mM $MgCl_2$, 50 mM urea, 1 mM HCl) were then added onto each test zone for litmus test. Images were sent to a computer and analyzed using ImageJ software. The image was split into its colour channels, and the green colour channel was selected and inverted. The green channel was selected because it is the complementary

colour of red, the reaction's endpoint colour. The colour intensity of each sample spot was then quantified.

2.6 References

1.   Urdea, M. *et al.* Requirements for high impact diagnostics in the developing world. *Nature* **444 Suppl,** 73–79 (2006).

2.   Yager, P., Domingo, G. J. & Gerdes, J. Point-of-Care Diagnostics for Global Health. *Annu. Rev. Biomed. Eng.* **10,** 107–144 (2008).

3.   Ali, M. M. *et al.* Rolling circle amplification: a versatile tool for chemical biology, materials science and medicine. *Chem. Soc. Rev.* **43,** 3324 (2014).

4.   Canceill, D., Viguera, E. & Ehrlich, S. D. Replication slippage of different DNA polymerases is inversely related to their strand displacement efficiency. *J. Biol. Chem.* **274,** 27481–27490 (1999).

5.   Blanco, L. *et al.* Highly efficient DNA synthesis by the phage Φ29 DNA polymerase. Symmetrical mode of DNA replication. *J. Biol. Chem.* **264,** 8935–8940 (1989).

6.   Ou, L., Sun, A. & Liu, K. Rolling Circle Amplification-Based Biosensors. *Anal. Lett.* **48,** 1199–1216 (2015).

7.   Liu, M. *et al.* Target-Induced and Equipment-Free DNA Amplification with a Simple Paper Device. *Angew. Chemie - Int. Ed.* **55,** 2709–2713 (2016).

8.   Liu, M. *et al.* Programming a topologically constrained DNA nanostructure into a
        sensor. *Nat. Commun.* **7,** (2016).

9.   Liu, M. *et al.* A DNAzyme Feedback Amplification Strategy for Biosensing. *Angew.*
        Chemie - Int. Ed. **56,** 6142–6146 (2017).

10.   Liu, M., Zhang, W., Zhang, Q., Brennan, J. D. & Li, Y. Biosensing by Tandem
        Reactions of Structure Switching, Nucleolytic Digestion, and DNA Amplification
        of a DNA Assembly. *Angew. Chemie - Int. Ed.* **54,** 9637–9641 (2015).

11.   Liu, M. *et al.* Target-Induced and Equipment-Free DNA Amplification with a
        Simple Paper Device. *Angew. Chemie - Int. Ed.* **55,** 2709–2713 (2016).

12.   Zhao, W., Ali, M. M., Brook, M. A. & Li, Y. Rolling circle amplification:
        Applications in nanotechnology and biodetection with functional nucleic acids.
        Angewandte Chemie - International Edition **47,** 6330–6337 (2008).

13.   Monsur Ali, M. & Li, Y. Colorimetric sensing by using allosteric-DNAzyme-
        coupled rolling circle amplification and a peptide nucleic acid-organic dye probe.
        Angew. Chemie - Int. Ed. **48,** 3512–3515 (2009).

14.   Chang, D. *et al.* Integrating deoxyribozymes into colorimetric sensing platforms.
        Sensors (Switzerland) **16,** (2016).

15.   Karplus, P. A., Pearson, M. A. & Hausinger, R. P. 70 Years of Crystalline Urease:
        What Have We Learned? *Acc. Chem. Res.* **30,** 330–337 (1997).

16. Tram, K., Kanda, P., Salena, B. J., Huan, S. & Li, Y. Translating bacterial detection by DNAzymes into a litmus test. *Angew. Chemie - Int. Ed.* **53,** 12799–12802 (2014).

17. Chang, D. *et al.* Detection of DNA Amplicons of Polymerase Chain Reaction Using Litmus Test. *Sci. Rep.* **7,** 3110 (2017).

18. Leslie, D. C. *et al.* New detection modality for label-free quantification of DNA in biological samples via superparamagnetic bead aggregation. *J. Am. Chem. Soc.* **134,** 5689–5696 (2012).

19. Lin, C., Zhang, Y., Zhou, X., Yao, B. & Fang, Q. Naked-eye detection of nucleic acids through rolling circle amplification and magnetic particle mediated aggregation. *Biosens. Bioelectron.* **47,** 515–519 (2013).

20. Liu, M. *et al.* A graphene-based biosensing platform based on the release of DNA probes and rolling circle amplification. *ACS Nano* **8,** 5564–5573 (2014).

21. Bock, L. C., Griffin, L. C., Latham, J. A., Vermaas, E. H. & Toole, J. J. Selection of single-stranded DNA molecules that bind and inhibit human thrombin. *Nature* **355,** 564–566 (1992).

22. Brummel-Ziedins, K. E., Pouliot, R. L. & Mann, K. G. Thrombin generation: Phenotypic quantitation. *J. Thromb. Haemost.* **2,** 281–288 (2004).

23. Andrae, J., Gallini, R. & Betsholtz, C. Role of platelet-derived growth factors in physiology and medicine. *Genes and Development* **22,** 1276–1312 (2008).

24. Disis, M. L. & Cheever, M. A. Oncogenic proteins as tumor antigens. *Current Opinion in Immunology* **8,** 637–642 (1996).

25. Khare, V. & Eckert, K. A. The proofreading 3′ → 5′ exonuclease activity of DNA polymerases: A kinetic barrier to translesion DNA synthesis. *Mutation Research - Fundamental and Molecular Mechanisms of Mutagenesis* **510,** 45–54 (2002).

26. Gersuk, G. M., Carmel, R. & Pattengale, P. K. Platelet-derived growth factor concentrations in platelet-poor plasma and urine from patients with myeloproliferative disorders. *Blood* **74,** 2330–2334 (1989).

27. Condon, C. & Putzer, H. The phylogenetic distribution of bacterial ribonucleases. *Nucleic Acids Res.* **30,** 5339–5346 (2002).

28. Liu, M. *et al.* A graphene-based biosensing platform based on the release of DNA probes and rolling circle amplification. *ACS Nano* **8,** 5564–5573 (2014).

Chapter 3

Detecting Epidemic Strains of *Clostridium difficile* using PCR and Urease-mediated Litmus Test

3.1 Abstract

We report on a new colorimetric DNA detection method that takes advantage of the power of polymerase chain reaction (PCR) and the simplicity of the classic litmus test. The strategy makes use of a modified set of primers for PCR to facilitate ensuing manipulations of resultant DNA amplicons: their tagging with urease and immobilization onto magnetic beads. The amplicon/urease-laden beads are then used to hydrolyze urea, resulting in the increase of pH that can be conveniently reported by a pH-sensitive dye. We have successfully applied this strategy for the detection of two hypervirulent strains of the bacterium *Clostridium difficile* that are responsible for the recent increase in the global incidence and severity of *C. difficile* infections. Furthermore, the viability of this test for diagnostic applications is demonstrated using clinically validated stool samples from *C. difficile* infected patients.

3.2 Introduction

Polymerase chain reaction (PCR) is a popular DNA amplification technique and can create millions of amplicons of a target sequence in a short period of time[1–4]. This technique has been widely utilized for a variety of applications, including the detection of pathogenic bacteria[5–8]. PCR-based DNA detection is attractive for bacterial detection simply because specific DNA sequences can serve as reliable bacterial biomarkers and the amplification power of PCR permits the detection of a small number of bacteria before they can grow to pathogenic quantities[5–8].

Although PCR has become a widely adopted technique in clinical laboratories, it has not become commonly used point-of-care or field tools. One significant roadblock that prevents such applications is the need of thermal cyclers that are often too expensive and bulky. However, there have been significant efforts towards miniaturizing PCR machines[9–12]. Another significant barrier that restricts PCR from becoming a popular field tool is the lack of simple yet effective signal transduction mechanisms that permit detection of PCR products without the use of expensive equipment (such as real-time PCR machine) and complicated process (such as DNA separation by gel electrophoresis). These issues reduce the utility of PCR as field tools. One approach to address this problem is to develop simple colorimetric assays that can be easily implemented in the field to detect DNA amplicons of PCR. Recently, our group reported on an approach of adopting the classic litmus test for bacterial detection using a protein-activated DNAzyme and the protein enzyme urease[13]. Herein we describe a strategy for adopting the same litmus test for the detection of PCR amplicons through the use of a set of specially modified DNA primers and urease.
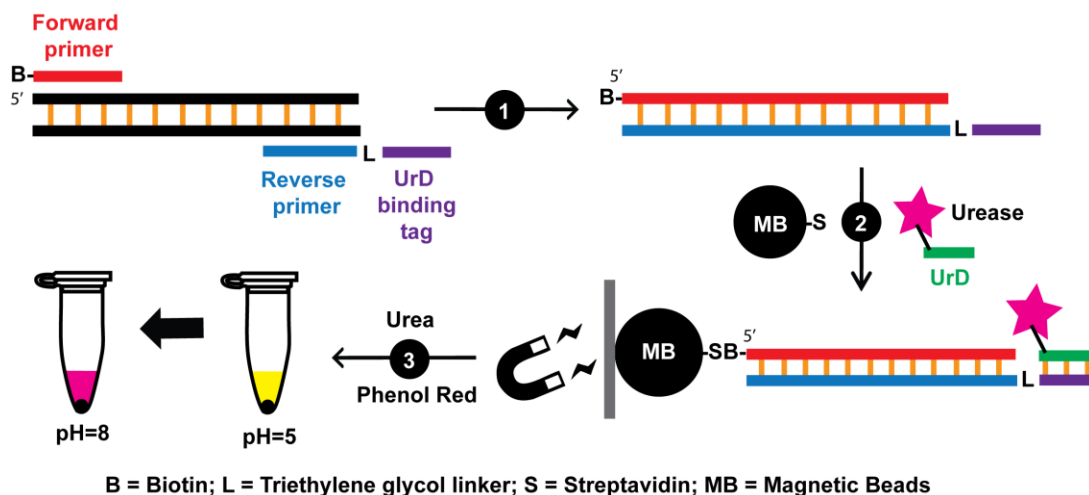
Figure 3-1. Assay principle. (1) PCR reaction. (2) Immobilization of PCR product and urease labelled DNA onto magnetic beads. (3) Litmus test.

Our devised strategy is illustrated in Figure 3-1. Two modified DNA primers are used to carry out PCR. The forward primer contains a 5′-biotin and the reverse primer contains a triethylene glycol linker that separates the target binding sequence (blue) from the sequence (purple) that is designed to hybridize with the DNA strand (green) coupled onto urease (a conjugate denoted "UrD" in this report). By this design, the PCR amplicons can be immobilized on the surface of magnetic beads containing streptavidin and the immobilized amplicons are capable of capturing UrD. The amplicon/urease-charged beads can then be used to hydrolyze urea, resulting in the increase of pH that can be reported by a pH-sensitive dye, such as phenol red (which can produce a sharp, yellow-to-pink transition when the solution pH changes from acidic to basic). Simply put, the proposed

strategy converts the detection of DNA into tracking of pH increases using procedures that are easy to carry out.

To validate the proposed idea, we chose to develop a test that can be used to detect two hypervirulent strains of *C. difficile*. known as 027/NAP1 and 078/NAP7. *C. difficile* is a gram-positive, spore-forming anaerobic bacterium that has been identified as the leading cause of diarrhea in developed countries and pseudomembranous colitis in humans[14]. The incidence and mortality of *C. difficile* infection (CDI) has increased dramatically over the past 15 years and CDI has become a common problem in hospitals across North America, Europe and some regions of Asia[15,16]. This has been mostly attributed to the emergence of highly virulent strains. One such strain was characterized as ribotype 027, as North America Pulsed-field type NAP1 by pulsed-field gel electrophoresis (PFGE) and was subsequently referred as 027/NAP1[17]. The 027/NAP1 strain is known for its high-level resistance to fluoroquinolones, with markedly high toxin production and a mortality rate three times as high as that associated with less virulent strains, such as the ribotype 001[17–20]. Another epidemic strain of *C. difficile*, known as 078/NAP7, has also been described as hypervirulent since it can cause symptoms of similar severity to strain 027/NAP1. However, 078/NAP7 affects the younger population and is more frequently community associated[21–24]. Identification of these epidemic strains may assist in determining relatedness of strains and recognizing transmission of CDI within healthcare facilities.

Current methods available for the diagnosis of CDI include cytotoxicity assays, anaerobic toxigenic culture, enzyme immunoassay (EIA) and nucleic acid amplification-based tests[16,25]. These methods generally target toxins or their associated toxin genes and

are unable to discriminate epidemic strains from non-epidemic strains[14,25–27]. Meanwhile, current strain typing methods for *C. difficile*, such as ribotyping, restriction endonuclease analysis and PFGE, require culture of the organism, lack discriminatory power and are performed in reference laboratories, with resulting delays of days to weeks[28,29]. Consequently, there is a significant need for a simple and rapid method for identifying epidemic *C. difficile* strains.

The virulence of *C. difficile* is mainly caused by toxin A and toxin B which are encoded by *tcdA* and *tcdB*, respectively, and their expression is regulated by *tcdR* (positive regulator) and *tcdC* (negative regulator)[30–32]. Interestingly, mutations in *tcdC* were found in both strains 027/NAP1 and 078/NAP7. A single-base deletion at nucleotide position 117 of *tcdC* (Δ1stop-*tcdC*) has been found in the strain 027/NAP1 and this single nucleotide deletion results in a frame shift that introduces a stop codon at nucleotide position 196[33,34].Consequently, this generates a shortened protein of 65 residues. Similarly, strain 078/NAP7 carries a *tcdC* with a C184T transition (*TAA stop-tcdC*) leading to a truncated protein of 61 residues[35]. These mutations in *tcdC* have been proposed as a possible explanation for the increased virulence of the epidemic strains. Meanwhile, since these mutations are well conserved in strains 027/NAP1 and 078/NAP7, they can serve as molecular markers for the rapid identification of the hypervirulent *C. difficile* strains[34–36].

It is well established that PCR can achieve highly specific DNA detection. For example, allele-specific PCR has been developed for Single Nucleotide Polymorphisms (SNP) detection using a DNA primer containing a single mismatch at 3′-end. This principle

was used in this study to achieve the detection of mutations in *tcdC* genes associated with 027/NAP1 and 078/NAP7.

3.3 Results

3.3.1 PCR primer design for identification of epidemic strains of C. difficile
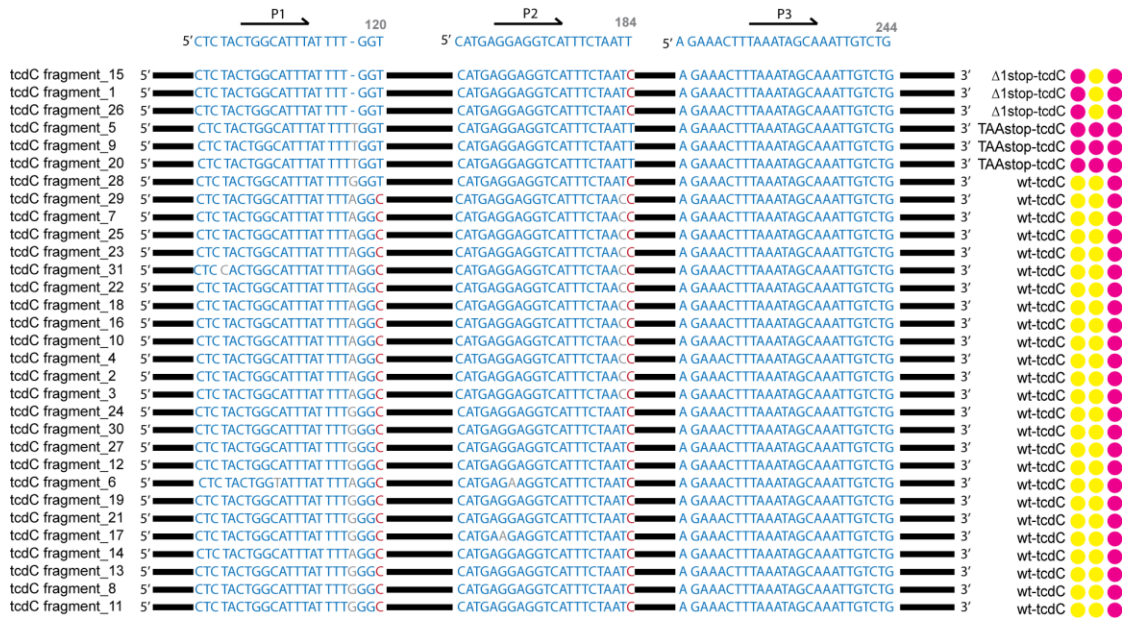

Figure 3-2. Sequence alignment and primer design for identification of epidemic strains of *C. difficile*. An alignment of 31 *tcdC*_fragment gene sequences (PubMLST http://pubmlst.org/) and corresponsive triplet patterns generated by PCR-litmus test are shown. The primer binding regions are colour-coded. The mismatched 3′ terminus between forward primer and template are shown in red.

Through sequence analysis of *tcdC* (Figure 3-2), three forward primers (FP1, FP2 and FP3) and one reverse primer (RP) were designed for the discrimination between four possible outcomes: wild-type *tcdC* (*wt-tcdC*), *Δ1stop-tcdC*, *TAAstop-tcdC* and no *tcdC* (sequences of the DNA molecules used for this work are provided in Table 3-1). We found that both *Δ1stop-tcdC* and *TAAstop-tcdC* have a thymine at position 120, whereas *wt-tcdC*

has a cytosine at this position. P1 with 3′-thymine was then designed to detect this difference. Similarly, P2 targets adenine at position 184 of *tcdC* to discriminate *TAAstop-tcdC* and Δ*1stop-tcdC*. P3 was designed to amplify all *tcdC* variants and could be used to identify the presence of *tcdC* gene and play the role of quality control during PCR. Since P1, P2 and P3 have similar T_m, they should theoretically have comparable PCR yields under same condition. The design of each primer was checked by BLAST to avoid nonspecific amplifications. Secondary structures and self-pairing of these primers were also examined.
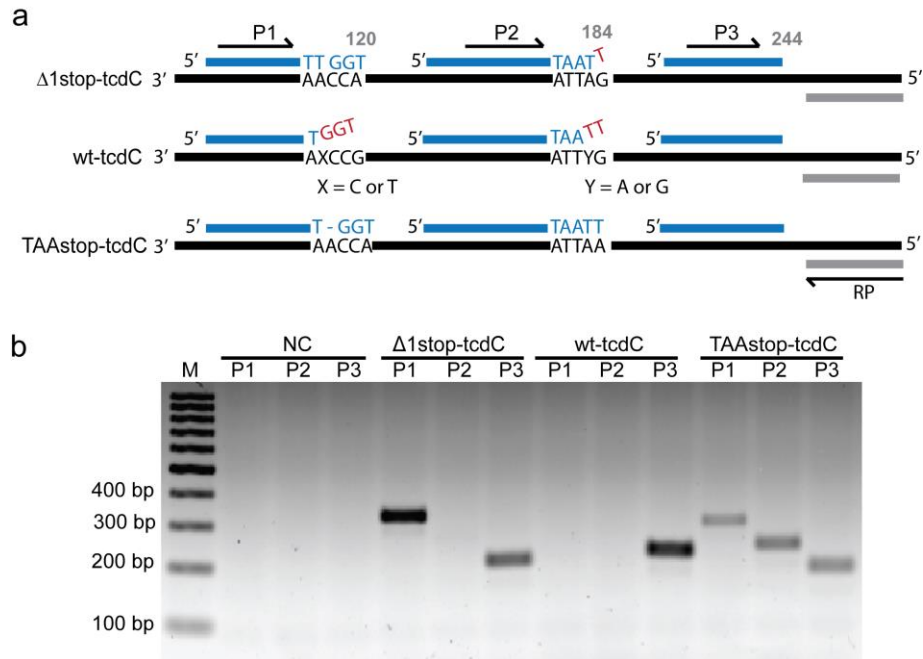
Figure 3-3. PCR-based tests for the wild and two mutated *tcdC* genes. a) Primer design. Primers for *tcdC* genes are colour-coded. The mismatched 3′ terminus between forward primer and template are shown in red. Red and yellow dots denote a successful and unsuccessful PCR reaction, respectively. b) Analysis of PCR products by 2% agarose gel electrophoresis.

Three *C. difficile* strains, 027/NAP1 (with Δ*1stop-tcdC*), 078/NAP7 (with *TAA stop-tcdC*) and 001/NAP2 (with *wt-tcdC*) were tested to examine the performance of the designed primers. Genomic DNA from each strain was extracted based on a previous described method. 200 ng of genomic DNA was used as starting material for 28 cycles of PCR amplification. Agarose gel analysis indicates that a significant amount of PCR product was generated when primers were matched the template, whereas no PCR product was observed in the absence of target gene or when using primers with mismatched 3′ termini (Figure 3-3). Based on the performances of three primer pairs toward each strain, we could successfully discriminate between epidemic *C. difficile* strains, 027/NAP1 and 078/NAP7 and non-epidemic *C. difficile* strain 001/NAP2. We also tested the performance of each primer set by changing the number of PCR cycles. Figure 3-4 indicates that non-specific products were generated after more than 30 cycles of PCR. This is consistent with previous findings that primer 3′ nucleotide mismatches could reduce PCR efficiency but not fully inhibit the reaction[26]. As a result, we proceeded to perform each assay within 30 cycles of PCR.
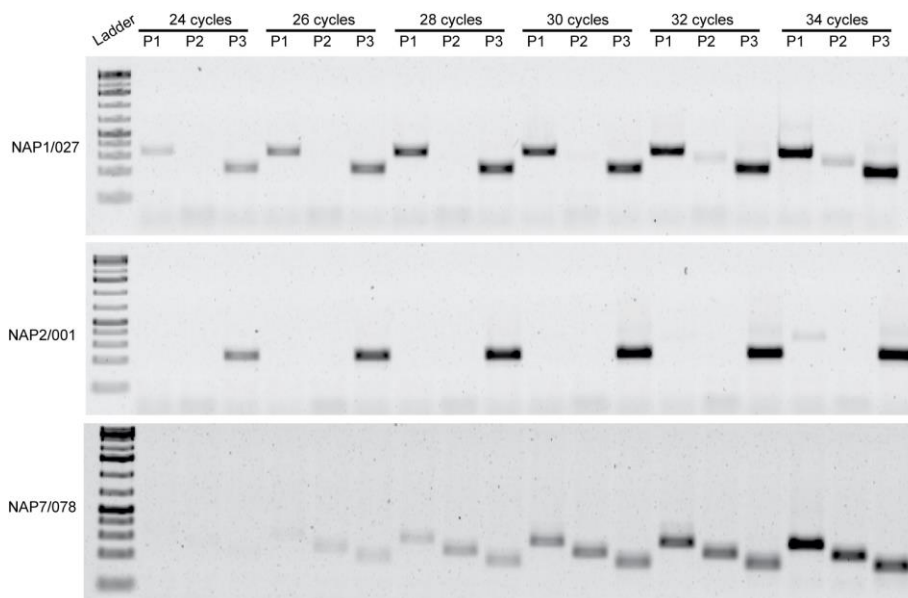
Figure 3-4. Evaluation of the effect of PCR cycles on primer specificity. 200 ng of genomic DNA prepared from strain 027/NAP1, 001/NAP2 and 078/NAP7 were used as starting material. PCR products are analyzed by 2% agarose gel electrophoresis.

3.3.2 Detection of PCR amplicons using litmus test

To achieve colorimetric detection of PCR products, we firstly conjugated urease with an oligonucleotide as reported in a previous method (see details in the supporting information). This conjugated urease-DNA (UrD) is used to hybridize to the extended binding region found in the reverse primer. Although the UrD does not contain a biotin modifier, the UrD has a tendency to non-specifically bind to magnetic beads at high concentrations and increase the background signal. To circumvent non-specific binding, varying concentrations of UrD was incubated with magnetic beads and tested with addition of indicator and urea after thorough washing of the beads. From this quick control assay, we can determine the right diluted UrD solution to be used in future assays. As presented

in Figure 3-5, we found that there was no observed colour change after 2 hours, when 1 μL

of 1 μM UrD in 10 μL of magnetic beads was used. Therefore, we chose to use this stock

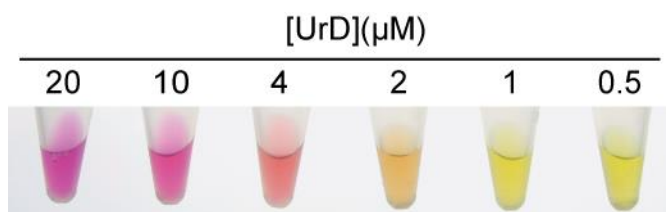concentration for further assay development and testing.

Figure 3-5. Optimization of concentration of UrD in litmus test. Different concentrations of UrD were incubated with binding buffer along with 10 μL of MB for 15 minutes. MB was then washed four times with 100 μL of binding buffer and resuspended in 70 μL of acetic acid buffer. This was followed by addition of 10 μL of 0.04% phenol red and 100 μL of substrate solution. The photograph was taken after a signal-producing time of 2 hours.

We then carried out the colorimetric test on the PCR sample, expecting that the

presence of PCR products would induce a colour change. Within 15 min, PCR positive

products yielded a colour change from yellow to pink while samples that remained yellow

indicated the absence of amplified PCR products and therefore did not capture the UrD. As

shown in figure 3-6, the results of three colorimetric reactions for each strain form a triplet

pattern (no colour change for absence of *tcdC*, one colour change for *wt-tcdC* (non-

epidemic strain), two colour changes for Δ*1stop-tcdC* (epidemic strain 027/NAP1), and

three colour changes for *TAA stop-tcdC* (epidemic strain 078/NAP7)). These patterns can

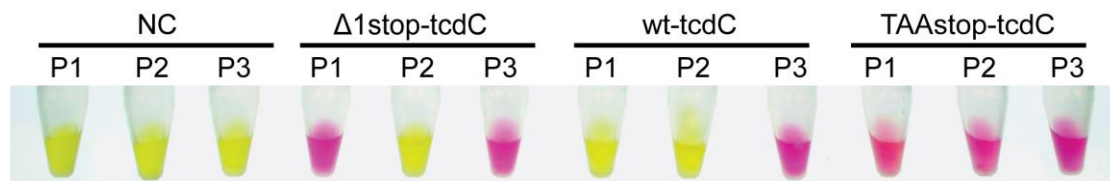then be used to identify epidemic *C. difficile* strains.

Figure 3-6. Litmus test with PCR products. The photographs were taken at 30 minutes.

3.3.3 Detection sensitivity of the PCR-litmus test

The sensitivity of the PCR-litmus assay was evaluated by testing genomic DNA isolated from serially diluted *C. difficile* stocks containing a known number of cells (Figure 3-7). A sharp colour transition was observed for the sample containing 2×10^6 cells after incubation for 1 minute (top panel) and 2×10^5 cells after incubation for 10 minutes (middle panel). A subtle but detectable colour transition, in comparison to the reference samples (without target), was observed for the sample containing 200 cells after colour development of 1 hour. We compared the colorimetric test to conventional agarose gel based test where PCR products were visualized through the staining of DNA-binding dye (SYBRsafe). As shown in Figure 3-7 b**,** we found the dye-staining methods resulted a detection limit of approximately 10^4–10^5 bacteria cells. Therefore, our litmus test exhibits a better detection sensitivity by as much as 100-fold. We have also performed spectroscopic analysis to quantify the detection sensitivity by plotting OD570/OD443 vs. cell numbers (see Figure 3-7c). This analysis confirms that our method can indeed detect as low as 200 cells; however, the spectroscopic analysis did not lead to improved detection sensitivity.
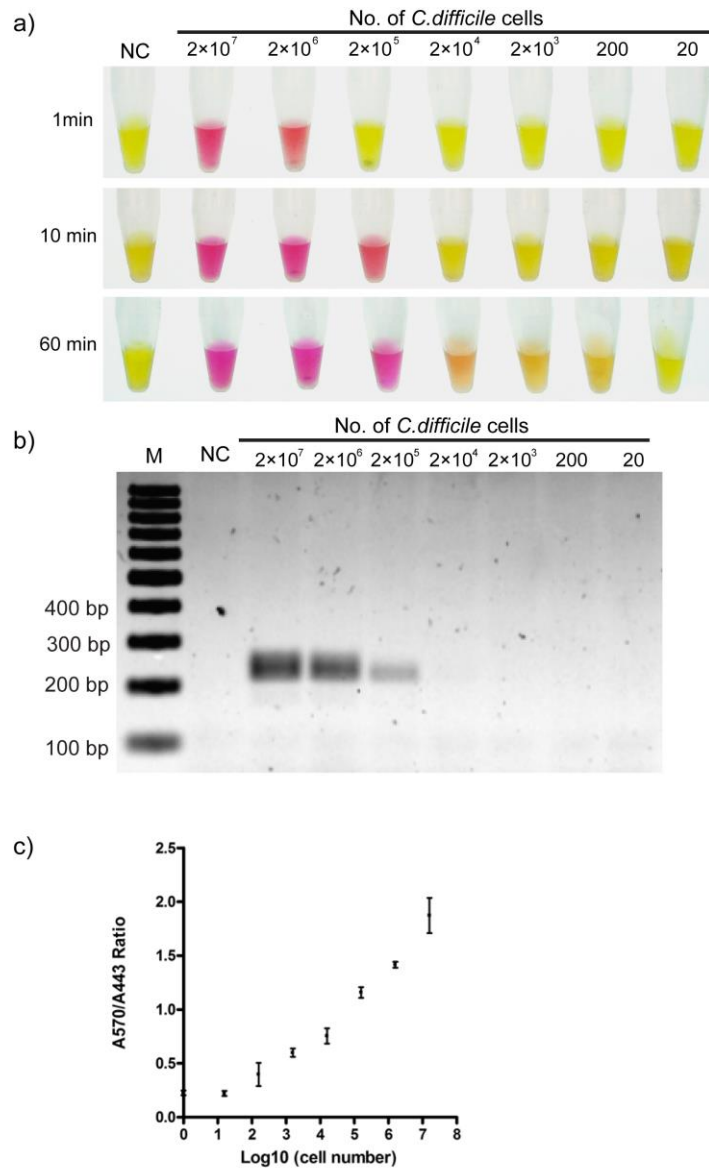
Figure 3-7. Sensitivity of PCR-litmus test for *C. difficile* detection. 28 cycles of PCR were performed with genome DNA prepared from various numbers of *C. difficile* cells. Strain ATCC 1803, forward primer P3 and reverse primer RP were used in this test. a) Litmus test with PCR products. The photograph was taken after a signal-producing time of 1 minute (top panel), 10 minutes (middle) and 60 minutes (bottom). b) Analysis of PCR products by 2% agarose gel electrophoresis. c) Quantification of PCR-litmus test. The absorbance of the reaction at 570 nm and 443 nm (A570 and A443) was measured. A570/A443 was plotted against cell numbers at logarithmic scale.

3.3.4 Validation of the PCR-litmus test in C. difficile strain identification

To further verify the accuracy of the assay in strain discrimination, we applied the assay towards genomic DNA extracted from 14 different strains of *C. difficile* (see Figure 3-8). In addition, the *tcdC* gene from all these strains were independently sequenced to confirm their identity. It was found that our PCR-litmus test accurately identified three 027/NAP1 strains and one 078/NAP7 strain of *C. difficile* in reference to the *tcdC* sequencing analysis and the documentation provided by ATCC.

Sample (ATCC)	Ribotype	tcdC Fragment	tcdC type	Pattern	Test
BAA-1801	010	–	no tcdC gene		
BAA-1803	027	1	Δ1stop-tcdC		
BAA-1804	053	23	wt-tcdC		
BAA-1805	027	1	Δ1stop-tcdC		
BAA-1812	024	24	wt-tcdC		
BAA-1814	251	21	wt-tcdC		
BAA-1870	027	1	Δ1stop-tcdC		
BAA-1871	001	2	wt-tcdC		
BAA-1872	207	3	wt-tcdC		
BAA-1875	078	5	TAAstop-tcdC		
43594	005	2	wt-tcdC		
43596	012	23	wt-tcdC		
43598	017	6	wt-tcdC		
43600	014	23	wt-tcdC		

Figure 3-8. PCR-litmus test with genomic DNA from 14 different *C. difficile* strains. The *tcdC* genes from all the strains were sequenced and their nucleotide sequences were compared with database entries by using PubMLST program. Ribotype of each strain is provided by ATCC. The photographs of test were taken at 30 minutes.

3.3.5 Detection of epidemic C. difficile strains in clinical samples

Evidence of a *C. difficile* infection can be determined non-invasively by analyzing a patient's stool sample. However, due to the composition and complexity of these samples, we next investigated the utility of our PCR-litmus assay in clinically relevant settings. We randomly selected stool samples of 12 CDI patients and 5 healthy donors obtained from St. Joseph's Healthcare (Hamilton, Canada). In addition, healthy stool samples were also spiked with known strains of *C. difficile* cells with a concentration of 10^8 cells/g. Total DNA from each sample was extracted using Powerfecal DNA isolate kit (MO BIO LABORATORIES, USA). 100 ng of total DNA from each sample was used for PCR amplification. From Figure 3-9, stool collected from healthy patients did not indicate colour change. All 3 spiked samples revealed colour patterns indicative of their respective spike strains. Of the 12 CDI patient samples, 4 presented a pattern of 027/NAP1 while the other 8 were identified as *C. difficile* (with *wt-tcdC*) but neither as 027/NAP1 nor 078/NAP7. These patterns are consistent to the sequencing results of *tcdC*. These tests demonstrated that our approach could potentially be used for clinical diagnosis.

Figure 3-9. PCR-litmus test with DNA from stool samples. The *tcdC* gene information was acquired by DNA sequencing. The photographs of test were taken at 30 minutes.

3.4 Summary

We have developed a novel assay that can sensitively and specifically detect mutations in the *tcdC* gene to identify epidemic strains of *C. difficile*. This assay relies on the difference in PCR amplification efficiency by using 3′ matched and 3′ mismatched primers to detect virulence-related mutations. By taking advantage of a reporting system based on pH increase by urease, this assay can provide a colorimetric detection of PCR products without using complex and expensive equipment. In addition, through the combined effect of a double amplification system of PCR and hydrolytic activity of urease, PCR-litmus test exhibits a great sensitivity in *C. difficile* detection. Another advantage is the platform's accuracy and robustness in discriminating epidemic strains of *C. difficile* in a complex matrix such as stool. To the best of our knowledge, this is the first time an assay is developed using regular PCR targeting *tcdC* gene to identify epidemic strains of *C. difficile*. It is also the first example where the product of PCR product detection is converted into a colorimetric pH test. This PCR-litmus design can be easily extended to other PCR-based applications simply by changing the primers. Considering the ubiquitous nature of PCR in biology, medical, and environmental field, we envision that the PCR-litmus design will add value to cheaper and simpler means of detection.

3.5 Experiments

3.5.1 Materials

All DNA oligonucleotides were prepared by automated DNA synthesis using standard phosphoramidite chemistry (Integrated DNA Technologies, Coralville, IA, USA) and purified by 10% denaturing (8 M urea) polyacrylamide gel electrophoresis (dPAGE). Their concentrations were determined spectroscopically. Deoxynucleoside 5′-triphosphates (dNTPs) were purchased from Thermo Scientific (Ottawa, ON, Canada). Thermus thermophilus DNA polymerase was acquired from Biotools. Streptavidin-coated magnetic beads of 1.5 μm (BioMag-SA) was purchased from Bangs Laboratories Inc. Urease powder from Canavaliaensiformis (Jack bean), maleimidobenzoic acid N-hydroxy-succinimide ester (MBS) and phenol red were obtained from Sigma-Aldrich. Water was purified with a Milli-Q Synthesis A10 water purification system. All other chemicals were purchased from Bioshop Canada and used without further purification.

Table 3-1. Sequences used in the PCR-litmus test.

Name	Sequences (5′-3′)
P1	Bio-CTCTACTGGCAT TTATTT TGGT
P2	Bio-CATGAGGAG GTCATTTCTAATT
P3	Bio-AGAAACTTTAAATAGCAAATTGTCTG
RP	CTTGACACTATTACGCACGCTTCACTATTTTTTTTT T-iSp9-TACCAGTATCATATCCTTTCTTCTC
NH$_2$-DNA	AmMC6T- TTTTTTAGTGAAGCGTGCGTAATAGTG TCAAG
FP-F	TTAATTAATTTTCTCTACAGCTATCC
RP-F	TCTAATAAAAGGGAGATTGTATTATG

Note: "Bio" represents biotin, "AmMC6T" represents amino modifier C6, and "iSp9" in the middle of the sequence is a triethylene glycol linker to stop extension of polymerase.

3.5.2 Bacterial strains and routine culture conditions

A panel of 14 *C. difficile* strains obtained from the American Type Culture Collection (ATCC; Manassas, USA) was used in this study. Cells were cultured in cooked meat broth medium (Sigma-Aldrich) under anaerobic condition with gas mixture of 80% N_2, 10% CO_2, 10% H_2 in a Whitley Anaerobic Workstation (Don Whitley Scientific).

3.5.3 Total DNA extraction from bacteria strains

Cells were grown in 5 mL of cooked meat broth medium until OD_{600} reached ~1. 200 μL of cultures were spun down (11000g, 5 min) in order to remove the culture medium; and the obtained pellets were suspended in 200 μL of 5% Chelex 100 (Bio-Rad) with 0.2 mg protease K. The mixture was then vortexed and incubated at 56°C for 30 min and then 95°C for 15 min. After centrifugation for 10 min at 10000 g, the supernatant was transferred into a fresh tube and stored at 4°C until PCR testing.

3.5.4 PCR primer design

For *tcdC* gene, primer design was conducted with the OligoAnalyzer 3.1(http://www.idtdna.com/calc/analyzer) after alignment of 26 *tcdC*_fragment gene sequences got from PubMLST (http://pubmlst.org/). All primers were checked using the alignments of sequences, and subsequently with the basic local alignment search tool (BLAST; http://www.ncbi.nlm.nih.gov/BLAST/). Secondary structures and self-pairing of all primers were also checked with the OligoAnalyzer 3.1. All primers are listed in Table 3-1.

3.5.5 PCR reaction

The PCR mixture (50 µL) contained 200 ng of DNA, 0.5 µM of forward primer (P1, P2 or P3) and reverse primer (RP), 200 µM of dNTPs (dATP, dCTP, dGTP and dTTP), 1× PCR buffer (75 mM Tris-HCl, pH 9.0, 2 mM $MgCl_2$, 50 mM KCl, 20 mM $(NH_4)_2SO_4$) and 1 units of Thermus thermophilus (Tth) DNA polymerase. The DNA was amplified using the following thermocycling steps: 94 ℃ for 5 min; 28 cycles of 94 ℃ for 1 min, 60 ℃ for 1 min and 72 ℃ for 1 min; 72 ℃ for 3 min.

3.5.6 DNA-urease conjugation

Urease-DNA was prepared according to a previously reported method[13]. An MBS solution (6.4 mM) was made by dissolving 2 mg MBS (6.4 µmol) in 1 mL of dimethyl sulphoxide (DMSO). Similarly, a urease solution was produced by dissolving 1.5 mg urease (3.3 nmol) powder in 1 mL of 1× PBS buffer (pH 7.2). 10 nmol NH_2-DNA and 3.2 µL of the MBS solution (20 nmol) were mixed and adjusted to a final reaction volume of 400 µL with 1× PBS buffer, and allowed to react at room temperature. After 30 min, the mixture was passed through a membrane-based molecular sizing centrifugal column with a molecular weight cut-off of 3,000 Daltons (NANOSEP OMEGA, Pall Incorporation) in order to remove excess MBS. The column was washed with 50 µL of 1× PBS buffer 3 times and the DNA was resuspended in 100 µL of 1× PBS buffer. The urease solution (1 mL, 3.3 nmol) was then added to the MBS activated DNA. The conjugation reaction was allowed to proceed at room temperature for 1 h. The mixture was filtered through a 300,000-Dalton

cut-off centrifugal column. The DNA-urease conjugate (UrD) was then washed with 50 μL of 1× PBS buffer 3 times and resuspended in 160 μL of 1× PBS buffer. The concentration of the UrD was estimated to be 20 μM.

3.5.7 Conjugate quantification

The average loading of DNA per urease can be calculated by measuring the absorbance at 260 and 280 nm. The concentration of the conjugate can be calculated as follows:[37]

$$A_{260UrD} = A_{260urease} + A_{260DNA} \qquad (1)$$

$$A_{280UrD} = A_{280urease} + A_{280DNA} \qquad (2)$$

$$A_{260DNA} / A_{280DNA} = \alpha \qquad (3)$$

$$A_{260urease} / A_{280urease} = \beta \qquad (4)$$

As shown in Figure 3-10, the ratio α and β of the absorbance at 260 and 280 nm of NH$_2$-DNA (α =1.72) and urease (β = 0.72) were determined by using Nanovue plus spectrophotometer. Insertion of Eqs. 3 and 4 into 1 and 2, respectively, leads to Eqs. 5 and 6

$$A_{260UrD} = \beta A_{280urease} + A_{260DNA} \qquad (5)$$

$$A_{280UrD} = A_{280urease} + (A_{260DNA} \times 1/\alpha) \qquad (6)$$

Insertion of Eqs.5 into 6, leads to

$$A_{260DNA} = (\alpha A_{260UrD} - \alpha\beta A_{280UrD})/(\alpha-\beta) \qquad (7)$$

$$A_{280urease} = (\alpha A_{280UrD} - A_{260UrD})/(\alpha-\beta) \qquad (8)$$

The absorbance of UrD was determined to be 0.278 at 260 nm and 0.235 at 280 nm. By insertion to Eqs. 7 and 8,

$$A_{260DNA} = (1.72 \times 0.278 - 1.72 \times 0.72 \times 0.235) / (1.72-0.72) = 0.187$$

$$A_{280urease} = (1.72 \times 0.235 - 0.278) / (1.72-0.72) = 0.126$$

Then, according to Lambert-Beers-Law: $c = A/(\varepsilon \times L)$, we can get

$$c_{DNA} = A_{260DNA}/(\varepsilon_{DNA} \times L) \qquad (9)$$

$$c_{urease} = A_{280urease}/(\varepsilon_{urease} \times L) \qquad (10)$$

According to OligoAnalyzer 3.1 (http://www.idtdna.com/calc/analyzer), ε_{260} of NH_2-DNA is 316,900 $M^{-1} \cdot cm^{-1}$. Based on previous study[38], ε_{280} of Jackbean urease monomer is 54,780 $M^{-1} \cdot cm^{-1}$. Here, L is 0.05 cm when using Nanovue plus spectrophotometer. Taking into Eqs. 9 and 10,

$$c_{DNA} = 0.187 / (316900\ M^{-1} \cdot cm^{-1} \times 0.05\ cm) = 11.8\ \mu M$$

$$c_{urease} = 0.126 / (54780\ M^{-1} \cdot cm^{-1} \times 0.05\ cm) = 46.0\ \mu M$$

Based on above calculations, the UrD concentration was 11.8 μM of DNA equals to about 46.0 μM of urease monomer. If ureases are in the form of monomers, the DNA/urease ratio will be 0.26. However, Jackbean ureases are known to exist in the form of homohexamers, the DNA/urease ratio will be 1.54.
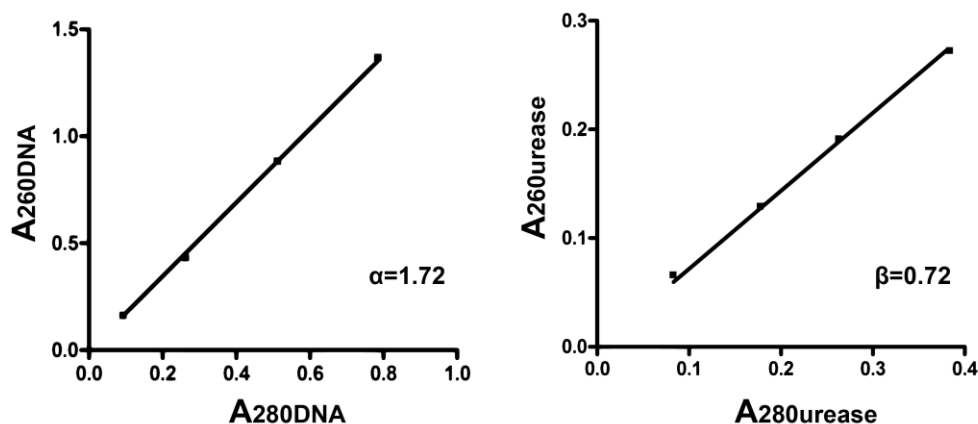
Figure 3-10. Determination of ratio α and β of the absorbance at 260 and 280 nm of NH_2-DNA and urease.

3.5.8 Litmus test

50 µL of the above PCR reaction mixture was incubated with 50 µL of binding buffer (10 mM Tris-HCl, pH 7.5, 3M NaCl, 1 mM $MgCl_2$, 0.01% tween 20) along with 10 µL of magnetic beads (MB) for 15 minutes. Then it was placed in a magnet holder to separate the supernatant and MB. Then the MB was suspended in 100 µL of binding buffer with 1 µL of 1 µM UrD (1 pmol). After 15 min of incubation, MB was washed with 100 µL of binding buffer four times and then resuspended in 70 µL of acetic acid buffer (0.1 mM, pH 5). Then 10 µL of 0.04% phenol red and 100 µL of substrate solution (3 M NaCl, 60 mM $MgCl_2$, 50 mM urea) were added. Note that this substrate solution should have a starting pH of 5.0. A photograph was taken after a signal-producing time of 0-1 h according to individual experiments.

3.5.9 Sequencing of tcdC genes

Each *tcdC* gene was amplified by PCR as previously described[33]. The reaction mixture contained $1\times$ PCR buffer, 200 pmol of each dNTPs, 25 pmol of the FP-F and RP-F (Table 3-1), and 1 U of Tth DNA polymerase. The template was denatured for 5 min at 94°C, and DNA was amplified for 30 cycles consisting of 1 min at 94°C, 1 min at 50°C, and 1 min at 72°C. The PCR products were sequenced at the Mobix Lab (McMaster University). The nucleotide sequences were compared with database entries by using the PubMLST program.

3.5.10 Sensitivity test

A single colony of strain ATCC1803 from an anaerobic cooked meat broth agar plate was taken and cultured in 5 mL of cooked meat broth medium overnight. The bacterial culture was then diluted in 10-fold intervals seven times with cooked meat broth medium; 100 μL of 10^{-5}, 10^{-6} and 10^{-7} dilutions were placed on a cooked meat broth plate and cultured for colony development in order to calculate the cell numbers (average colony-forming units) for each dilution. Meanwhile, 200 μL of each diluted cultures were used for DNA extraction and PCR reaction.

3.5.11 Stool sample test

The Stool samples used in this study were obtained from St. Joseph's Healthcare. Stool samples from 5 healthy donors and 12 patients infected by *C. difficile* were used in

this study. 3 spiked samples were also prepared by adding $\sim 2 \times 10^7$ *C. difficile* cells (ATCC 1870, ATCC1871 or ATCC1875) into 200 mg of stool sample from healthy donors. A Powerfecal DNA isolate kit (MO BIO LABORATORIES, USA) was used to extract total DNA from stool samples, and 100 ng of total DNA from each sample was used as template DNA for PCR-litmus test. The DNA was amplified using the following thermocycling steps: 94 ℃ for 5 min; 30 cycles of 94 ℃ for 1 min, 60 ℃ for 1 min and 72 ℃ for 1 min; 72 ℃ for 3 min.

3.6 References

1.   Saiki, R. K. *et al.* Primer-directed enzymatic amplification of DNA with a thermostable DNA polymerase. *Science* **239,** 487–491 (1988).

2.   Li, H. H. *et al.* Amplification and analysis of DNA sequences in single human sperm and diploid cells. *Nature* **335,** 414–7 (1988).

3.   Mullis, K. B. & Faloona, F. A. [21] Specific synthesis of DNA *in vitro* via a polymerase-catalyzed chain reaction. *Methods Enzymol.* **155,** 335–350 (1987).

4.   Mullis, K. B. The unusual origin of the polymerase chain reaction. *Scientific American* **262,** 56–61, 64–65 (1990).

5.   Law, J. W.-F., Ab Mutalib, N.-S., Chan, K.-G. & Lee, L.-H. Rapid methods for the detection of foodborne bacterial pathogens: principles, applications, advantages and limitations. *Front. Microbiol.* **5,** 770 (2014).

6.   Yamamoto, Y. PCR in diagnosis of infection: detection of bacteria in cerebrospinal fluids. *Clin. Diagn. Lab. Immunol.* **9,** 508–514 (2002).

7.   Erlich, H. A., Gelfand, D. & Sninsky, J. J. Recent advances in the polymerase chain reaction. *Science* **252,** 1643–51 (1991).

8.   Murakami, K. *et al.* Identification of methicillin-resistant strains of staphylococci by polymerase chain reaction. *J. Clin. Microbiol.* **29,** 2240–2244 (1991).

9.   Chan, K. *et al.* A rapid and low-cost PCR thermal cycler for infectious disease diagnostics. *PLoS One* **11,** e0149150 (2016).

10.   Wong, G., Wong, I., Chan, K., Hsieh, Y. & Wong, S. A Rapid and Low-Cost PCR Thermal Cycler for Low Resource Settings. *PLoS One* **10,** e0131701 (2015).

11.   Agrawal, N., Hassan, Y. A. & Ugaz, V. M. A pocket-sized convective PCR thermocycler. *Angew. Chemie - Int. Ed.* **46,** 4316–4319 (2007).

12.   Marx, V. PCR heads into the field. *Nat. Methods* **12,** 393–397 (2015).

13.   Tram, K., Kanda, P., Salena, B. J., Huan, S. & Li, Y. Translating bacterial detection by DNAzymes into a litmus test. *Angew. Chemie - Int. Ed.* **53,** 12799–12802 (2014).

14.   Leffler, D. A. & Lamont, J. T. *Clostridium difficile* Infection. *N. Engl. J. Med.* **372,** 1539–1548 (2015).

15.   Ekma, N., Yee, L. Y. & Aziz, R. A. Prevalence of *Clostridium difficile* infection in Asian countries. *Rev. Med. Microbiol.* **23,** 1–4 (2012).

16. M., R., M.H., W. & D.N., G. *Clostridium difficile* infection: New developments in epidemiology and pathogenesis. *Nat. Rev. Microbiol.* **7,** 526–536 (2009).

17. McDonald, L. C. *et al.* An epidemic, toxin gene-variant strain of *Clostridium difficile*. *N. Engl. J. Med.* **353,** 2433–41 (2005).

18. Loo, V. G. *et al.* A predominantly clonal multi-institutional outbreak of *Clostridium difficile*-associated diarrhea with high morbidity and mortality. *N. Engl. J. Med.* **353,** 2442–9 (2005).

19. Warny, M. *et al.* Toxin production by an emerging strain of *Clostridium difficile* associated with outbreaks of severe disease in North America and Europe. *Lancet* **366,** 1079–1084 (2005).

20. Pépin, J., Valiquette, L. & Cossette, B. Mortality attributable to nosocomial *Clostridium difficile*-associated disease during an epidemic caused by a hypervirulent strain in Quebec. *CMAJ* **173,** 1037–1041 (2005).

21. Goorhuis, A. *et al.* Emergence of *Clostridium difficile* infection due to a new hypervirulent strain, polymerase chain reaction ribotype 078. *Clin. Infect. Dis.* **47,** 1162–70 (2008).

22. Jhung, M. A. *et al.* Toxinotype V *Clostridium difficile* in humans and food animals. *Emerg. Infect. Dis.* **14,** 1039–1045 (2008).

23.   Rupnik, M., Widmer, A., Zimmermann, O., Eckert, C. & Barbut, F. *Clostridium difficile* toxinotype V, ribotype 078, in animals and humans. *Journal of Clinical Microbiology* **46,** 2146 (2008).

24.   Costa, M. C. *et al.* Prevalence and molecular characterization of *Clostridium difficile* isolated from feedlot beef cattle upon arrival and mid-feeding period. *BMC Vet. Res.* **8,** 38 (2012).

25.   Planche, T. *et al.* Diagnosis of *Clostridium difficile* infection by toxin detection kits: a systematic review. *The Lancet Infectious Diseases* **8,** 777–784 (2008).

26.   Longtin, Y. *et al.* Impact of the type of diagnostic assay on *Clostridium difficile* infection and complication rates in a mandatory reporting program. *Clin. Infect. Dis.* **56,** 67–73 (2013).

27.   Bélanger, S. D., Boissinot, M., Clairoux, N., Picard, F. J. & Bergeron, M. G. Rapid detection of *Clostridium difficile* in feces by real-time PCR. *J. Clin. Microbiol.* **41,** 730–734 (2003).

28.   Citron, D. M. *et al.* Typing and susceptibility of bacterial isolates from the fidaxomicin (OPT-80) phase II study for *C. difficile* infection. *Anaerobe* **15,** 234–236 (2009).

29.   Brazier, J. S. Typing of *Clostridium difficile*. *Clin. Microbiol. Infect.* **7,** 428–431 (2001).

30. Braun, V., Hundsberger, T., Leukel, P., Sauerborn, M. & Von Eichel-Streiber, C. Definition of the single integration site of the pathogenicity locus in *Clostridium difficile*. *Gene* **181,** 29–38 (1996).

31. Thelestam, M. & Chaves-Olarte, E. Cytotoxic effects of the *Clostridium difficile* toxins. *Curr Top Microbiol Immunol* **250,** 85–96 (2000).

32. Matamouros, S., England, P. & Dupuy, B. *Clostridium difficile* toxin expression is inhibited by the novel regulator TcdC. *Mol. Microbiol.* **64,** 1274–1288 (2007).

33. Spigaglia, P. & Mastrantonio, P. Molecular analysis of the pathogenicity locus and polymorphism in the putative negative regulator of toxin production (TcdC) among *Clostridium difficile* clinical isolates. *J. Clin. Microbiol.* **40,** 3470–3475 (2002).

34. Curry, S. R. *et al. tcdC* genotypes associated with severe TcdC truncation in an epidemic clone and other strains of *Clostridium difficile*. *J. Clin. Microbiol.* **45,** 215–221 (2007).

35. Dingle, K. E. *et al.* Clinical *Clostridium difficile*: Clonality and pathogenicity locus diversity. *PLoS One* **6,** e19993 (2011).

36. Wilmer, A. *et al.* Polymerase chain reaction assay to detect *Clostridium difficile tcdC* variants is valuable in characterizing hospital epidemiology. *J. Hosp. Infect.* **84,** 252–255 (2013).

37. Kukolka, F., Lovrinovic, M., Wacker, R. & Niemeyer, C. M. Covalent coupling of DNA oligonucleotides and streptavidin. *Methods Mol. Biol.* **283,** 181–96 (2004).

38.   Real-Guerra, R., Carlini, C. R. & Stanisçuaski, F. Role of lysine and acidic amino

acid residues on the insecticidal activity of Jackbean urease. *Toxicon* **71,** 76–83

(2013).

Chapter 4

Isolation of RNA-cleaving Fluorogenic Aptazymes for Identification of Epidemic Strains of *Clostridium difficile*

4.1 Abstract

Hypervirulent epidemic strains of *Clostridium difficile* can cause serious infectious diseases and there is a growing demand for molecular probes that can specifically identify them. Here we report four classes of RNA-cleaving fluorogenic aptazyme (RFA), RFA7-1, RFA7-2, RFA12-1, and RFA12-10, that have the potential to be used for *C. difficile* detection. These RFA probes were isolated through *in vitro* selection where a DNA pool containing a random-sequence DNA library was incubated with the crude extracellular mixture (CEM) derived from an epidemic strain of *C. difficile*, coupled with counter-selection steps to remove non-specific species cross-reactive to unintended *C. difficile* strains and other bacterial species. We have demonstrated that the four selected RFA probes are capable of generating unique cleavage patterns when incubating with CEM from *C. difficile* NAP1, NAP2, or NAP7 strains, and these cleavage patterns can be used for strain identification. Some strategies that allow the probes to specifically detect *C. difficile* have also been discussed in this chapter.

4.2 Introduction

As described in Chapter 1, the incidence and mortality of *C. difficile* infections (CDI) have increased dramatically over the past two decades[1,2]. This is largely associated with the emergence of several hypervirulent strains of *C. difficile,* such as 027/BI/NAP1 strain[3]. These strains not only appear to be more virulent but also show high resistance to antibiotics that are used for CDI treatment[4,5]. Early and specific detection of these pathogens is crucial in disease management and infection control. Molecular probes that can identify the epidemic strains of *C. difficile* are highly desirable.

Functional DNAs are single-stranded DNA molecules capable of forming well-defined structures to carry out molecular recognition and enzymatic catalysis[6,7]. DNA sequences that can bind specific targets are called aptamers; those with the ability to speed up a chemical transformation are termed DNAzymes; those capable of performing both functions are named aptazymes. All the functional DNA molecules are generated by a method called Systematic Evolution of Ligands by Exponential Enrichment (SELEX), or *in vitro* selection, a simple technique allowing for the isolation of desired functional DNA sequence from a random DNA pool[8,9]. Functional DNAs have been employed as molecular tools for a wide array of applications including biosensing, imaging, and therapeutics[8–12].

The functional DNA used in this study is an RNA-cleaving fluorogenic aptazyme (RFA). As depicted in Figure 4-1, it can perform three linked functions: target binding, enzymatic catalysis and fluorescence generation. These molecules are composed of two main components: 1) a DNA sequence that can sense and bind a ligand and perform a

catalytic function; 2) a stretch of DNA flanking a single RNA moiety that can be cleaved

by the DNA catalytic core (in orange). The RNA moiety is located between a fluorophore-

modified deoxythymine and a quencher-modified deoxythymine (fluorescein and dabcyl,

respectively). The proximity of the quencher to the fluorophore prevents fluorescence

emission. However, in the presence of target, the RFA catalyzes the cleavage of the single

RNA moiety, which separating the fluorophore from the quencher, thereby enhancing

fluorescence. Since the RFA can be mixed into contaminated samples to generate a

fluorescent signal, it can be used to develop a 'mix-and-read' type assay for the detection

of a target of interest[13–16].
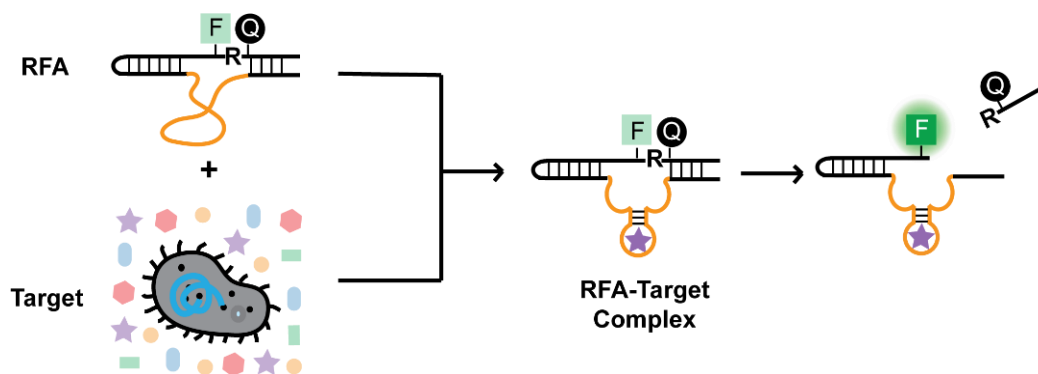
Figure 4-1. Conceptual design of RFA that fluoresce upon contact with the CEM produced by bacterial cells.

Recently, our group has successfully developed one RFA probe (RFA-CD1) for *C. difficile*[16]. RFA-CD1 shows exquisite specificity for a pathogenic strain of *C. difficile* (BI/027-H) which has been isolated from a CDI patient in St. Joseph's Healthcare-Hamilton

(Ontario, Canada). RFA-CD1 remains active in the fecal extracts of CDI patients allowing it to be directly used in fecal samples for detection of *C. difficile*. The discovery of RFA-CD1 and the verification of its functionality within clinical specimens represent a significant step towards our goal. The target of RFA-CD1 was identified to be TcdC, a transcription factor that regulates the expression of toxins A and B in *C. difficile*[17]. The TcdC expressed by *C. difficile* BI/027-H is not wild-type, but a TcdC variant that has a 6-amino acid deletion. RFA-CD1 can only be activated by this TcdC variant and cannot be cleaved by other types of TcdC, leading to the high strain-specificity of RFA-CD1. However, further studies indicated that *C. difficile* BI/027-H is not the epidemic strain BI/027/NAP1 despite the same restriction endonuclease analysis type (BI) and ribotype (027). RFA-CD1 was unable to detect the epidemic strain BI/027/NAP1 which does not express the TcdC variant. Therefore, we set to isolate new probes that can target the epidemic strains of *C. difficile*.

Herein, we present the RFAs that we isolated for the detection of epidemic strains of *C. difficile*. When live bacteria grow under nutritious conditions, they constantly exchange materials with their environment and leave behind a mixture of small or macromolecular substances that can be highly characteristic for each bacterium. This mixture was termed crude extracellular mixture (CEM). During the selection process, the CEM prepared from BI/027/NAP1 strain was utilized as target for positive-selection, and the CEM from unintended cell types, such as non-pathogenic strains, were used as target for counter-selection. The use of the combined positive-selection/counter-selection strategy

is intended to eliminate the sequences without strain-selectivity and ensure the derived

RFAs have high specificity for the intended strain.

4.3 Results

4.3.1 In vitro selection

L1:   5'-CAA CCT AAA CTC CCT ACAC C-N_{50}-TGA TGT GGA AGC AGA TGT CG

FS1:   5'-CAT CAG ACT CCG-**Q**-R-**F**-AAC CTC ACT ACC AAG

FP1:   5'-CAA CCT AAA CTC CCT ACAC C

RP1:   5'-CGA CAT CTGCTT CCA CAT CA

RP2:   5'-AAAAAAAAAAAAAAAAAAAA-L-CGA CAT CTGCTT CCA CAT CA

LT1:   5'-G AGT TTA GGT TGC TTG GTA GTG AGG
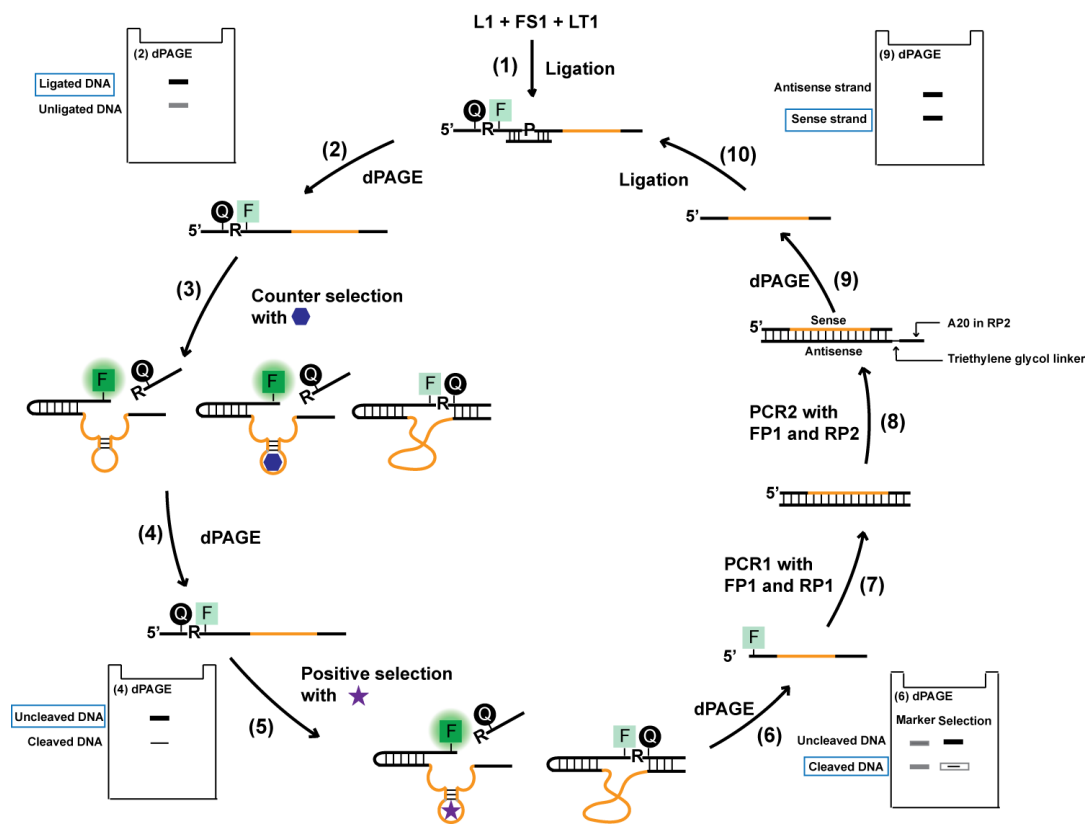
Figure 4-2. *In vitro* selection scheme for RNA-cleaving fluorogenic aptazyme. The DNA sequences used in the selection are shown in the top panel.

The *in vitro* selection strategy was similar to the one employed in our previous study[15,16]. A pool of 10^{14} DNA molecules, containing 50 random nucleotides, was used for *in vitro* selection experiment. The *in vitro* selection scheme is shown in Figure 4-2. 2 nmol of L1 was first phosphorylated and ligated to FS1 that contained a single ribonucleotide as the cleavage site. Upon purification using denaturing gel electrophoresis (dPAGE), the ligated construct was first incubated with selection buffer (SB; 50 mM HEPES, pH 7.5, 150 mm NaCl, 15 mm $MgCl_2$, and 0.01% Tween 20) for 3 hours at room temperature to eliminate self-cleaving sequences. The activity of these self-cleaving sequences is often promoted in the presences of buffers containing divalent metal ions. The uncleaved DNA library was collected and used for positive selection. The target of positive selection was CEM prepared from *C. difficile* BI/NAP1/027. The cleavage product was then purified by dPAGE and subject to two polymerase chain reactions. The first PCR (PCR1) used two standard primers, forward primer FP1 and reverse primer RP1; however, the reverse primer (RP2) used in the second PCR reaction (PCR2) contains an A20 tail separated by a non-amplifiable linker. Therefore, PCR2 produced two DNA strands with different sized, permitting the separation of the coding strand by dPAGE. The purified DNA was then used as the DNA pool for the next cycle of selection enrichment. From the second round, around 200 pmol of DNA library was used in the selection as this was the final yield obtained following the purification of PCR2. A counter-selection step was performed in each round against the unintended target (Figure 4-3a). In order to isolate highly efficient RFAs, the reaction time in the positive-selection step was reduced from 3 hours in round 1 to 30 minutes in round 8. Meanwhile, the incubation time in the counter-selection step was

extended to 17 hours after round 8 to further eliminate nonspecific species. By round 12,

approximately 2.3% of cleavage was detected after 17 hours of counter selection, and 1.2%

of cleavage was observed after 30 minutes of positive selection (see Figure 4-3b). The DNA

population at the end of the 7th round and 12th round were sent for deep sequencing analysis.

a)

	R1	R2-3	R4-7	R8	R9-12
Counter selection	SB (3H)	CM (3H)	NAP2,4,7 CEM(3H)	Other bacteria CEM(17H)	NAP2,4,7 CEM(17H)
Positive selection	NAP1 CEM(3H)	NAP1 CEM(2H)	NAP1 CEM(1H)	NAP1 CEM(0.5H)	NAP1 CEM(0.5H)

b)
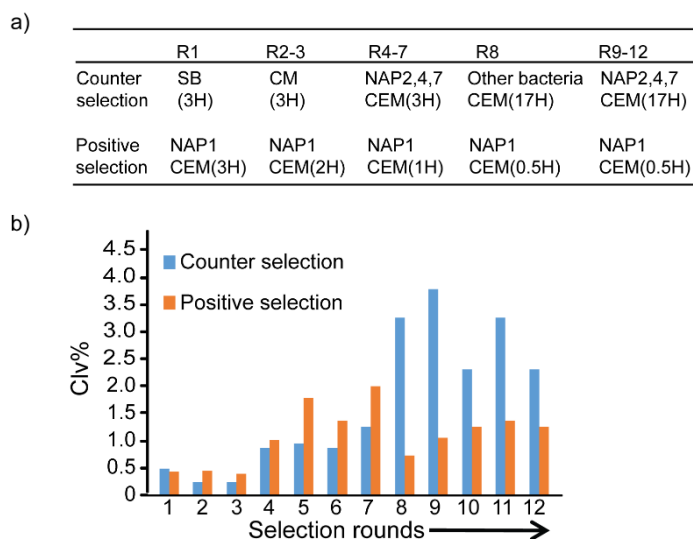
Figure 4-3. *In vitro* selection a) Strategies and b) progress. SB: selection buffer. CM: cooked meat broth media. Other bacteria: *Escherichia coli Δrna*, and *Streptococcus salivarius*. The cleavage rate percentages (Clv%) at each round was quantified using ImageQuant 5.2.

4.3.2 Identification of RFA probes targeting C. difficile

Deep sequencing results from round 7 revealed a total of 208,635 classes of

sequences. The most dominant class is named RFA7-1, which accounts for 0.017% of the

DNA pool. At round 12, the sequence diversity decreased, and a total of 70,682 classes was

found in the DNA pool. Meanwhile, the level of enrichment improved as indicated by the

increased frequency of the top classes. The top classes from round 7 and 12 were ordered

and tested. Four classes of *C. difficile*-responsive RFAs (RFA7-1, RFA7-2, RFA12-1,

RFA12-10) were discovered. As shown in Figure 4-4a, the rank and frequency of these classes changed drastically during selection, especially those of for RFA12-10. This could be attributed to the adjustment of the selective pressure after round 8 as previously described (see Figure 4-3a).

The sequence information of the four RFA classes is provided in Figure 4-4b. Their recognition specificities towards *C. difficile* strains were examined by dPAGE analysis. The CEMs prepared from 7 strains of *C. difficile* were tested. The detailed information on these strains is summarized in Table 4-1. The cleavage of RFAs was expected to generate two DNA fragments; the 3′-fragment carries the fluorophore and can be detected by fluorescence imaging, and the 5′-fragment does not fluoresce. As shown in Figure 4-4c, the absence of cleavage bands in the negative controls suggests that the isolated RFAs are not self-cleaving DNAzymes. Meanwhile, all *C. difficile*-CEMs induced cleavage of each of the RFAs. This indicated that the RFAs did not have strain-specificity and that activators of the RFAs probably exist in the CEM from all tested strains. Moreover, as indicated by their cleavage percentages, the RFAs generally had low cleavage efficiency. Low cleavage activity of 5% or less (except for the reaction involving RFA12-10 and ATCC1872, 13%) was observed after 4 hours of incubation. We also noticed that the RFAs might not have the same activator in CEM. For example, the CEM from the NAP2 strain generated a relatively high cleavage (44%) of RFA12-10 and a low cleavage (4%) of RFA7-2. The NAP7 strain, on the other hand, produced a relatively low cleavage (7%) of RFA12-10 and a high cleavage (19%) of RFA7-2. This difference suggests that RFA12-10 and RFA7-2 are primarily activated by different molecules and the concentration of the molecules were

different in the NAP2 strain from the NAP7 strain. Based on these discoveries, ratiometric-

based strategies could be applied to identify the different *C. difficile* strains.
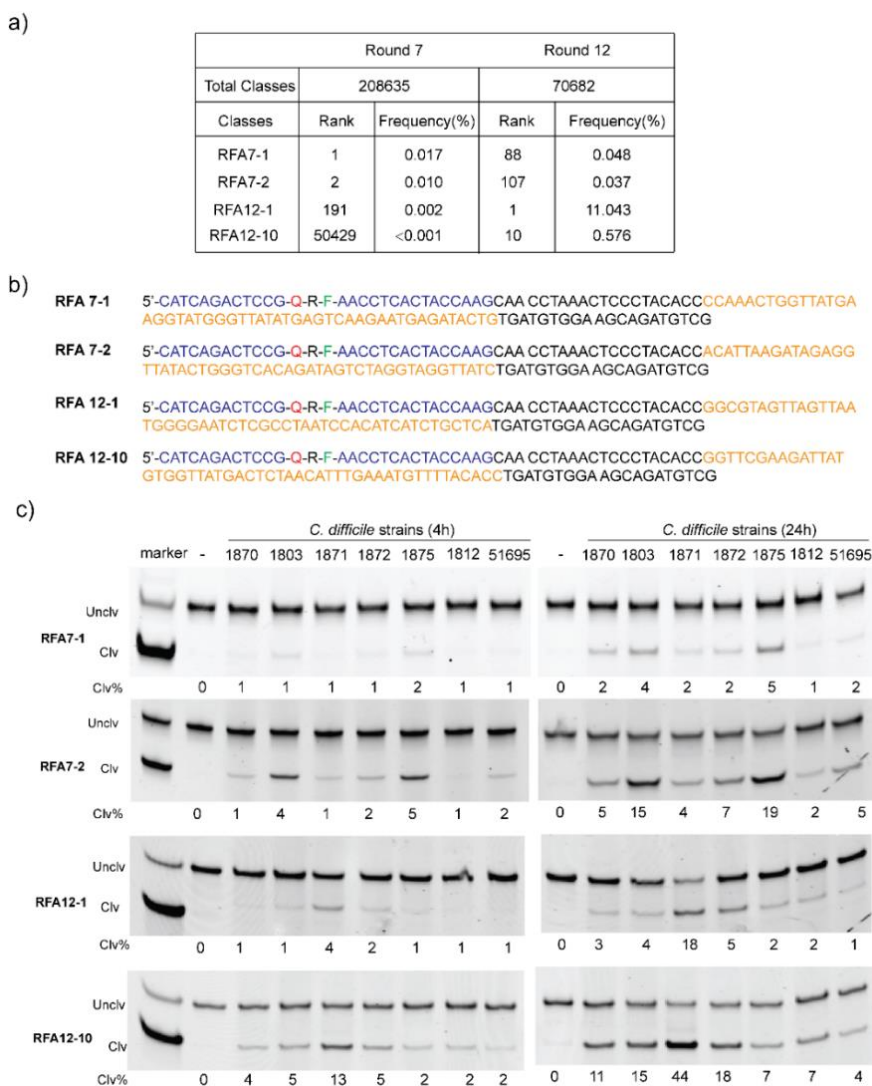
Figure 4-4. Characterization of the RFA classes isolated through *in vitro* selection. a) Deep sequencing analysis. b) Sequence information for the four RFA classes. FS1 is in blue. The isolated sequences are in orange. Q: Debcyl-dT. R: adenine ribonucleotide. F: fluorescein-dT. c) Responses of RFA probes towards CEMs prepared from different *C. difficile* strains. Unclv: uncleaved RFA probes; Clv: cleaved RFA probes; Clv% = $(F_{Clv}/6)/[(F_{Clv}/6) + F_{Unclv})]$. F_{Clv} and F_{Unclv}: fluorescence intensity of cleaved and uncleaved fractions of RFA probe. Note that cleavage leads to six-fold fluorescence enhancement, which was taken into consideration for cleavage percentage calculation. M: marker for cleavage. NC: Negative control (RFAs in the selection buffer)**.**

4.3.3 Identification of C. difficile strains using multiple RFAs

Four *C. difficile* strains, NAP1 (ATCC1870), NAP1 (ATCC1803), NAP2 (ATCC1871) and NAP7(ATCC1875) were tested with the isolated RFA classes (RFA7-1, RFA7-2, RFA12-1, and RFA12-10). As shown in Figure 4-5a, the four RFA classes generated distinct cleavage patterns towards each strain. The cleavage percentages were calculated and are presented in Figure 4-5b. Both NAP1 strains (ATCC 1870 and ATCC 1803) produced a similar pattern with the highest cleavage of RFA12-10 and the second highest cleavage of RFA 7-2. The NAP2 strain also induced the highest cleavage of RFA12-10, but the second highest is of RFA 12-1. The NAP7 strain, however, produced the highest cleavage of RFA 7-2. Therefore, based on the cleavage patterns of the four RFA classes towards each strain, we can successfully discriminate between *C. difficile* epidemic strain NAP1, NAP7, and nonepidemic strain NAP2. The results here, suggest we can potentially identify a specific strain of *C. difficile* using multiple RFA probes together, however, further experiments are still required to validate this approach.
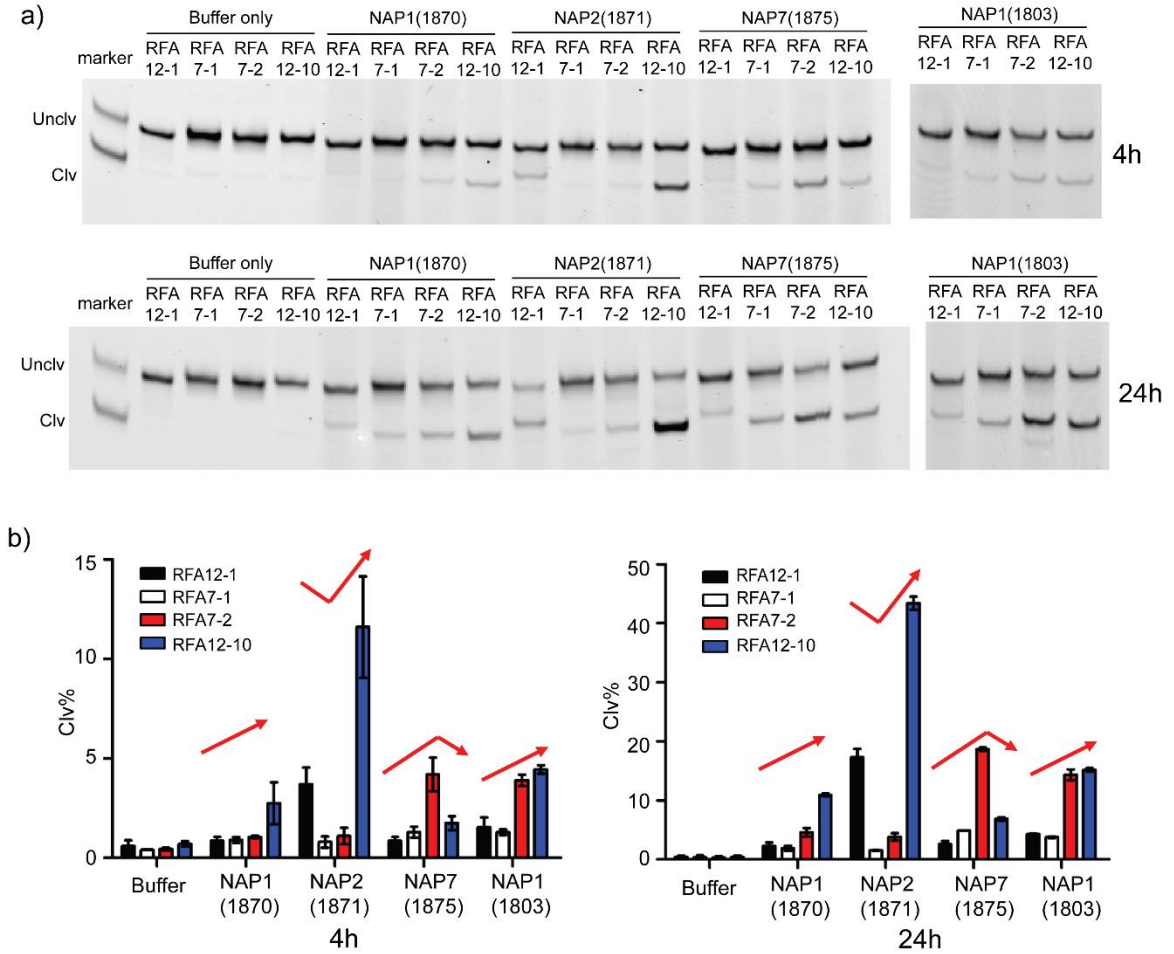
Figure 4-5. Discrimination of *C. difficile* strains using multiple RFA probes. a) 10% dPAGE analysis of the cleavage reaction between RFA probe (RFA12-1, RFA7-1, RFA7-2 or RFA12-10) and CEM prepared from *C. difficile* (ATCC1870, ATCC1871, ATCC1875, or ATCC1803) after an incubation time of 4 hours and 24 hours. b) The percentage cleavage (Clv%) of the reactions. The cleavage rate percentages were calculated using ImageQuant 5.2. Error bars denote standard deviation (n=2). The red arrows indicate the different cleavage patterns.

4.3.4 Determination of the species-specificity of the RFAs

Next, the species-specificity of the RFA classes were examined. The cleavage activities of the four RFA classes (RFA7-1, RFA7-2, RFA12-1, RFA12-10) were tested in response to the CEM of 12 bacterial species including five Gram-positive bacteria and seven Gram-negative bacteria as shown in Figure 4-6. After 4 hours of incubation, we found that RFA classes were activated not only by *C. difficile* but also by several other bacterial species. A clear cleavage signal was observed when RFA7-1, RFA7-2, or RFA12-10 was incubated with the CEM from *Fusobacterium nucleatum*, a pathogenic bacterium with previously demonstrated association with colon cancer[18]. Both RFA12-1 and RFA 12-10 generated a cleavage signal when reacting with the CEM from *Listeria monocytogenes,* a foodborne pathogen which has been responsible for multiple food contamination outbreaks in recent years[19]. The fact that the CEMs from *F. nucleatum* and *L. monocytogenes* were not used as counter-selection targets during *in vitro* selection explains the cross-reactivity of the isolated probes to these bacteria. We also found that several bacteria including *Escherichia coli, Salmonella enterica* and *Shigella sonnei,* induced nuclease degradation of the RFAs based on the nonspecific banding patterns on the dPAGE gel. These bacteria are all from the phylum of *Proteobacteria* which are known to express ribonucleases with the highest diversity [20].
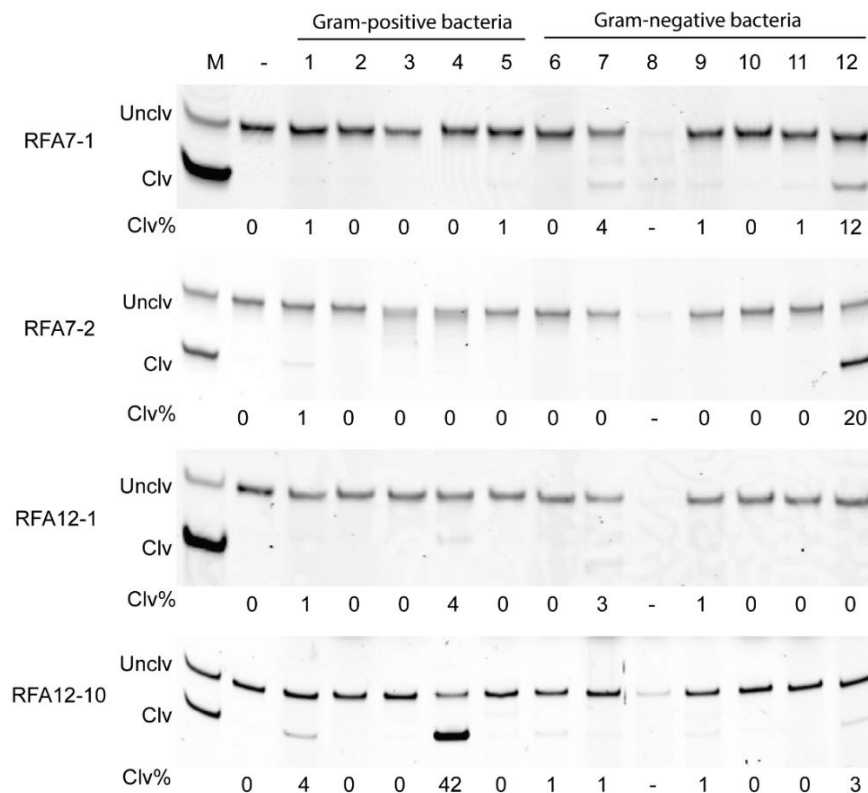
Figure 4-6. Responses of RFA classes to CEMs prepared from various bacteria. Lane 1-5: *C. difficile* (ATCC1870), *Streptococcus salivarius, Bacillus subtilis, Listeria monocytogenes, and Actinomyces orientalis.* Lane 6-12: *Klebsiella aerogenes, Escherichia coli, Salmonella enterica, Shigella sonnei, Legionella pneumophila, Bacteroides fagillis,* and *Fusobacterium nucleatum.* Incubation time: 4 hours.

4.3.5 Strategies to eliminate the problem of low species-specificity of the RFAs

The low species-specificity of the RFAs limit their usefulness in the identification of *C. difficile.* In this section, several strategies are discussed that can help achieve specific detection of *C. difficile* by these probes, despite their low specificity. For example, RFA7-2, as previously discussed is cleaved in the presence of the CEM from both *C. difficile* and *F. nucleatum.* However, here we propose strategies that allow RFA7-2 to specifically detect *C. difficile.*

Although both *C. difficile* and *F. nucleatum* can activate RFA7-2, the molecular target from the CEMs can be different. If one target is proteinaceous and the other one is non-proteinaceous, then proteinase inhibitors can be employed to help discriminate between the two bacteria. Here we treated the CEM from *C. difficile* (CEM-CD) and *F. nucleatum* (CEM-FN) with proteinase K and found that both CEMs after proteinase-treatment were unable to activate the RFA7-2 (Figure 4-7a). This suggests the target of RFA7-2 in both cases are proteins. Thus, the strategy of using proteinase-treatment to distinguish between *C. difficile* and *F.* nucleatum is not applicable.

Similarly, RNase inhibitor-treatment can help discriminate between RNase-mediated cleavage signal and non-RNase mediated cleavage signal. To examine whether the protein target that exists in the CEMs is a ribonuclease, we treated CEM-CD and CEM-FN with RNase Inhibitor (SUPERase). This treatment did not cause any activity reduction signifying the target of RFA7-2 in both CEMs are not RNases (Figure 4-7b).

We next evaluated the heat-resistance of the protein target in CEM-CD and CEM-FN. Both CEMs were heated at 90 °C for various durations ranging from 0 to 60 minutes and then incubated with RFA7-2 for 4 hours. The cleavage activity induced by CEM-CD was abolished entirely after 30 minutes of heat-treatment (Figure 4-7c). However, CEM-FN heated at 90 °C for 1 hour still generated a clear, albeit reduced, cleavage signal. This suggests that the protein target in CEM-FN is more heat-resistant compared to CEM-CD. Based on this discovery, we propose that a heat-treatment step can be incorporated into our RFA approach to distinguish *C. difficile* and *F. nucleatum* as demonstrated in Figure 4-7d.
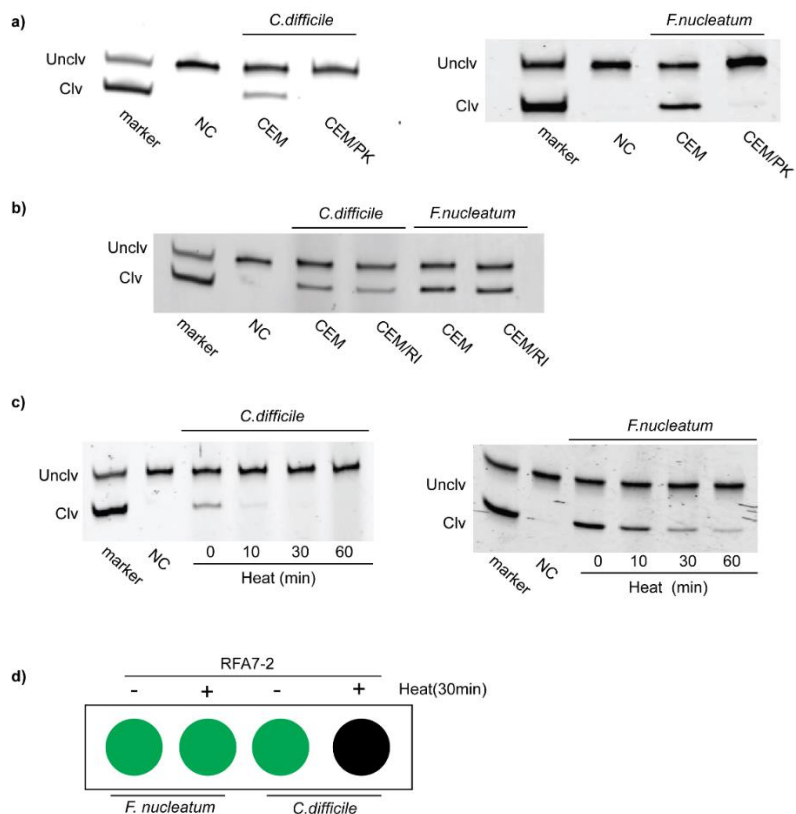
Figure 4-7. Investigation of strategies that allow RFA7-2 to specifically detect *C. difficile.* a) Responses of RFA7-2 to protease-treated CEMs. PK: proteinase K. b) Responses to RFA7-2 to RNase inhibitor-treated CEMs. RI: SUPERase In. RNase inhibitor. c) Responses of RFA7-2 to heat treated-CEMs from *C. difficile* and *F. nucleatum. C. difficile* ATCC1803 were used in the above tests. Heating temperature: 90 °C. d) strategy of using heat-treatment to discriminate between *F. nucleatum* and *C. difficile.* Green circle: positive signal. Black circle: negative signal.

Also, our group has already developed several RFAs targeting *E. coli*[20], *L. monocytogenes* (unpublished) and *F.* nucleatum (unpublished). These probes exhibit high species-specificity and have no cross-activity with *C. difficile*. Thus, they can be used together with the probes isolated here to help discriminate between *C. difficile* and other bacteria.

4.4 Summary

In summary, through *in vitro* selection using the CEM prepared from epidemic strains of *C. difficile,* we have successfully isolated four *C. difficile* responsive RNA-cleaving aptazyme classes (RFA7-1, RFA7-2, RFA12-1, and RFA 12-10). Although none of the RFAs is strain-specific, they can be used together to generate unique cleavage patterns when conducting tests using the CEM from *C. difficile* epidemic strain NAP1, NAP7, and non-epidemic strain NAP2. These patterns show great potential for *C. difficile* epidemic strain identification. Although the activities and specificities of the RFAs are still under optimization, the discovery of these novel molecular probes for *C. difficile* presents opportunities for developing biosensors for identification of epidemic strains of *C. difficile* that can be translated into simple point-of-care devices.

4.5 Experiments

4.5.1 Enzymes, chemicals, and other materials

T4 polynucleotide kinase (PNK) and T4 DNA ligase were purchased from Thermo Scientific (Ottawa, ON, Canada). Urea (ultrapure) and 40% polyacrylamide solution (29:1) were acquired from BioShop Canada (Burlington, ON, Canada). The water used was purified via Milli-Q Synthesis A10 water purifier. All other chemicals were purchased from Bioshop Canada and used without further purification.

4.5.2 Synthesis and purification of oligonucleotides

The sequences of oligonucleotides are listed in Figure 4-2. The DNA library L1, the special fluorogenic substrate FS1, the forward PCR primer FP1, the two reverse PCR primers RP1 and RP2, the template LT1 for ligating FS1 to L1 were purchased as synthetic oligonucleotides either from Yale University Keck Facilities or from Integrated DNA Technologies (IDT). All oligonucleotides were purified by 10% denaturing polyacrylamide gel electrophoresis (dPAGE) before use. Each random position in L1 represents a 25% probability of A, C, G or T nucleotide. FS1 contains an adenosine ribonucleotide (R), flanked by a fluorescein-dT (F) and a dabcyl-dT (Q). The reverse primer RP2 contains a triethylene glycol spacer and A20 tail at the 5' end. The spacer prevents the poly(dA) tail from being amplified, making the non-DNAzyme-coding strand 20 nucleotides longer than the coding strand. This allows for the separation of the two strands by 10% dPAGE. The RNA-containing substrate FS1 was deprotected and purified by 10% dPAGE following a previously reported protocol[15,21].

4.5.3 Bacterial strains and culture conditions

C. difficile NAP1 strain in this study was obtained from the American Type Culture Collection (ATCC; Manassas, Va.). The *E. coli* strains used were *E. coli* K12 and *E. coli* K12 BW25113Δ*rna*. The bacteria *K. aerogenes* was obtained as gifts from the laboratory of Professor Gerard Wright (Michael G. DeGroote Institute for Infectious Disease Research, McMaster University). Other bacteria used in this study are routinely cultured and

maintained in our laboratory. For aerobic bacteria, cells were cultured (37°C; shaking at 200 rpm) in LB medium. *C. difficile* cultures were grown in chopped meat glucose medium (ATCC medium 593), anaerobically, at 37 °C in an anaerobic workstation (D. Whitley).

Table 4-1. Information on the tested *C. difficile* strains

Strain names	North American pulsed-field type	Toxin type	Ribotype	Toxin A	Toxin B	Binary Toxin
BAA-1870	NAP1	IIIb	027	+	+	+
BAA-1803	NAP1	III	027	+	+	+
BAA-1871	NAP2	0	001	+	+	-
BAA-1872	NAP4	0	207	+	+	-
BAA-1875	NAP7	V	078	+	+	+
BAA-1812	unknown	XII	024	+	+	-
BAA-51696	unknown	0	001	+	+	-

4.5.4 Preparation of crude extracellular mixture (CEM) from bacterial strains

Both aerobic and anaerobic bacteria were grown in 5 mL of the appropriate medium (LB for aerobic bacteria, chopped meat glucose medium for anaerobic bacteria) until OD600 reached ~1. Pellets from the culture were removed by centrifugation at 11,000 g at 4 ℃ for 5 min. The crude supernatant was collected and passed through a 0.22 µm filter, and then aliquoted into microcentrifuge tubes, and stored at -80℃.

4.5.5 In vitro selection

Procedures were performed similarly as previously described[15,21]. Briefly, 1 nmol of L1 was phosphorylated (reaction volume: 100 µL) with ATP and 20 U of T4 polynucleotide kinase (PNK) in 1× PNK buffer A at 37°C for 45 min. The reaction was quenched by heating the mixture at 90°C for 5 min. Equimolar FS1 and LT1 were then added to this solution, and the mixture was heated at 90°C for 1 min and cooled to room temperature. Then, 15 µL of 10× T4 DNA ligase buffer was added, and the volume was adjusted to 150 µL with ddH$_2$O. T4 DNA ligase (20 U) was added, followed by incubation at room temperature for 2 h. The DNA molecules in the mixture were concentrated by ethanol precipitation, and the ligated FS1-L1 molecules were purified by 10% dPAGE and then dissolved in 50 µL of 1× selection buffer (1× SB) (50 mM HEPES, pH 7.5, 150 mM NaCl, 15 mM MgCl$_2$, and 0.01% Tween 20). This mixture was incubated with 50 µL of the unintended target (See Figure 4-3a for more details). After ethanol precipitation, the uncleaved CDFS1-RFL1 molecules were purified by 10% dPAGE, dissolved in 10 µL of ddH$_2$O. The purified FS1-L1 was again dissolved in 50 µL of 1× SB. This mixture was incubated with 50 µL of CEM from *C. difficile* NAP1(ATCC1870) in 1× SB at room temperature for 30 min. The reaction was quenched by the addition of 100 µL of stop solution containing 100 mM EDTA and 8 M urea. After ethanol precipitation, the cleaved FS1-L1 molecules were purified by 10% dPAGE, dissolved in 10 µL of ddH$_2$O, and stored at -20°C. The PCR1 mixture (50 µL) contained 4 µL of the template prepared above, 0.5 µM each of FP1 and RP1, 200 µM each of dNTPs (dATP, dCTP, dGTP and dTTP), 1× PCR buffer (75 mM Tris-HCl, pH 9.0, 2 mM MgCl$_2$, 50 mM KCl, 20 mM (NH$_4$)$_2$SO$_4$) and

2.5 U of Thermus thermophilus (Tth) DNA polymerase. The DNA was amplified using the following thermocycling steps: 94°C for 1 min; 11-13 (dependent on the amount of cleavage of the DNA pool) cycles of 94°C for 45 s, 53°C for 45 s and 72°C for 45 s; 72°C for 1 min. For the PCR2 reaction, 1 µL of the PCR1 product was diluted with ddH$_2$O to 20 µL, 2-5 µL of which was used as the template for this additional PCR step (a total of 8× 50-µL reactions were conducted to generate enough DNA) using primers FP1 and RP2 and the same protocol for PCR1. The L1 strand was purified by 10% dPAGE and used for the next selection round.

4.5.6 High-throughput sequencing

The cleavage product from the round 7 and 12 of selection was amplified by PCR to obtain sufficient DNA for sequencing. PCR1 was conducted using FP1 and RP1 following the same protocol as described above. 1 µL of the PCR1 product was diluted into 100 µL with ddH2O, and 2 µL was used as the template for PCR2 using deep sequencing primers SFP and SRP following the same protocol above for PCR1. 8 individual PCR reactions were performed, and the PCR products were purified by 2% agarose gel electrophoresis. DNA extraction from agarose gel was done using GenElute Gel Extraction Kit (Sigma Aldrich). Purified PCR products were sequenced using paired-end next-generation sequencing (NGS) using an Illumina Miseq system at the Farncombe Metagenomics Facility, McMaster University. Raw sequencing reads were first trimmed of their primers using Geneious. The resulting 50 nt reads were filtered for quality using

PrinSeq v0.20.4 to make sure only high-quality reads were used for further analysis[22]. All sequences with any bases of Phred scores < 20 (base-call probability < 99%) were eliminated. Using a clustering algorithm CD-HIT-EST, sequences were grouped into clusters (also known as classes)[23]. The following input parameters were used: identity threshold (-c), 0.9; word length (-n), 7; (-d), 0; (-g), 1. Grouped classes were then ranked by size, defined by the number of sequences in that class, to identify the dominating sequences in the pool.

4.5.7 Cleavage test with CEM prepared from bacteria

Cleavage test for each CEM was carried out as follows: 10 µL of 2× SB containing 1 pmol RFA molecules was incubated with 10 µL of CEM at room temperature for 4 h or 24 h. The reaction was quenched by the addition of 20 µL of 2× denaturing gel loading buffer (GLB, containing 100 mM of EDTA and 8 M urea). The cleavage was then analyzed by 10% dPAGE. The image of cleaved and uncleaved DNA bands was obtained with a Typhoon Trio+ Imager.

4.5.8 Cleavage test using CEM treated with protease

To evaluate the nature of the target of RFA, CEM with 1 µL of 5 U/µL proteinase K stock (PK; New England Biolabs) was mixed with 9 µL of CEM and 10 µL of 2× SB, and the resulting solution was incubated at room temperature for 1 h. Following this step, 1 µL of 1 µM RFA stock was added to the mixture, which was further incubated at room

temperature for 4 h. The reaction was then quenched by 20 µL of 2× GLB and the reaction mixture was analyzed using 10% dPAGE.

4.5.9 Heat resistance analysis

To evaluate the thermal stability of the potential targets, the CEM was subjected to further heating at 90ºC for 5, 10, 20, 30 or 60 min. The cleavage activity of the RFA probe was induced by adding CEM heated for different times in the same assay set up as described above.

4.6 References

1. He, M. *et al.* Emergence and global spread of epidemic healthcare-associated *Clostridium difficile*. *Nat. Genet.* **45,** 109–13 (2013).

2. Martin, J. S. H., Monaghan, T. M. & Wilcox, M. H. *Clostridium difficile* infection: Epidemiology, diagnosis and understanding transmission. *Nat. Rev. Gastroenterol. Hepatol.* **13,** 206–216 (2016).

3. Freeman, J. *et al.* The changing epidemiology of *Clostridium difficile* infections. *Clin. Microbiol. Rev.* **23,** 529–49 (2010).

4. McDonald, L. C. *et al.* An epidemic, toxin gene-variant strain of *Clostridium difficile*. *N. Engl. J. Med.* **353,** 2433–41 (2005).

5. Pépin, J., Valiquette, L., Gagnon, S., Routhier, S. & Brazeau, I. Outcomes of *Clostridium difficile*-associated disease treated with metronidazole or vancomycin before and after the emergence of NAP1/027. *Am. J. Gastroenterol.* **102,** 2781–2788 (2007).

6. Silverman, S. K. Catalytic DNA: Scope, Applications, and Biochemistry of Deoxyribozymes. *Trends Biochem. Sci.* **41,** 595–609 (2016).

7. Silverman, S. K. Artificial Functional Nucleic Acids: Aptamers, Ribozymes, and Deoxyribozymes Identified by *In Vitro* Selection. *Funct. Nucleic Acids Anal. Appl.* 47–108 (2009).

8. Ellington, a D. & Szostak, J. W. *In vitro* selection of RNA molecules that bind specific ligands. *Nature* **346,** 818–22 (1990).

9. Tuerk, C. & Gold, L. Systematic Evolution of Ligands By Exponential Enrichment - Rna Ligands To Bacteriophage-T4 DNA-Polymerase. *Science* **249,** 505–510 (1990).

10. Liu, M., Chang, D. & Li, Y. Discovery and Biosensing Applications of Diverse RNA-Cleaving DNAzymes. *Acc. Chem. Res.* **50,** 2273–2283 (2017).

11. Liu, J., Cao, Z. & Lu, Y. *Functional Nucleic Acid Sensors Functional Nucleic Acid Sensors*. **109,** (2009).

12. Mok, W. & Li, Y. Recent progress in nucleic acid aptamer-based biosensors and bioassays. *Sensors* **8,** 7050–7084 (2008).

13. Ao, F. G., Iu, F. L., Heng, J. Z., Eng, M. Z. & Iang, Y. J. A Catalytic DNA Probe with Stem-loop Motif for Human T47D Breast Cancer Cells. **31,** (2015).

14. Tram, K., Kanda, P. & Li, Y. Lighting Up RNA-cleaving DNAzymes for biosensing. *J. Nucleic Acids* **2012,** (2012).

15. Ali, M. M., Aguirre, S. D., Lazim, H. & Li, Y. Fluorogenic DNAzyme Probes as Bacterial Indicators. *Angew. Chemie Int. Ed.* **50,** 3751–3754 (2011).

16. Shen, Z. *et al.* A Catalytic DNA Activated by a Specific Strain of Bacterial Pathogen. *Angew. Chemie - Int. Ed.* **55,** (2016).

17. Curry, S. R. *et al. tcdC* genotypes associated with severe TcdC truncation in an epidemic clone and other strains of *Clostridium difficile*. *J. Clin. Microbiol.* **45,** 215–221 (2007).

18. Shang, F.-M. & Liu, H.-L. Fusobacterium nucleatum and colorectal cancer: A review. *World J. Gastrointest. Oncol.* **10,** 71–81 (2018).

19. Ramaswamy, V. *et al.* Listeria--review of epidemiology and pathogenesis. *J. Microbiol. Immunol. Infect.* **40,** 4–13 (2007).

20. Condon, C. & Putzer, H. The phylogenetic distribution of bacterial ribonucleases. *Nucleic Acids Res.* **30,** 5339–5346 (2002).

21. Shen, Z. *et al.* A Catalytic DNA Activated by a Specific Strain of Bacterial Pathogen. *Angew. Chem. Int. Ed. Engl.* **55,** 2431–4 (2016).

22.   Schmieder, R. & Edwards, R. Quality control and preprocessing of metagenomic datasets. *Bioinformatics* **27,** 863–864 (2011).

23.   Li, W. & Godzik, A. Cd-hit: a fast program for clustering and comparing large sets of protein or nucleotide sequences. *Bioinformatics* **22,** 1658–9 (2006).

Chapter 5

RFA13-1: An Unintentional Discovery of a Fluorogenic DNA Probe for Ribonuclease I

5.1 Abstract

Ribonuclease I belongs to a class of non-specific endoribonucleases and plays many important roles in a variety of biological and cellular processes. While their ubiquitous nature and high activity contribute to the well-known problem of RNase contamination in experimentation, their abundance can potentially be leveraged as a biosensor target. As a result, there is substantial interest in generating a specific and reliable probe for RNase detection for a variety of purposes. To that end, we report on our unintentional discovery of the RNase I probe RFA13-1 isolated through *in vitro* selection with the crude extracellular matrix from *C. difficile* contaminated with *K. aerogenes* as a selection target. Characterization of RFA13-1 revealed that it exhibited high sensitivity to *E. coli* RNase I with detection limits within the 5 pM range. Furthermore, RFA 13-1 also demonstrated high specificity towards RNase I produced only in select bacteria from the *Enterobacteriaceae* class. As a result, this probe offers a simple tool for RNAse I detection with potential applications in RNase functional studies, ribonuclease contamination monitoring, and bacterial detection.

5.2 Introduction

Ribonucleases are a class of ubiquitous enzymes that play important roles in many biological processes such as gene expression and regulation, genome replication and maintenance, host defence, stress response, and viral strategies of infection[1]. However, while ribonucleases are important for cellular function, the presence of RNase contamination represents a major problem in experiments involving RNA as they may damage precious samples and invalidate the experimental outcomes. Therefore, there is substantial interest in monitoring RNase activity in connection to various applications.

Ribonuclease I (RNase I) is a nonspecific endoribonuclease belonging to the RNase T2 superfamily and found primarily in the periplasmic space in *E. coli*[2–4]. In the presence of EDTA, ~99% of the total RNase activity is due to RNase I[5,6]. Currently, the biological role of RNase I remains incompletely understood. Early reports have proposed a role for the enzyme in scavenging extracellular RNA to supply nutrients for cells[7,8]. However, the physiological substrate(s) in this process remains unclear due to a lack of *in vivo* investigations. A recent study has found that RNase I can be inhibited by helix 41 of the *E. coli* 16s rRNA which provides a physiological benefit for the host cells in coping with the potential cytotoxicity of this enzyme[9]. Moreover, cytoplasmic RNase I was shown to be involved in the degradation of mRNA and rRNA to yield 2', 3'-cNMPs[10]. This study has also demonstrated that RNase I and 2', 3'-cNMPs levels play an important role in controlling biofilm formation[10]. However, the biological function of periplasmic RNase I is still unclear. In addition, RNase I has only been identified in the α- and γ-subdivisions of the Proteobacteria exclusively[11]. This allows this enzyme to act as a potential biomarker

for bacteria from these subdivisions, including pathogenic bacteria like *Salmonella enterica* and *Escherichia coli*.

A specific and reliable probe for RNases I detection is not only important for biological function studies of this enzyme but it can also be employed for nucleases contamination monitoring and bacterial detection. Traditionally, gel electrophoresis and capillary electrophoresis are the predominant means of studying enzyme activity. However, these methods have significant limitations as they often require radioisotope-labelled DNA substrates and can only provide discontinuous enzyme kinetic analysis[12–14]. Several innovative approaches have been proposed recently based on the detection of fluorescent or electrochemical signals, colorimetric changes, or surface plasmon resonance[15–18]. However, none of these methods are designed to specifically detect RNase I.

SELEX (or *in vitro* selection) is an *in vitro*, test-tube evolution method that begins with a large pool of randomized DNA or RNA sequences that are subjected to multiple rounds of selective pressure[19,20]. Only the sequences that are capable of performing a desired function, such as binding to a specific target are isolated, amplified and subject to further rounds of evolution. This allows one to isolate the sequences that can perform the expected function with the greatest efficiency. This method has already been adopted in the past to understand substrate preferences of nucleic acid interacting enzymes[21,22]. In this work, we presented an RNA-cleaving fluorescent probe isolated through *in vitro* selection that is capable of identifying RNase I with high sensitivity and specificity.

5.3 Results

5.3.1 Isolation of RFA13-1 though in vitro selection
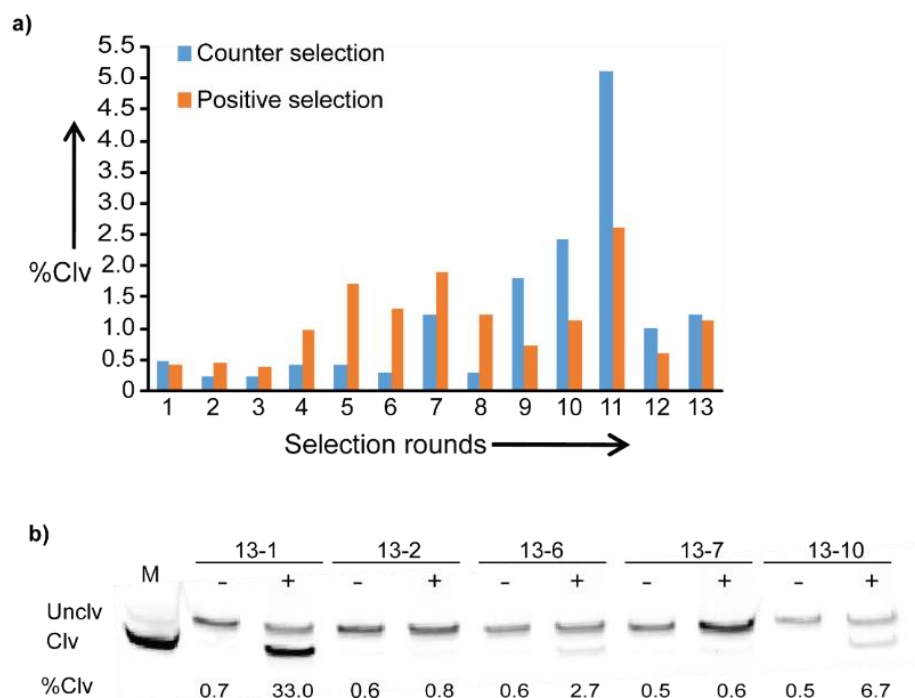
Figure 5-1. a) The progress of *in vitro* selection. b) Responses of top RFAs towards CEM-SELEX. Incubation time: 4 hours.

Our discovery of the RNase I probe was unintentional. In our lab, we are interested in isolating RNA-cleaving fluorescent aptazyme (RFA) for pathogenic bacteria detection[23–26]. Recently, we attempted to isolate RFA probes targeting a specific strain of *Clostridium difficile*, an intestinal pathogen related to infectious diarrhea. The crude extracellular mixture (CEM) prepared from *C. difficile* culture was used as a target for selection. The selection was carried out according to our previously established protocols[23,25]. See Figure 4-2 in Chapter 4 for the DNA sequences used in this work and Table 5-2 for the selection

strategy. After 13 rounds of selection, the DNA pool was sent for high-throughput sequencing. Several active RFA classes were discovered (Figure 5-1). The RFA probe with the highest cleavage activity (Class 1) was named RFA13-1(Figure 5-2a). However, upon further investigation, it was discovered that RFA13-1 could only be activated by the CEM prepared from a particular *C. difficile* glycerol stock with no activity observed when testing CEM prepared from another C. *difficile* resource. To uncover why this had occurred, we re-cultured *C. difficile* from the initial glycerol stock for selection in cooked meat broth for 48 hours and then spread the diluted bacterial culture on agar plates. After overnight culture at 37 degrees, colonies with different appearance and size were observed suggesting that the glycerol stock used may have been contaminated. By utilizing16s rRNA sequencing analysis, the larger colonies were confirmed to be *C. difficile*, while the smaller colonies were identified as *Klebsiella aerogenes,* a Gram-negative pathogenic bacterium (Figure 5-2b). The CEM from *C. difficile* (CEM-CD) and *K. aerogenes* (CEM-KA) were then prepared separately and tested with RFA13-1. As shown in Figure 5-2c, CEM-KA generated a cleavage signal, while CEM-CD did not. Therefore, this study explains the observed cleavage and suggests that RFA13-1 targets *K. aerogenes* instead of *C. difficile.* As the CEM used during the selection was contaminated by the metabolites from *K. aerogenes*, it would not be surprising to isolate a probe targeting *K. aerogenes*.
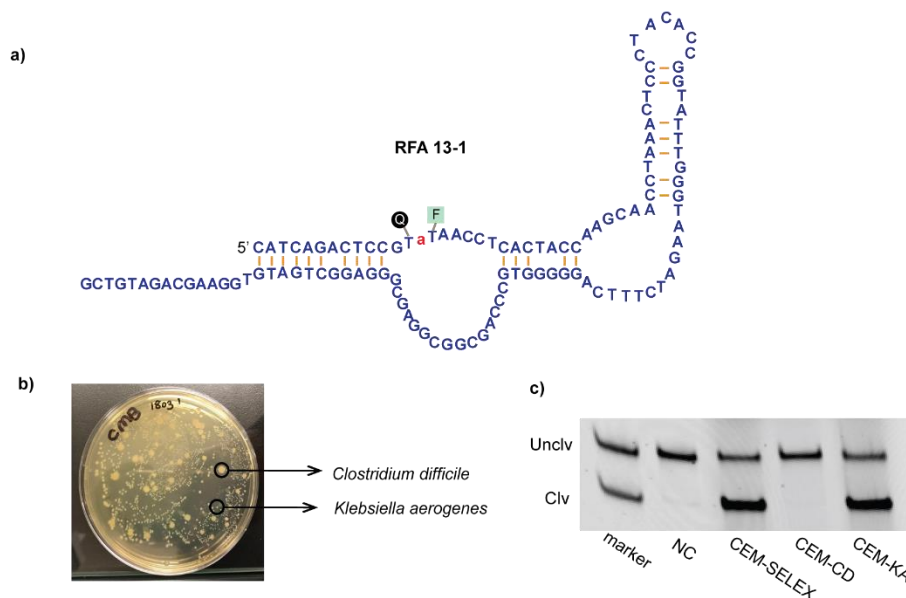
Figure 5-2. Isolation of RFA13-1. a) Secondary structure of RFA13-1. b) Colonies of *C. difficile* and *K. aerogenes* on an agar plate. d) Responses of RFA13-1 to CEM used in selection, or produced by *C. difficile* NAP1, and *K. aerogenes*. Incubation time: 1 hour.

5.3.2 Responses of RFA13-1 towards different bacteria

We subsequently investigated the response of RFA13-1 to CEM produced by different microbes. Eleven bacteria from the *Enterobacteriaceae* family and eleven bacteria from other families were chosen for this experiment. Detailed information surrounding these bacteria are summarized in Table 5-1. Eight out of eleven bacteria from the *Enterobacteriaceae* family were able to activate RFA13-1, whereas none of the other bacteria were able to induce cleavage (see Figure 5-3).
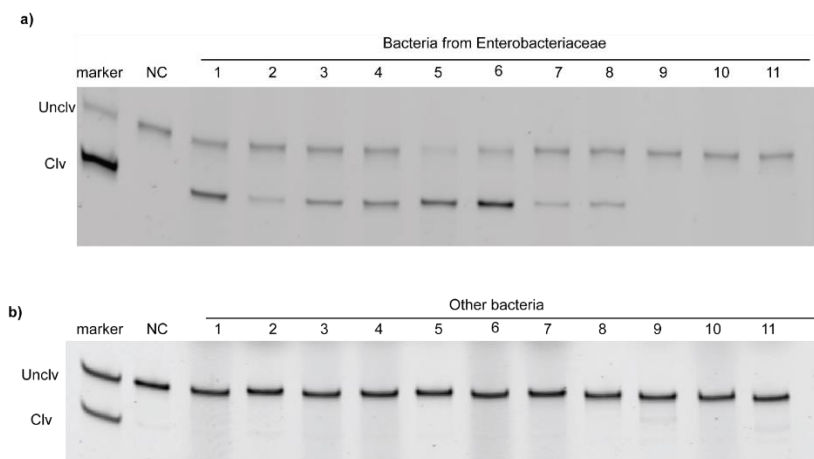
Figure 5-3. Responses of RFA13-1 towards CEM prepared from bacteria from the family of *Enterobacteriaceae*. Lane 1-11: *K. aerogenes, K. pneumoniae, E. aerogenes, E. cloacae, S. enterica, E. coli, S. sonnei, S. flexneri, Y. ruckeri, H. alvei,* and *S. fonticola.* b) Responses of RFA13-1 toward various other bacteria. Lane 1-11: *A. lwoffii, L. pneumophila, O. gringonese, B. diminuta, A. xylosoxidans, F. nucleatum, E. faecium, L. monocytogenes, B. subtilis, C. difficile,* and *A. orientalis.* Incubation time: 1 hour.

5.3.3 Identification of RNase I as the target of RFA13-1

To discover the targets in the CEM that activate RFA13-1, we first treated the CEM-KA with proteinase K and found that the protease-treated CEM was no longer able to activate RFA13-1 (Figure 5-4a). This observation suggests that the responsive target is a protein. We then treated the CEM-KA with two protein-based RNase inhibitors, NxGen RNase inhibitor (RI-NG) and SUPERase RNase inhibitor (RI-SP), to examine whether the observed cleavage was generated by RNases that may exist in the CEM. As shown in Figure 5-4b, the cleavage activity was fully inhibited by adding RI-SP. In contrast, the addition of RI-NG did not affect the cleavage activity. Subsequently, we compared the targets of RI-NG and RI-SP and found that RI-SP can inhibit RNases A, B, C, I, and T1, whereas RI-NG is only able to inhibit RNase A, B and C. Since RNase T1 is a fungal ribonuclease

which is not expressed by bacteria, we then suspected that RNase I is the likely target of

RFA13-1. It is also important to note that RI-SP can also inhibit the cleavage activity of

RFA13-1 towards all tested bacteria (Figure 5-5).
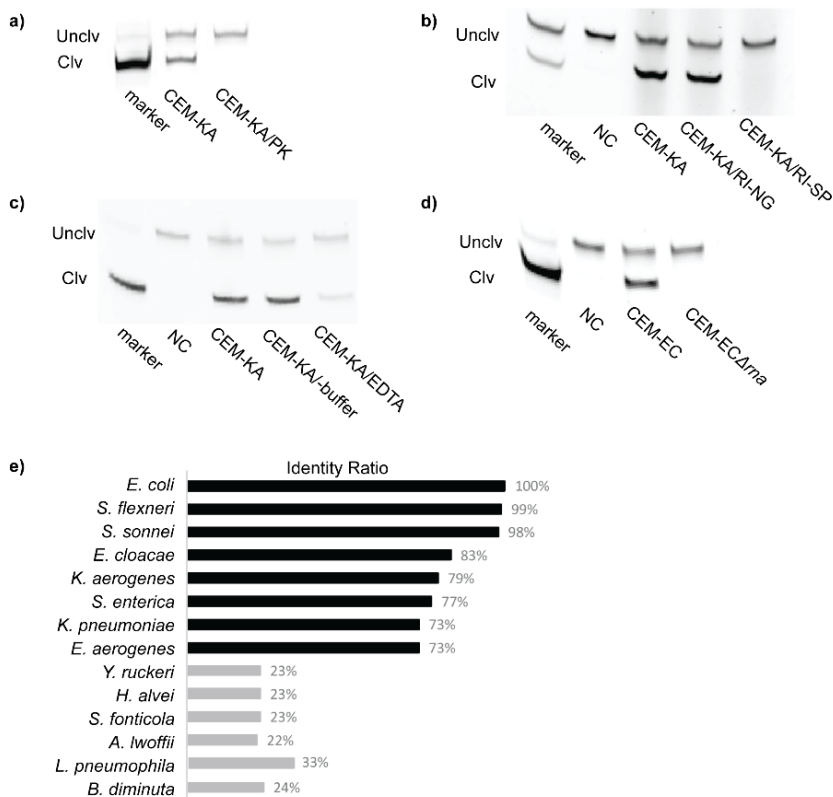
Figure 5-4. Identification of the activator of RFA13-1. a) Responses of RFA13-1 to protease-treated CEM-KA. PK: proteinase K. b) Responses of RFA13-1 to RNase inhibitor-treated CEM-KA. RI-NG: NxGen RNase inhibitor. RI-SP: SUPERase RNase inhibitor. c) Responses of RFA13-1 to CEM-KA in the absence of reaction buffer or in the presence of reaction buffer with EDTA. d) Responses of RFA13-1 to CEM-EC and CEM-ECΔrna. Incubation time: 1 hour. e) Comparison of the identity of RNase I from different bacteria. The *E. coli*-RNase I protein sequence had served as the subject sequence during Blast.

To test our hypothesis, we examined the metal ion dependence of RFA13-1 as

RNase I does not require any divalent cations for activity. We tested the activity of RFA13-

1 with CEM-KA in the absence of reaction buffer or in the presence of reaction buffer with EDTA, a chelating agent that can sequester divalent metal ions. As shown in Figure 5-4c, cleavage activity was still observed in both cases, although an activity reduction was observed in the presence of EDTA. This reduced activity could have been caused by DNA probe misfolding in the absence of divalent metal ions. These results suggest that metal ions are not necessary for the cleavage reaction of RFA13-1, and supports the idea that the target of RFA13-1 is RNase I.
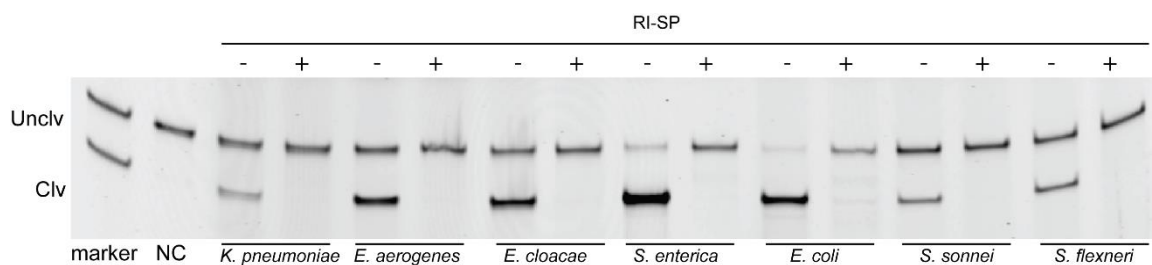
Figure 5-5. Responses of RFA13-1 to RNase inhibitor-treated CEM from various bacteria. RI-SP: SUPERase RNase inhibitor. Incubation time: 1 hour.

We then compared the cleavage activity of RFA13-1 in the presence of CEM from wild-type *E. coli* strain K12 (CEM-EC) and an *E. coli* RNase I-knockout strain (CEM-ECΔ*rna*). As shown in Figure 5-4d, CEM-EC generated a cleavage signal while CEM-ECΔRNase1 did not. This experiment confirmed that RNase I is the target of RFA13-1, at least in the case of *E. coli*.

As mentioned above, RNase I has only been identified in the α- and γ-subdivisions of the proteobacteria. Unsurprisingly, from the data presented in Figure 5-3, the bacteria

responsive to RFA13-1 are all from these two divisions. However, not all bacteria species from these divisions are able to trigger the probe. To investigate why this occurred, we then compared the RNase I protein sequence from these bacteria using Blast analysis (*E. coli*-RNase I protein sequence was used as subject sequence and other bacteria's RNase I sequences were used as the query sequence). The sequence identity was calculated and summarized in Figure 5-4e. We found that the RNase I from RFA13-1-responsive bacteria all have a high sequence identity to *E. coli*-RNase1 (> 73%), while RNase1 from other bacteria have a low sequence identity (<33%). These results explain the microbial selectivity of RFA13-1 and suggest that RFA13-1 is targeting specific types of RNase I.

5.3.4 Evaluation of the specificity of RFA13-1 against different RNases
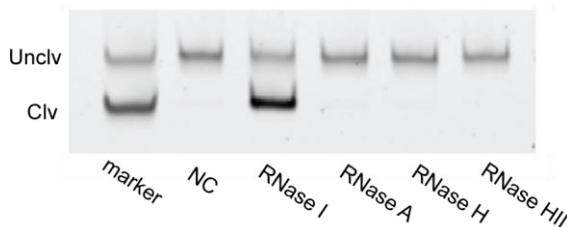
Figure 5-6. Responses of RFA13-1 towards endoribonucleases I, A, H, and HII. The concentration of RNases is 50 pM. Incubation time: 1 hour.

The specificity of RFA13-1 towards other ribonucleases was also evaluated. As RFA13-1 is a stretch of DNA containing a single RNA moiety located between a fluorophore-modified deoxythymine and a quencher-modified deoxythymine (fluorescein and dabcyl, respectively), this design gives RFA13-1 a great protection from exoribonuclease. Here, endoribonucleases, RNase I, RNase A, RNase H, and RNase HII,

were employed (Figure 5-6). We found RFA13-1 only responded to RNase I signifying a

strong ribonuclease-specificity.

5.3.5 Evaluation of the sensitivity of RFA13-1 in RNases I detection
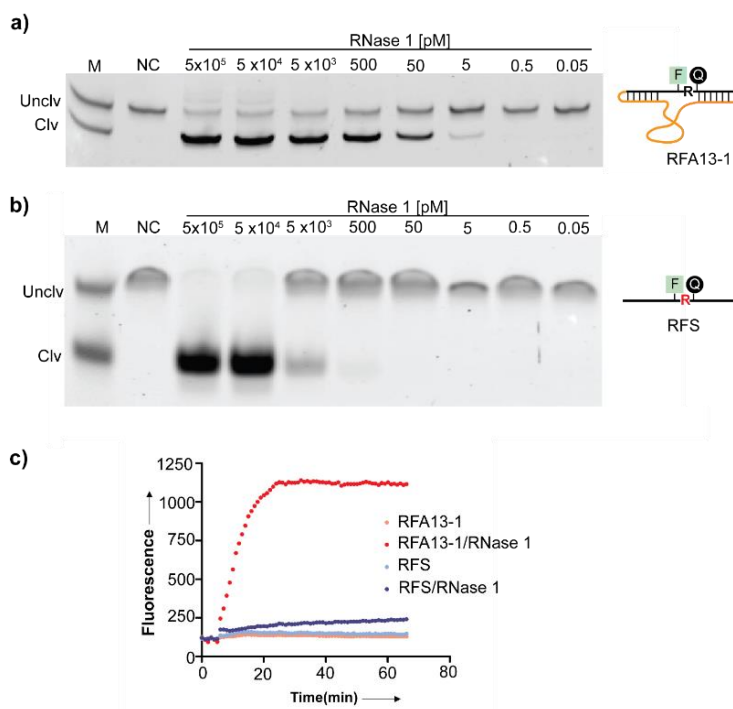
Figure 5-7. Sensitivity analysis of a) RFA13-1 and b) RFS towards RNase I. RFA13-1 and RFS concentration: 50 nM. Reaction time: 1 hour. c) Signalling profiles of 100 nm RFA13-1 or RFS in the presence or absence of 500 pM RNase I. DNA probe was incubated in SB alone for 5 min, followed by the addition of RNase I and further incubation for 1 hour.

The sensitivity of RFA13-1 was also investigated by using different concentrations

of *E. coli*-RNase I. As shown in Figure 5-7a, RFA 13-1 offers a detection limit of 5 pM,

which is comparable or even lower than that of many commercial RNase detection kits.

However, by removing the part of the selected sequence from RFA13-1, the RNA-cleaving

fluorogenic substrate (RFS) alone (see Figure 5-7b) was only able to detect 500 pM of

RNase I. The activity of RFA13-1 and RFS against RNase I was also examined by

fluorescence measurement. These results suggest that the selected DNA sequence in

RFA13-1 is able to significantly improve the RNase I mediated cleavage activity.

5.3.6 Kinetic analysis of RFA13-1-RNase I reaction
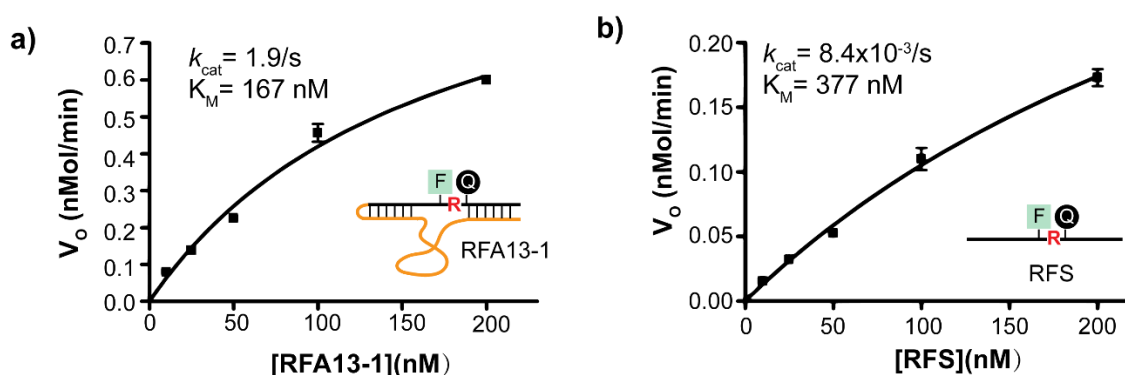
Figure 5-8. Kinetics analysis of a) RFA13-1 and b) RFS towards RNase I. The RNase I concentration is 10 pM and 1 nM for RFA13-1 and RFS respectively.

Kinetics analysis was then performed to investigate why the selected sequence in

RFA13-1 could enhance the cleavage activity of RNase I. As shown in Figure 5-8, a

comparison of k_{cat} indicates that RNase I has a ~230-fold higher catalytic turnover towards

RFA13-1 than RFS. The K_M value for RFA13-1 was less than half of that for RFS,

suggesting a stronger affinity between RFA13-1 and RNase I. As a result, compared to RFS,

RFA13-1 serves as a significantly better substrate for RNase I in the cleavage reaction. We

also performed kinetics analysis for the probes (5'F-RFA13-1 and 5'F-RFS) which do not

have a fluorophore and a quencher beside the cleavage site (see Figure 5-9). Compared with the original probes, the catalytic turn over increased by ~10 times for 5'F-RFA13-1 and ~3000 times for 5'F-RFS. The binding affinity against RNase I was also improved for 5'F-RFA13-1, but not for 5'F-RFS. These results suggest that the fluorophore- and quencher- modifications have a role in protecting the ribonucleotide from RNase cleavage as they could significantly decrease the catalytic turnover of RNase I. However, the selected DNA is able to recover the turnover and also improve the binding affinity between RNase I and the probe.
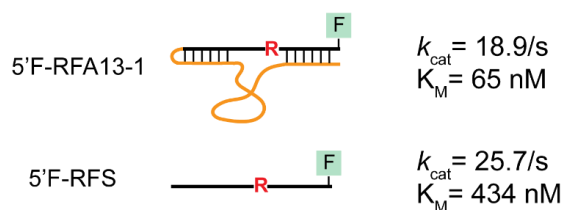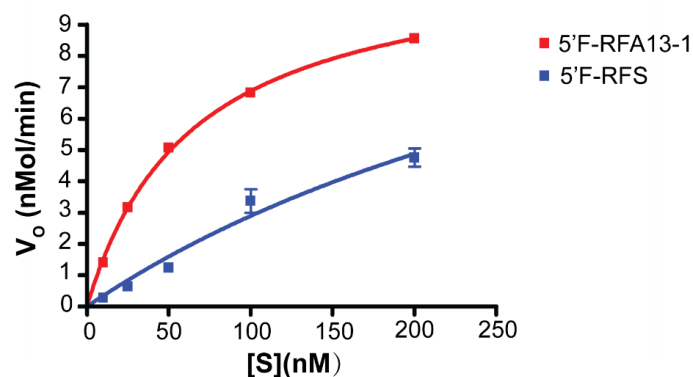
Figure 5-9. Kinetics analysis of 5'F-RFA13-1 and 5'F-RFS towards RNase I. RNase I concentration: 10 pM.

5.4 Summary

In summary, we performed an *in vitro* selection experiment for generating *C. difficile* probes, but unintentionally isolated a probe, RFA13-1, targeting RNase I, due to the contamination of the *C. difficile* glycerol stock used for selection. However, despite the unexpected result, RFA13-1 may nonetheless serve as a useful probe as it exhibited high sensitivity being able to detect as low as 5 pM of RNase I. RFA13-1 also presented great specificity as it only responds to specific types of RNase I expressed in *Enterobacteriaceae* bacteria, such as *K. aerogenes* and *E. coli*. Thus, this multifaceted probe can be applied for bacterial pathogen detection in addition to other numerous applications such as being employed as a sensitive tool for RNase I detection or in biological function studies of the RNase enzyme.

5.5 Experiments

5.5.1 Enzymes, chemicals, and other materials

T4 DNA ligase, T4 polynucleotide kinase (PNK), Ribonuclease I (RNase I) and RNase A were purchased from Thermo Scientific (Ottawa, ON, Canada). RNase H was purchased from New ENGLAND BioLabs (Whitby, ON, Canada). RNase HII was cloned and expressed in our lab. Urea (ultrapure) and 40% polyacrylamide solution (29:1) were acquired from BioShop Canada (Burlington, ON, Canada). The water used was purified via Milli-Q Synthesis A10 water purifier. All other chemicals were purchased Bioshop Canada and used without further purification.

5.5.2 Synthesis and purification of oligonucleotides

The sequences of oligonucleotides are listed in Figure 4-2. The DNA library L1, the special fluorogenic substrate FS1, the forward PCR primer FP1, the two reverse PCR primers RP1 and RP2, the template LT1 for ligating FS1 to L1 were purchased as synthetic oligonucleotides either from Yale University Keck Facilities or from Integrated DNA Technologies (IDT). All oligonucleotides were purified by 10% denaturing polyacrylamide gel electrophoresis (dPAGE) before use. Each random position in L1 represents a 25% probability of A, C, G or T nucleotide. FS1 contains an adenosine ribonucleotide (R), flanked by a fluorescein-dT (F) and a dabcyl-dT (Q). The reverse primer RP2 contains a triethylene glycol spacer and A20 tail at the 5' end. The spacer prevents the poly(dA) tail from being amplified, making the non-DNAzyme-coding strand 20 nucleotides longer than the coding strand. This allows for the separation of the two strands by 10% dPAGE. The RNA-containing substrate FS1 was deprotected and purified by 10% dPAGE following a previously reported protocol[25,26].

5.5.3 Bacterial strains and culture conditions

C. difficile NAP1 strain in this study was obtained from the American Type Culture Collection (ATCC; Manassas, Va.). The *E. coli* strains were *E. coli* K12 and *E. coli* K12 BW25113Δ*rna*. The bacteria *Klebsiella aerogenes, Klebsiella pneumoniae, Enterobacter aerogenes, Enterobacter cloacae* were obtained as gifts from the laboratory of Professor Gerard Wright (Michael G. DeGroote Institute for Infectious Disease Research, McMaster University). *Salmonella enterica, Escherichia coli, Shigella sonnei, Shigella flexneri,*

Yersinia ruckeri, Hafnia alvei, Serratia fonticola, Acinetobacter lwoffii, Legionella pneumophila, Ochrobactrum gringonese, Brevundimonas diminuta, Achromobacter xylosoxidans, Fusobacterium nucleatum, Enterococcus faecium, Listeria monocytogenes, Bacillus subtilis, and *Actinomyces orientalis* are routinely cultured and maintained in our laboratory. For aerobic bacteria, cells were cultured (37°C; shaking at 200 rpm) in LB medium. *C. difficile* cultures were grown in chopped meat glucose medium (ATCC medium 593), anaerobically, at 37 °C in an anaerobic workstation (D. Whitley).

Table 5-1. The information on bacteria tested in Figure 5-3. The bacteria labelled in blue are able to activate RFA13-1.

Bacteria	Phylum	Class	Order	Family	Genus
Klebsiella aerogenes	Proteobacteria	Gammaproteobacteria	Enterobacteriales	Enterobacteriaceae	Enterobacter
Klebsiella pneumoniae	Proteobacteria	Gammaproteobacteria	Enterobacteriales	Enterobacteriaceae	Klebsiella
Enterobacter aerogenes	Proteobacteria	Gammaproteobacteria	Enterobacteriales	Enterobacteriaceae	Enterobacter
Enterobacter cloacae	Proteobacteria	Gammaproteobacteria	Enterobacteriales	Enterobacteriaceae	Enterobacter
Salmonella enterica	Proteobacteria	Gammaproteobacteria	Enterobacteriales	Enterobacteriaceae	Salmonella
Escherichia coli k12	Proteobacteria	Gammaproteobacteria	Enterobacteriales	Enterobacteriaceae	Escherichia
Shigella sonnei	Proteobacteria	Gammaproteobacteria	Enterobacteriales	Enterobacteriaceae	Shigella
Shigella flexneri	Proteobacteria	Gammaproteobacteria	Enterobacteriales	Enterobacteriaceae	Shigella
Yersinia ruckeri	Proteobacteria	Gamma Proteobacteria	Enterobacteriales	Enterobacteriaceae	Yersinia
Hafnia alvei	Proteobacteria	Gammaproteobacteria	Enterobacteriales	Enterobacteriaceae	Hafnia alvei
Serratia fonticola	Proteobacteria	Gammaproteobacteria	Enterobacteriales	Enterobacteriaceae	Serratia
Acinetobacter lwoffii	Proteobacteria	Gammaproteobacteria	Pseudomonadales	Moraxellaceae	Acinetobacter
Legionella pneumophila	Proteobacteria	Gammaproteobacteria	Legionellales	Legionellaceae	Legionella
Ochrobactrum gringonese	Proteobacteria	Alphaproteobacteria	Rhizobiales	Brucellaceae	Ochrobactrum
Brevundimonas diminuta	Proteobacteria	Alphaproteobacteria	Caulobacterales	Caulobacteraceae	Brevundimonas
Achromobacter xylosoxidans	Proteobacteria	Beta Proteobacteria	Burkholderiales	Alcaligenaceae	Achromobacter
Fusobacterium nucleatum	Fusobacteria	Fusobacteria	Fusobacteriales	Fusobacteriaceae	Fusobacterium
Enterococcus faecium	Firmicutes	Bacilli	Lactobacillales	Enterococcaceae	Enterococcus
Listeria Monocytogenes	Firmicutes	Bacilli	Bacillales	Listeriaceae	Listeria
Bacillus subtilis	Firmicutes	Bacilli	Bacillales	Bacillaceae	Bacillus
Clostridium difficile	Firmicutes	Clostridia	Clostridiales	Clostridiaceae	Clostridium
Actinomyces orientalis	Actinobacteria	Actinobacteria	Actinomycetales	Actinomycetaceae	Actinomyces

5.5.4 Preparation of CEM from bacterial strains

Both aerobic and anaerobic bacteria were grown in 5 mL of the appropriate medium (LB for aerobic bacteria, chopped meat glucose medium for anaerobic bacteria) until OD600 reached ~1. Pellets from the culture were removed by centrifugation at 11,000 g at 4ºC for 5 min. The crude supernatant was collected and passed through a 0.22 µm filter, and then aliquoted into microcentrifuge tubes, and stored at -80ºC.

5.5.5 In vitro selection and sequencing analysis

The protocols for *In vitro* selection and deep sequencing were described in Section 4.5.5 and 4.46. The selection strategies were summarized in Table 5-2.

Table 5-2. Strategies used during *in vitro* selection

		Counter selection		Positive selection
R1	3h	Selection buffer	3h	
R2-3		Selection buffer Culture media	2h	Selection buffer NAP1 CEM
R4-7		Selection Buffer NAP2 CEM NAP4 CEM NAP7CEM	1h	
R8-13	17h	Selection Buffer NAP2 CEM NAP4 CEM NAP7CEM	0.5h	

5.5.6 Specificity test with different bacteria cells

The dPAGE based specificity test for each CEM was carried out as follows: 10 µL of 2× SB containing 1 pmol RFA13-1 was incubated with 10 µL of CEM at room temperature for 60 min. The reaction was quenched by the addition of 20 µL of 2× loading buffer (containing 100 mM of EDTA and 8 M urea). The cleavage was then analyzed by 10% dPAGE. The image of cleaved and uncleaved DNA bands was obtained with a Typhoon Trio+ Imager.

5.5.7 Cleavage test using CEM-KA treated with protease

1 µL of 5 U/µL proteinase K (PK; New England Biolabs) stock was mixed with 9 µL of CEM-KA and 10 µL of 2× SB, and the resulting solution was incubated at room temperature for 1 h. Following this step, 1 µL of 1 µM RFD-CD1 stock was added to the mixture, which was further incubated at room temperature for 60 min. The reaction was then quenched by 20 µL of 2× loading buffer and the reaction mixture was analyzed using 10% dPAGE.

5.5.8 The activity of RFA13-1 in the presence of ribonuclease inhibitors

To treat CEM with ribonuclease inhibitors (RI). 1 µL of RI stock, either NxGen RNase inhibitor (RI-NG) or SUPERase RNase inhibitor (RI-SP), was mixed with 9 µL of CEM and 10 µL of 2× SB, and the resulting solution was incubated at room temperature for 1 h. Following this step, 1 µL of 1 µM RFD-CD1 stock was added to the mixture, which

was further incubated at room temperature for 60 min. The reaction was then quenched by 20 µL of 2× loading buffer and the reaction mixture was analyzed using 10% dPAGE.

5.5.9 Bioinformatics analysis

RNase I protein sequences of tested bacteria from NCBI were collected. The sequence identity was compared with that in *E. coli* using BLAST (http://www.ncbi.nlm.nih.gov/BLAST/).

5.5.10 The fluorescence-based analysis of the cleavage reaction

To set up the reaction mixture, 50 µL of 2× SB,10 µL of RNase I with different concentration and 35 µL of ddH$_2$O were mixed in a 96 plate which was placed in a microplate scanning spectrometer (TECAN M1000). Fluorescence intensities at 1-min intervals were collected continuously for 5 min; 5 µL of 1µM RFA13-1 or RFS was then added into the wells and the solution was quickly mixed by pipetting the mixture up and down a few times. Following this step, the fluorescence intensity of the solution was recorded every minute for 60 min. All the reactions were conducted in 3 replicates.

5.5.11 Kinetic analysis

The cleavage reaction was conducted in a 50 µL mixture containing 50 nM RFA construct in 1× SB. A 10 µL aliquot was withdrawn from the reaction mixture at the

following time points: 0, 2, 5, 10, and 20 min. These DNA samples were then mixed with $2\times$ loading buffer and subjected to 10% dPAGE for DNA separation. Rate constants were obtained by curve fitting using $Y = Y_m [1-e^{-kt}]$, where Y represents cleavage yield at the time t, Y_m is the maximal cleavage yield, and k is the first-order rate constant.

5.6 References

1. Nichols, N. M. & Yue, D. Ribonucleases. *Curr. Protoc. Mol. Biol.* 1–8 (2008).

2. Neu, H. C. & Heppel, L. A. The release of ribonuclease into the medium when E.coli cells are converted to spheroplasts. *Biochem. Biophys. Res. Commun.* **14,** 109–112 (1964).

3. Abrell, J. W. I Released from Escherichia co / i by Osmotic Shock fractions depending upon the method of cell. (1971).

4. Kaplan, R. & Apirion, D. The involvement of ribonuclease I, ribonuclease II, and polynucleotide phosphorylase in the degradation of stable ribonucleic acid during carbon starvation in Escherichia coli. *J. Biol. Chem.* **249,** 149–151 (1974).

5. Zhu, L. & Deutscher, M. P. The Escherichia coli *rna* gene encoding RNase I: sequence and unusual promoter structure. *Gene* **119,** 101–106 (1992).

6. Zhu, L. Q., Gangopadhyay, T., Padmanabha, K. P. & Deutscher, M. P. Escherichia coli *rna* gene encoding RNase I: cloning, overexpression, subcellular distribution of the enzyme, and use of an *rna* deletion to identify additional RNases. *J. Bacteriol.* **172,** 3146–51 (1990).

7. Beacham, I. R. Periplasmic enzymes in gram-negative bacteria. *Int. J. Biochem.* **10,** 877–83 (1979).

8. Anraku, Y. & Mizuno, D. Ribonuclease-Cyclic Phosphodiesterase System in

Escherichia coli. *J. Biochem.* **61,** 81–88 (1967).

9.   Kitahara, K. & Miyazaki, K. Specific inhibition of bacterial RNase T2 by helix 41 of 16S ribosomal RNA. *Nat. Commun.* **2,** 547–549 (2011).

10. Fontaine, B. M. *et al.* RNase I Regulates E. coli 2',3'-Cyclic Nucleotide Monophosphate Levels and Biofilm Formation. *Biochem. J.* **475,** BCJ20170906 (2018).

11. Condon, C. & Putzer, H. The phylogenetic distribution of bacterial ribonucleases. *Nucleic Acids Res.* **30,** 5339–5346 (2002).

12. Hogrefe, H. H., Hogrefe, R. I., Walder, R. Y. & Walder, J. A. Kinetic analysis of Escherichia coli RNase H using DNA-RNA-DNA/DNA substrates. *J. Biol. Chem.* **265,** 5561–6 (1990).

13. Chan, K. C. *et al.* A capillary electrophoretic assay for ribonuclease H activity. *Anal. Biochem.* **331,** 296–302 (2004).

14. Subbarayan, P. R. & Deutscher, M. P. Escherichia coli RNase M is a multiply altered form of RNase I. *RNA* **7,** 1702–1707 (2001).

15. Ye, Y. *et al.* Direct Electrochemical Monitoring of RNase Activity. *Electroanalysis* **20,** 919–922 (2008).

16. Kim, J. H., Estabrook, R. A., Braun, G., Lee, B. R. & Reich, N. O. Specific and sensitive detection of nucleic acids and RNases using gold nanoparticle–RNA–fluorescent dye conjugates. *Chem. Commun.* **0,** 4342 (2007).

17. Liu, B., Xiang, D., Long, Y. & Tong, C. Real time monitoring of junction ribonuclease activity of RNase H using chimeric molecular beacons. *Analyst* **138,** 3238 (2013).

18. Tripathy, D. R., Dinda, A. K. & Dasgupta, S. A simple assay for the ribonuclease activity of ribonucleases in the presence of ethidium bromide. *Anal. Biochem.* **437,** 126–129 (2013).

19.   Ellington, a D. & Szostak, J. W. *In vitro* selection of RNA molecules that bind specific ligands. *Nature* **346,** 818–22 (1990).

20.   Tuerk, C. & Gold, L. Systematic Evolution of Ligands By Exponential Enrichment - Rna Ligands To Bacteriophage-T4 DNA-Polymerase. *Science* **249,** 505–510 (1990).

21.   Phadtare, S. & Inouye, M. Sequence-selective interactions with RNA by CspB, CspC and CspE, members of the CspA family of Escherichia coli. *Mol. Microbiol.* **33,** 1004–14 (1999).

22.   Frank, D. N., Ellington, A. E. & Pace, N. R. *In vitro* selection of RNase P RNA reveals optimized catalytic activity in a highly conserved structural domain. *RNA* **2,** 1179–88 (1996).

23.   Zhang, W., Feng, Q., Chang, D., Tram, K. & Li, Y. *In vitro* selection of RNA-cleaving DNAzymes for bacterial detection. *Methods* **106,** 66–75 (2016).

24.   Liu, M., Chang, D. & Li, Y. Discovery and Biosensing Applications of Diverse RNA-Cleaving DNAzymes. *Acc. Chem. Res.* **50,** 2273–2283 (2017).

25.   Shen, Z. *et al.* A Catalytic DNA Activated by a Specific Strain of Bacterial Pathogen. *Angew. Chem. Int. Ed. Engl.* **55,** 2431–4 (2016).

26.   Ali, M. M., Aguirre, S. D., Lazim, H. & Li, Y. Fluorogenic DNAzyme Probes as Bacterial Indicators. *Angew. Chemie Int. Ed.* **50,** 3751–3754 (2011).

Chapter 6

Conclusion and Outlook

This thesis research has exploited the use of functional DNAs in the identification of epidemic strains of *Clostridium difficile*. Several strategies, based on the use of aptamers, RNA-cleaving aptazymes, and PCR have been configured to detect various biomarkers from *C. difficile*. We have also developed two colorimetric biosensing platforms that make use of RCA or PCR in conjunction with a urease-mediated litmus test to achieve sensitive biosensing with the naked eye.

Sensitive and colorimetric biosensors are desirable in point-of-care diagnosis applications. In Chapter 2, a colorimetric double-amplified biosensing platform was created using both the RCA technique and a urease-mediated litmus test. By making use of the strong amplification power of RCA and the robust activity of urease, we demonstrated that the sensitivity of the RCA-urease assay could reach sub-picomolar level. In addition, by coupling the assay with the use of structure-switching signalling aptamers for target recognition, the platform was capable of detecting different targets. Currently, our studies have shown that the platform can be used to detect thrombin and PDGF. The next milestone of this project is to expand our approach for the detection of *C. difficile*. The anti-*C. difficile* aptamers which have been mentioned in Chapter 1 can be employed as the recognition element in biosensor development. We have also demonstrated that the platform could be

incorporated into a simple paper-based device for colorimetric detection of DNA. To achieve detection of different targets on paper, we are interested in next exploring the possibility of incorporating structure-switching aptamers into paper-based devices.

In Chapter 3, we extended the use of urease-mediated litmus test in the detection of PCR amplicons and developed a novel assay that can sensitively and specifically detect mutations in the *tcdC* gene to identify epidemic strains of *C. difficile*. Through the combined effect of a double amplification system of PCR and hydrolytic activity of urease, the PCR-litmus test exhibited high sensitivity for *C. difficile* detection. This method can be used to identify the epidemic strains of *C. difficile* in stool samples and has shown great potential in clinical applications. We believe this method can be easily extended to other PCR-based applications simply by using different primers. Considering the broad applications of PCR in biology, medicinal, and environmental studies, we believe that the PCR-litmus design will add great value to cheaper and simpler means of detection.

The studies in Chapter 2 and 3 highlight the versatility of the urease-mediated litmus test. It can not only serve as a signal transducer to generate a colorimetric signal but also has an intrinsic signal amplification mechanism making it a strong signal amplifier. Moreover, it can be easily incorporated into various biosensor designs to achieve colorimetric detection of different targets. However, there are still areas in which the assay can be improved. Currently, several washing steps are involved in the detection process to remove any unused urease-labelled DNA. Magnetic separation and pipetting are required in each of the washing steps, which decrease the simplicity of the detection process. Therefore, lateral-flow technologies and filtration-based technologies need to be

investigated in the future to simplify the detection process and make it more suitable for point-of-care applications.

In Chapter 4, we explored the possibility of isolating RNA-cleaving fluorogenic aptazymes for epidemic strains of *C. difficile* through *in vitro* selection. We used the CEMs prepared from an epidemic *C. difficile* strain (027/NAP1) as the target for the positive-selection and the CEMs prepared from unintended *C. difficile* strains and other bacterial species as the target for the counter-selection. After 12 rounds of selection, four classes of *C. difficile*-responsive probes were successfully isolated. Although none of the RFAs showed strain-specificity, the four RFAs could be used together and generate unique cleavage patterns toward each of the *C. difficile* strains (NAP1, NAP2, and NAP7). These patterns can be used for strain identification of *C. difficile*. This study not only confirmed that RFAs could be isolated to target *C. difficile*, but also provided a novel ratiometric-based strategy for strain identification.

In the future, several experiments are required to validate the relevance of the cleavage patterns and *C. difficile* strain types. For example, to examine whether the cell growth stage would affect the RFA cleavage patterns, CEMs prepared from different growth phases of *C. difficile,* including log phase, stationary phase, and death phase should be tested. More *C. difficile* strains should also be queried to examine the diversity and consistency of the cleavage patterns. Moreover, the molecular targets of the RFAs should be investigated to help us understand why the different patterns have been generated. In addition, the sequence of the RFAs should be optimized to improve their cleavage activity and target selectivity. To do this, mutation and truncation analysis can be performed.

In Chapter 5, we discovered RFA13-1, a RNase I-cleaving fluorogenic probe. This probe was isolated due to the contamination of the glycerol stock for *C. difficile* that was used for *in vitro* selection. Despite the unexpected result, RFA13-1 may serve as a useful probe for RNase I or RNase I-containing bacteria as it exhibited high sensitivity and was able to detect as low as 5 pM of RNase I. Additionally, the probe presented great specificity as it only responds to specific types of RNase I expressed in the bacteria from the family of *Enterobacteriaceae*. This study also highlighted the importance of showing extreme care during *in vitro* selection. While *in vitro* selection is a powerful method for isolating highly specific sequences, any amount of contamination has the potential to significantly affect the end outcome. In addition, results from this study revealed that ribonucleases in CEM can significantly interfere with the selection system. This is particularly important for the selection for RNA-cleaving aptazymes, due to the potential for non-specific degradation of RNA. To address this issue, several approaches can be applied for future *in vitro* selections: 1) redesigning the library using modified ribonucleic acids, such as L-ribonucleic; 2) adding RNases inhibitors to the system; 3) heating the CEM to denature the enzyme; or 4) preparing a pure molecular target instead of CEM for selection.

In conclusion, this thesis describes the development and characterization of novel approaches that have the potential to be used in the identification of epidemic strains of *C. difficile*. I hope my work serves as a stepping-stone for the development of practical biosensors that can be eventually used in the clinical diagnosis of *C. difficile* infections. I believe the general biosensing strategies discussed in this thesis can also be utilized in other bioanalytical applications.